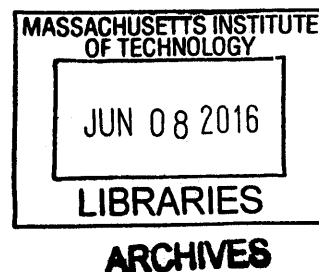


Molecular imaging with engineered physiology

by

Adrian L. Slusarczyk

BA (Hons.), MSci cantab.
University of Cambridge, 2009



Submitted to the Department of Biological Engineering
in Partial Fulfillment of the Requirements for the Degree of

Doctor of Philosophy in Biological Engineering
at the
Massachusetts Institute of Technology

June 2016

© 2016 Adrian L. Slusarczyk. All rights reserved.

The author hereby grants to MIT permission to reproduce
and to distribute publicly paper and electronic
copies of this thesis document in whole or in part
in any medium now known or hereafter created.

Signature redacted

Signature of Author: _____

Department of Biological Engineering
April 15, 2016

Signature redacted

Certified by: _____

Alan P. Jasanoff
Professor of Biological Engineering,
Nuclear Science and Engineering, and Brain and Cognitive Sciences
Thesis Supervisor

Signature redacted


Accepted by: _____

Forest White
Professor of Biological Engineering
Chair, Graduate Program Committee

Thesis Committee

Signature redacted


Accepted by: _____


S.E.T.I. Professor of Biological Engineering and Mechanical Engineering
Chair of Thesis Committee

Linda Griffith

Signature redacted


Accepted by: _____


Professor of Biological Engineering,
Nuclear Science and Engineering, and Brain and Cognitive Sciences
Thesis Supervisor

Alan P. Jasanoff

Signature redacted

Accepted by: _____


C.P. Dubbs Professor of Chemical Engineering and Biological Engineering
Thesis Committee Member

K. Dane Wittrup

Molecular Imaging with Engineered Physiology

by

Adrian L. Slusarczyk

Submitted to the Department of Biological Engineering
on April 15, 2016 in Partial Fulfillment of the
Requirements for the Degree of Doctor of Philosophy in
Biological Engineering

ABSTRACT

Using molecular imaging *in vivo*, biomolecular and cellular phenomena can be investigated within their relevant physiological context, addressing a central challenge for 21st century biomedicine and basic research. To advance neuroscience in particular, molecular-level measurements across the brain inside the intact organism are required. However, existing imaging strategies and available probes have been limited by serious constraints.

Magnetic resonance imaging (MRI) provides deeper tissue penetration depth than optical imaging and better spatial resolution and greater versatility in sensor design than radioactive probes. The most important drawback for MRI probes has been the need for high concentrations in the micromolar to millimolar range, leading to analyte sequestration, complications for noninvasive brain delivery, and toxicity. Efforts to address the sensitivity problem, such as nuclear hyperpolarization, introduce their own technical constraints and so far lack generality.

Here, we introduce a conceptually novel molecular imaging technique based on artificially induced physiological perturbations, enabling molecular MRI with nanomolar sensitivity. In this imaging strategy, we take advantage of blood as an abundant endogenous source of contrast compatible with multiple imaging modalities including MRI and optical imaging to decouple the concentration requirement for molecular sensing from the concentration requirement for imaging contrast. Highly potent vasoactive peptides are engineered to respond to specific biomolecular phenomena of interest at nanomolar concentrations by inducing dilation of the microvasculature, increased local bloodflow, and consequently, large changes in T_2^* -weighted MRI contrast.

This principle is exploited to design activatable probes for protease activity based on the calcitonin gene-related peptide (CGRP) and validate them for brain imaging in live rats; to use CGRP as a genetic reporter for cell tracking; and to create fusions of a vasoactive peptide from flies to previously characterized antibodies capable of crossing the blood-brain barrier (BBB), suggesting the possibility of minimally invasive brain delivery of such probes.

We demonstrate the feasibility of highly sensitive molecular MRI with vasoactive probes at concentrations compatible with *in situ* expression of probes and delivery across the BBB, and show that vasoactive peptides are a versatile platform for MRI probe design which promises unprecedented *in vivo* molecular insights for biomedicine and neuroscience.

Thesis Supervisor: Alan P. Jasanoff

Title: Professor of Biological Engineering, Nuclear Science and Engineering, and Brain and Cognitive Sciences

Acknowledgements

I would like to convey my deep appreciation to my advisor, Alan Jasanoff, for the journey of the last several years. I'd like to thank him for the opportunity to labor in freedom towards the completion of this dissertation, but not without the benefit of his scientific creativity, encouragement, and sound guidance along the way which made the success of this project possible. More broadly, he has fostered in the lab an intellectually fertile, highly collegial, and collaborative environment that was both conducive to getting things done and a pleasure to work in.

I would like to thank my committee chair, Linda Griffith, for her crucial support during my PhD and her scientific and strategic advice throughout. Her guidance was instrumental in shaping my understanding of practical and productive avenues for research.

I am in debt to Dane Wittrup, member of my thesis committee and also my former undergraduate research advisor, for many things. Foremost among them is a way of thinking that begins with the end in mind, prioritizes the quality of the problem to be solved, and applies rigorous reasoning at every level.

Much of the credit for the work presented in this dissertation belongs to my co-authors and colleagues. My thanks go out to Mitul Desai, for all the challenging and intricate *in vivo* work in Chapters 2 and 3; to Mariya Barch for her help in getting started with CGRP; to Agata Wisniewska for being my collaborator on Chapter 4; and to Ashley Chapin, who during her two years as an undergraduate student in the lab made numerous contributions throughout this project with unusual energy and independence. Beside these contributions, I would also like to thank them for being the wonderful colleagues that they've been.

For their helpful discussions and practical advice in relation to this work, I would also like to thank Victor Lelyveld, Yuri Matsumoto, Ali Barandov, Ben Bartelle, Vivian Hsieh, Souparno Ghosh, Jacob Simon, Alessandro Angelini, Byron Kwon, and Sarah Bricault, as well as Prof. Eric Shusta (UWisconsin) and Dr. Jens Niewoehner (Roche).

Many more colleagues, friends, and mentors provided me with invaluable support unconnected to the particular experimental work included in this dissertation, but needed and appreciated just as much. To you, my heartfelt thanks go out as well.

During my graduate studies, I have been fortunate to be supported by fellowships from the Andrew Viterbi Family Foundation, the Boehringer Ingelheim Fonds, and the Friends of the McGovern Institute.

Finally, I am grateful to my parents for always having been encouraging and unconditionally supportive of my choices and endeavors.

Most of all, I thank Lizzie for her companionship and support.

Table of Contents

Background and Introduction	6
Modalities for molecular brain imaging.....	7
Imaging probes for molecular MRI and the challenge of sensitivity	14
Strategy for implementation using vasoactive neuropeptides.....	19
Objective and organization of this document	21
Caged neuropeptides as vasoactive molecular imaging probes for protease activity	25
Abstract.....	25
Introduction.....	25
Results.....	27
Discussion.....	30
Materials and Methods.....	31
Figures and tables	42
Vasoactive probes as genetic reporters for cell tracking by MRI	61
Abstract.....	61
Introduction.....	61
Results.....	63
Discussion	64
Materials and methods	65
Figures and tables	68
A protein engineering platform for BBB-crossing vasoactive imaging probes	75
Abstract.....	75
Introduction.....	75
Results.....	79
Conclusions and future work	83
Materials and methods	84
Figures and tables	89
Conclusions and future directions.....	118
Synopsis, significance, and impact	118
Limitations	120
Future work.....	123
References.....	125

Background and Introduction

Biologists seek to understand phenomena across multiple scales in space, in time, and in complexity, from near-instantaneous chemical transformations of individual molecules to the complex concert of molecules and cells that gives rise to higher-order functions in an organism. Over the past several decades of experimental biological research, from the “golden years” of molecular biology in the 1950s to the “-omics” era of the early 21st century, a dramatic expansion of what might be called reductionist insight into the nature and function of isolated molecules and of cultured cells has been achieved. However, the integrative study of molecular and cellular phenomena inside the physiological context of intact tissues and organs remains a daunting challenge in basic research and in biomedicine.

Two fundamental experimental approaches are at the forefront of efforts to expand our ability to investigate “molecules-in-context” in biology: on the one hand, the re-creation of a relevant physiological context within an experimental apparatus that allows convenient access for measurement, exemplified by tissue engineering, organoids, or organs-on-a-chip¹⁻⁴; and on the other hand, molecular imaging of intact organisms^{5,6}.

Our understanding of the central nervous system especially has the potential to greatly benefit from molecular imaging because much of the brain’s functionality in perception, learning, and cognition requires integrity of the whole organ if not of the entire organism, and has not been reproduced in any kind of *in vitro* device; and because brain function critically hinges on the spatial location and connectivity of neurons and other tissue components, making noninvasive measurement of molecular events as well as spatiotemporal information essential.

Modalities for molecular brain imaging

Given the strong impetus for molecular imaging of the brain, it is no wonder that intense engineering efforts have been exerted to develop suitable methods⁷. Most such methods rely on one of three main modalities: imaging with radionuclide-based probes, optical imaging, and magnetic resonance imaging (MRI). In this section, I outline the principles, available probes, exemplary applications, and strengths and limitations for each.

Brain imaging with radionuclide-based probes

Single-photon emission computed tomography (SPECT) and positron emission tomography (PET) are among the oldest and most established techniques for tomographic imaging of specific molecular probes in intact organisms. Notably, in the publication of the first general-purpose SPECT scanner in 1977⁸, its use was reported (a) in human patients in the clinic, (b) in conjunction with molecular probes, and (c) in the brain for the delineation of tumors, thus illustrating the suitability of the technique for brain imaging and the feasibility of clinical translation.

Principle. The principle of both SPECT and PET is to detect high-energy photons stemming from a radioactive decay event associated with a specifically introduced radionuclide-containing probe. In PET, a radionuclide such as ^{11}C or ^{18}F is selected which undergoes positive beta decay, resulting in the emission of a positron. When this positron collides with an electron, typically after travelling a distance of less than 1 mm through tissue, the two particles are annihilated and two high-energy photons (gamma rays) are emitted at an angle of 180 degrees. These photons are then detected by the scanner and the location of the original decay event is tomographically reconstructed. SPECT uses a different class of radionuclides such as $^{99\text{m}}\text{Tc}$ which directly emit a single gamma ray when they decay.

Probes. Radionuclides decay at a steady rate which cannot be biochemically modulated; thus, all radionuclide probes are continually emitting and no activatable probes can be designed. Nonetheless, two principal classes of molecular reporters for PET and SPECT are in broad use: affinity probes, which enrich in regions where they can bind a molecular target; and labelled substrates, which enrich upon enzymatic conversion or targeted transport. One important difference between PET and SPECT with regards to probe design lies in the kind of isotope compatible with each modality: Common PET isotopes can be chemically substituted for the basic building blocks of biomolecules (^{11}C for carbon, ^{18}F bound to carbon), which enables PET labeling even of small molecules such as glucose or neurotransmitters. Typical radioisotopes for SPECT, on the other hand, require the attachment of large chelating moieties. This makes it hard to label small molecules without interfering with their biology, while it is generally unproblematic for labeling affinity reagents such as antibodies. Both small-molecule metabolites and affinity probes can be designed to target endogenous enzymes or epitopes, or can be targeted at reporter gene products.

Exemplary applications in the brain. As mature clinically validated modalities, PET and SPECT have been widely used in human patients for molecular medicine. Notable examples in neurology include PET ligands for beta-amyloid used for patient selection for clinical trials in Alzheimer's disease⁹ and metabolic brain imaging with [^{18}F]-fluorodeoxyglucose (FDG), which has since been superseded by functional MRI (see below). Another key application of neuroimaging with radioligands worth highlighting is the quantitative mapping of neurotransmitter binding with PET-labelled neurotransmitter analogues, including competition studies of spatiotemporal dynamics¹⁰.

Advantages and limitations. The chief advantages of PET and SPECT are their suitability for deep-tissue imaging with superb (sub-nanomolar) sensitivity, as well as their clinical maturity which facilitates human translation of new probes and techniques. Images can be obtained from intact specimen

or patients and the opacity of the skull does not interfere with signal transmission, which is of particular relevance for minimally invasive brain imaging. The most important limitations of radioisotopes for molecular imaging are the low spatial resolution on the order of 1 mm, the continually emitting (“always-on”) nature of radioisotopes which prevents the facile construction of dynamic probes for enzyme activities or ligand concentrations, and the need for a local source of isotopes (such as a cyclotron or reactor) due to their short half-lives.

Optical brain imaging

Few techniques have repeatedly revolutionized biology as much as optical imaging, from Leeuwenhoek’s microscope to organic dyes for histology to the multitude of applications of fluorescent proteins. It also a major modality for molecular imaging *in vivo*, especially in animals.

Principle. Several conceptually different techniques for brain imaging make use of visible light. Fluorescence imaging probes for a wide variety of analytes and applications have been developed and validated for microscopy, and have been translated *in vivo*¹¹. The development of two-photon microscopy especially has boosted the *in vivo* use of fluorescent probes. Its key advantages include a reduction in light absorption by using two photons of double wavelength, thus increasing penetration depth; and a limited excitation volume due to the characteristic shape of the point spread function, which reduces out-of-focus excitation and decreases heating of the tissue. A different broadly used class of optical imaging probes based on luciferases make use of bioluminescence, which offers lower background signal due to the lack of crosstalk from tissue autofluorescence and better penetration depth since light only has to travel out of the tissue unidirectionally. Finally, the last decade has seen tremendous progress in photoacoustic tomography, which records optical absorption events by measuring the ultrasound waves emanating from an irradiated tissue as a consequence of thermoelastic expansion upon absorption of light energy^{12,13}. Since

all optical imaging methods are limited by (a) depth of penetration even in soft tissue and (b) additionally by the opacity of the skull, their application for brain imaging *in vivo* often includes access to the tissue by thinning and polishing the skull, by installing a cranial window, or by intravital microscopy.

Probes. Many classes of probes are available for fluorescence imaging, from small-molecule dyes to fluorescent proteins to quantum dots, and each class has been adapted to report on a wide array of biochemical events from ligand binding to enzymatic conversion to translocation between biological compartments to genetic events at each level. Luciferase reporters are not as numerous but still well developed. Finally, virtually any molecule (including endogenous analytes and all existing fluorescent probes) can in principle be detected by photoacoustic imaging since all molecules absorb light at some wavelength, and the physiological concentration of the analyte of interest as well as crosstalk from other biomolecules impose the main practical limitations. A vast review literature exists for this field^{5,11}.

Exemplary applications in the brain. While the uses of optical imaging in basic neuroscience are too diverse and numerous to comprehensively review here, the following examples illustrate the flexibility and importance of this modality. Firstly, the development of widely used calcium indicators both based on small molecules (such as fura-2) and also based on genetically encodable proteins has been the basis for the direct realtime imaging of neuronal firing *in vivo* and, consequently, many important discoveries in perception and behavior¹⁴. Secondly, cell-based reporters have been created and engrafted in live animals which make it possible to detect a specific neurotransmitter via its endogenous cell surface receptor, triggering a calcium or cyclic AMP-mediated response inside the reporter cell, which in turn is measured via a genetically encoded fluorescent reporter¹⁵. Finally, photoacoustic imaging using hemoglobin as an endogenous absorptive analyte has been used to image hemodynamic responses following sensory stimulation in active brain regions of rats through an intact skull¹⁶. One intriguing feature of many optical imaging studies is the ease with which *in vivo* imaging can build on and be compared with data from *in vitro* measurements using the same probes.

Advantages and limitations. One of the most important advantages of optical imaging is its versatility, due to the broad range of optically active moieties, of specific probes that utilize them, and of the ease of iterative engineering as probes can be synthesized and evaluated with high throughput *in vitro*. Furthermore, optical imaging offers excellent spatiotemporal resolution and sensitivity *in vivo* ranging from nanomolar for fluorescence and photoacoustics to even better for bioluminescence. The most important limitation is the limited tissue penetrance of optical imaging. Imaging depth can generally be no greater than a few millimeters for fluorescence and luminescence, or a few centimeters for photoacoustics in soft tissue and much worse if the opaque skull is left intact. This is highly limiting in rodents and all but rules out translation to humans with their larger brains.

Magnetic resonance imaging

Magnetic resonance imaging (MRI) is a versatile and widely used imaging modality both in the clinic and in basic research. MRI combines many of the favorable properties of radioactive and optical imaging.

Principle. The MRI signal arises from the behavior of the magnetic moments of nuclear spins of suitable atoms in the sample, most commonly ^1H which is abundant in tissues. Importantly, the chemical environment of these atoms modulates their magnetic behavior, giving rise to contrast. While a complete theoretical account of MRI principles requires a quantum mechanical treatment, a simplified description can be given as follows. In a typical MRI experiment, a strong magnetic field B_0 is applied to the specimen which aligns nuclear spins in the sample longitudinally in the field. Then, a brief radiofrequency (RF) pulse is applied at an appropriate resonant frequency (the Larmor frequency), causing the alignment of nuclear spins to flip 90 degrees into a transverse plane relative to B_0 upon absorption of

the provided RF energy. After the RF pulse ends, the nuclear spins can relax to lower-energy states in two ways: the excited spins can lose their transverse alignment with each other, causing net transverse magnetization to relax to zero with a characteristic time constant T_2 ; and they return to their longitudinally aligned equilibrium state under B_0 with relaxation time T_1 . Both types of relaxation occur simultaneously, although T_1 relaxation is usually faster. Pure T_2 relaxation results from spin-spin interactions among excited protons, while T_2^* relaxation arises from the convolution of T_2 relaxation and the effect of local inhomogeneities in the magnetic field, giving rise to faster loss of phase coherence in the transverse plane.

As protons return to their equilibrium alignment with B_0 , they engage in a rotating motion (precession) which induces a current in the coils of the MRI apparatus. This current is the recorded signal, and it is computationally processed to reconstruct an image. Spatial differences in this signal, and hence image contrast, can result from local differences in proton density; from tissue-specific differences in relaxation times; and from differences in water mobility. Since tissues vary in chemical composition and water diffusivity, MRI without extrinsic probes can be used to obtain structural anatomical images.

Probes. MRI contrast agents can be used to enhance the contrast between tissue components of interest, to visualize functional features of tissue such as metabolite accumulation or transport phenomena, or to act as specific probes for molecular imaging. MRI contrast agents can be classified into different categories based on the mechanism through which they modulate the MRI signal¹⁷: (1) T_1 agents which chiefly affect T_1 , (2) T_2 agents which chiefly affect T_2 , (3) chemical exchange saturation transfer (CEST) agents which exchange protons with the solvent¹⁸, and (4) heteronuclear agents requiring MRI at substantially different Larmor frequencies, including compounds based on ^{19}F and hyperpolarized ^{13}C or ^{129}Xe . Since MRI contrast can be modulated in a variety of ways, including changes in the electrochemical environment of atomic nuclei and (for proton MRI) changes in solvent access to a contrast agent moiety, MRI contrast can be modulated by a wide variety of molecular strategies, enabling flexibility and ingenuity in the design of molecular imaging probes. Different classes of molecular MRI probes will be discussed more comprehensively in subsequent sections.

Exemplary applications in the brain. The most prominent application of MRI in neuroscience is blood-oxygenation level dependent (BOLD) functional MRI (fMRI)¹⁹. Hemoglobin is abundant in blood, and when deoxygenated, its iron center is in a paramagnetic state and acts as an MRI contrast agent. Since neuronal activity exacts a high metabolic cost and oxygen consumption, neuronal firing causes the dilation of the local microvasculature and an increase in local bloodflow, a phenomenon known as neurovascular coupling. This has been exploited to infer brain activity patterns from BOLD MRI tomographs and applied to the mapping of brain regions for sensory perception, aversion and reward, and somewhat more speculative ascriptions of higher cognitive functions to specific brain regions in animals and humans. Manganese (Mn^{2+}) has been used as an MRI contrast agent due to its tendency to accumulate in active neurons²⁰. More recently, molecular MRI contrast agents based on engineered metalloproteins have been used in the brains of live animals to visualize neurotransmitter dynamics during stimulation²¹.

Advantages and limitations. MRI combines several attributes which render it an excellent candidate for molecular brain imaging: It offers (1) the versatility of optical probes because a wide range of biochemical mechanisms such as binding, conformational changes, and catalytic conversion can be linked to a modulation of MRI contrast by a contrast agent, unlike the continual signaling of radioprobes; (2) limitless depth of penetration just like radionuclide probes and unlike optical probes, because biological tissues are permeable to radio waves; (3) excellent resolution on the order of 10-100 micron spatially and seconds temporally, comparable to optical probes and 1-2 orders of magnitude better than PET probes; (4) a general lack of toxicity enabling human longitudinal studies, unlike radiotracers; and (5) mature and widely available scanner technology and algorithms for image reconstruction and annotation. The single most critical drawback of MRI as a modality which has so far restricted its broad use for molecular brain imaging (despite a proliferation of probe designs) is the low sensitivity of the method to molecular probes, requiring a concentration on the order of 10-100 μM of a contrast agent.

Imaging probes for molecular MRI and the challenge of sensitivity

Imaging probes for molecular MRI are contrast agents which modulate the MRI signal strength in response to specific molecular and cellular events, such as ligand binding, enzymatic conversion, transport between physiological compartments, or gene expression.

Criteria for an ideal molecular MRI probe

A probe for molecular MRI should be designed so as to harness the advantages of the modality, including whole-organ coverage, unlimited penetration depth, high spatial resolution on the sub-mm scale, high temporal resolution on the scale of seconds, and lack of toxicity; and specifically recognize a molecular or cellular event of biological or medical interest to trigger a change in MRI contrast. In addition, an ideal probe design should allow for robust and minimally invasive delivery to the site of interest, allow application both in basic research in animals and for human clinical translation, and enable unambiguous and quantitative interpretation of the resulting data. Finally, an ideal probe design is versatile so that many different biomolecular events can in principle be detected, modular so that probe variants for different analytes of interest can be created easily without lengthy ad-hoc re-engineering, and allows for simple, robust, and inexpensive production of the probe.

Existing molecular MRI probes and the challenge of sensitivity

The development of molecular imaging probes for MRI is an active field and progress in it has been extensively reviewed^{5,17,22,23}.

Single-metal probes. Molecular probes in which a ligand-binding moiety modulates MRI contrast from a gadolinium chelate (for example, in a small molecular calcium sensor^{24,25}) or from a metalloprotein (for example, in neurotransmitter sensors based on bacterial cytochromes²¹) contain a single metal ion that modulates the MRI contrast of solvent protons and therefore require concentrations on the order of 100 μM *in vivo* for appreciable contrast changes. While it is a highly significant development that these probes have been used for the realtime recording of chemical signaling in the brain noninvasively and with good spatial resolution using MRI, the high concentration requirement necessitated delivery by intracranial injection, a highly invasive process. Further problems associated with this high concentration requirement include sequestration of the analyte and hence interference with the biomolecular process under study; exacerbated toxicity, for example due to leaching of gadolinium²⁶; and consequently, no possibility of clinical translation. Several approaches have been developed to address the challenge of sensitivity in molecular MRI, but none of them are fully satisfactory.

Mineralized nanoparticles. In one class of approaches, probes are used with many MRI-active atoms per probe molecule. For example, superparamagnetic iron oxide (SPIO) nanoparticles²⁷ typically contain thousands of iron atoms and can be detected at concentrations in the low μM range for iron and hence a low nM range for the nanoparticles. SPIO nanoparticles have been used as labels for cell tracking²⁸ and for affinity labeling of vascular targets, and have been developed into aggregation-based molecular sensors for calcium²⁹. However, the large size of SPIO nanoparticles of typically 30-100 nm impedes delivery to non-exposed target sites. Furthermore, the mechanism of aggregation-based sensors is concentration-dependent and may require delivery of relatively large amounts. The delivery problem of SPIO-based sensors can be partially addressed with a protein-based, genetically encodable variant in the form of ferritin, an iron-storage protein on the basis of which molecular MRI sensors have been developed³⁰. However, this approach only circumvents the delivery problem when used in genetically modified animals

and does not generalize to clinical applications nor to the detection of extracellular analytes, and its robustness in mammalian cells has yet to be demonstrated.

CEST probes. CEST MRI agents are analogous to mineralized iron particles in that they utilize many MRI-active atoms per molecule of probe. CEST agents based on proteins can have thousands of protons available for exchange³¹. However, the versatility of CEST-based agents for a wide range of neurobiological analytes of interest has yet to be shown and high expression levels are still required, since sensitivity is inherently lower than for relaxation agents.

Hyperpolarized heteronuclei. Finally, hyperpolarized nuclei such as ¹²⁹Xe have been incorporated into molecular MRI probes³², but their short half-lives mean that complex strategies are required for delivery, ruling out multiple observations over time, and limiting the versatility of such probes.

Conclusion. Despite the great effort and creativity expended to establish the imaging tools above, it bears repeating that there are no molecular MRI probes in widespread use today which function at nanomolar concentrations, can be delivered noninvasively, and can be readily engineered to detect a variety of neurobiologically or clinically important molecular events¹⁷. The invention of molecular MRI techniques which remove or circumvent the sensitivity limit of existing agents while also fulfilling the other criteria of good probes (including versatility and ease of engineering and usage) therefore remains an important and unsolved problem.

Molecular imaging with engineered hemodynamic responses

Instead of trying to synthesize exogenous MRI contrast agents with improved sensitivity, we sought to altogether decouple the high concentration requirement for MRI detection from the

concentration requirement for the molecular probe, by perturbing an abundant biological source of endogenous multimodal contrast.

Blood as a contrast agent for MRI

Deoxyhemoglobin, but not oxyhemoglobin, is paramagnetic and causes a darkening of the T_2^* -weighted proton MRI signal, which can be exploited for blood oxygenation level-dependent (BOLD) functional MRI¹⁹. Neuronal signaling activity leads to a large acute demand for metabolic energy, causing (1) oxygen consumption and (2) local vasodilation and increased bloodflow, which overcompensates for the increase in oxygen demand. Consequently, neuronal activity in a certain brain region both increases the local blood volume and thus the concentration of total hemoglobin, and increases oxygenation. These changes in the concentration of deoxyhemoglobin are reflected in changes of the BOLD MRI signal, which has been widely exploited in neuroscience for functional imaging of brain activity³³.

Characteristics of the BOLD response

Despite this complex relationship, a net effect can typically be observed in MRI wherein the T_2^* -weighted signal dips briefly following neuronal activation (indicating an increased contribution from deoxyhemoglobin) followed by a rise in the signal which lasts several seconds³⁴. The typical magnitude of the BOLD MRI signal change is several percent, or an order of magnitude greater than typical noise fluctuations. This is enabled by the high concentration of hemoglobin of around 10 mM in blood and 100-300 μ M in total brain tissue (assuming 1-3% cerebral blood volume³⁵), making it an abundant endogenous contrast source. The spatial resolution is potentially constrained by three factors: imaging resolution, spatial extent of neuronal activity (i.e. what is the smallest spatial unit of brain tissue which is activated at a given time), and the spatial scale of cerebral vascularization. Cerebral vascularization is fine-

grained with roughly one microvessel per each individual neuron and a mean distance from the nearest bloodvessel of 15 μm at any point in the murine cortex³⁶. While changes in bloodflow are not independent among connected vessels, leading to a practical limit on spatial resolution worse than the average distance between capillaries, these length scales are nonetheless much below the typical imaging resolution of hundreds of micrometers.

A concept for linking vasodilation to specific molecular events

The main drawback of BOLD fMRI for neuroscientific investigation and medical use is its lack of specificity and the consequent difficulty in interpreting the observed signal changes. For basic neuroscience, for example, it would typically be desirable to know what subpopulations of neurons are active in a given situation and through which neurotransmitter pathways they communicate. Such molecular-level information cannot be obtained with BOLD fMRI currently.

We envisioned a novel concept for molecular imaging which takes advantage of the favorable spatial resolution, temporal resolution, signal-to-noise ratio, and the endogenous nature of the contrast agent characteristic of BOLD MRI, but which links the signal change to a specific molecular event of interest. In this concept, the neurovascular coupling underlying the endogenous BOLD MRI effect would be pharmacologically inhibited; a molecular sensor would be introduced which has been engineered to detect the molecular event of interest and in response, to cause dilation of the local microvasculature and a consequent change in bloodflow; and the resulting MRI signal changes would be recorded as a measure of the molecular event of interest. One potential platform for engineering such vasoactive imaging agents could be to start with vasodilatory peptides which act with low nanomolar potency (see next section) and to bring the toolbox of protein engineering to bear on them in order to create a wide variety of molecular sensors.

Molecular imaging with engineered bloodflow according to this concept would have several important advantages over existing molecular imaging techniques:

1. ***Versatility*** and ease of engineering of sensors for a wide range of neurobiologically and medically interesting analytes, due to the ability to use protein engineering approaches;
2. ***Unlimited depth of penetration*** and whole-brain coverage through the optically opaque skull;
3. ***Molecular specificity*** for an event or analyte of interest unattainable by current fMRI;
4. ***Sensitivity*** in the low nanomolar range, due to (a) decoupling of the concentration requirement for the probe from the concentration requirement for MRI detection, (b) the use of blood hemoglobin as an abundant endogenous source of imaging contrast, and (c) the use of highly potent vasoactive species as probes;
5. ***No need for invasive delivery*** as high sensitivity could enable in situ expression of such peptide-based probes in genetically engineered animals or delivery of peripherally injected probes across the blood-brain barrier (BBB).

Strategy for implementation using vasoactive neuropeptides

Neuropeptide signaling is ubiquitous in the brain and the periphery, occurs on timescales of seconds to minutes and on length scales from vesicular release to receptor binding of micrometers, acts through G protein-coupled receptors (GPCRs) of Class B, and can occur among neurons or other cell types, including vascular endothelial cells (VECs) and vascular smooth muscle cells (VSMCs)³⁷.

The calcitonin-gene related peptide (CGRP) is the most potent known human vasodilatory neuropeptide^{38,39}. Endogenous CGRP occurs as two closely-related 37 residue isoforms that act on widely expressed RAMP1/CLR receptor heterodimers to induce dilation of intracerebral arterioles with a half-effective concentration (EC₅₀) below 10 nM⁴⁰. The vasodilatory activity of CGRP results from its action on receptors expressed on the surface of VSMCs. Upon binding of CGRP, these receptors activate adenylate cyclase, leading to an increase in cyclic AMP (cAMP) and a decrease in cytosolic calcium in the smooth muscle cells, which in turn lead these cells to relax and allow the microvasculature to dilate.

CGRP is an attractive platform for implementing vasoactive molecular imaging agents. The potency of CGRP suggests that the vascular action of nanomolar concentrations should be detectable using well-established MRI protocols and pulse sequences used for BOLD fMRI, and that CGRP can therefore act as an MRI imaging agent with 3 to 4 orders of magnitude better sensitivity than conventional MRI contrast agents. Since CGRP is a peptide and exerts its action through a known cell surface receptor, variants of CGRP can be engineered using the toolkit of protein engineering, manufactured recombinantly or using solid-state peptide synthesis, and evaluated using a range of common cell-based activity assays *in vitro*. Furthermore, the large body of biomolecular engineering work implementing modulation of ligand-receptor interactions by small molecules, by protein ligands, by enzymes, or by cell-level molecular phenomena suggests that it should be possible to link modulation of the activity of vasoactive peptides to a wide range of neurobiologically and clinically relevant molecular phenomena, ensuring the versatile potential of the method. Finally, since CGRP effects vasodilation through a pathway independent of the major signaling pathways which underlie neurovascular coupling in BOLD fMRI⁴¹, it might be possible to modulate them independently to achieve deconvolution.

Objective and organization of this document

The objective of this dissertation is thus to establish highly sensitive molecular imaging with engineered physiological responses such as vasodilation as a conceptually unprecedented technique for specific biomolecular and cellular measurement in intact organisms.

The experimental strategy chosen to achieve the above objective is to engineer variants of vasoactive neuropeptides which can locally modulate cerebral bloodflow by acting on VSMCs in a manner that is responsive to, and thus reports, biomolecular events of interest.

To that end, experimental evidence is presented in the next several chapters for the following specific claims:

1. That the fundamental concept of molecular imaging with vasoactive probes is feasible; that molecular sensors for specific biomolecular analytes of interest, such as proteases, can be engineered on the basis of vasoactive peptides; and that their action can be imaged by MRI;
2. That the nanomolar sensitivity of vasoactive probes enables their functional expression *in situ*, for example as genetic reporters for cell tracking;
3. That vasoactive probes can be engineered which retain their nanomolar potency and engineerability when fused to well-characterized antibodies which act as molecular shuttles for delivery across the blood-brain barrier, making such probes potentially compatible with molecular imaging after minimally invasive delivery.

In a final chapter, a discussion is offered of the experimental achievements, the limitations, and future work to be done in establishing this imaging method and its applications in neuroscience and in biomedicine.

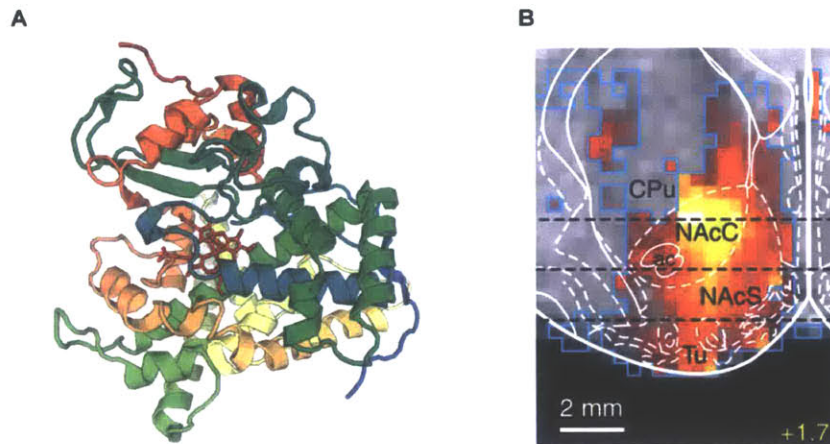


Fig. 1-1: Example of a bioengineered protein-based molecular MRI probe used to record neurotransmitter release dynamics in rat brains *in vivo*.

- (A) The probe (PDB 4DUF). The heme domain of the bacterial cytochrome P450-BM3 contains heme as a prosthetic group (shown in red in the center of the structure). A pocket in the immediate vicinity of the heme group has been engineered by directed evolution to reversibly bind a variety of ligands, including the neurotransmitters dopamine and serotonin. The specificity and affinity of these binding interactions have been tuned. Ligand binding modulates the T_1 MRI contrast due to the iron center in the heme, rendering this protein a molecular probe for MRI.
- (B) Imaging neurotransmitter release *in vivo*. This is an exemplary *in vivo* application of BM3h-9D7, a dopamine sensor based on the heme domain of P450-BM3. The probe was intracranially injected at a concentration of 500 μ M and used to record second-scale dynamics of dopamine release in a distal brain region upon electrical stimulation of the medial forebrain bundle. Reproduced with permission from Lee et al. 2014²¹.

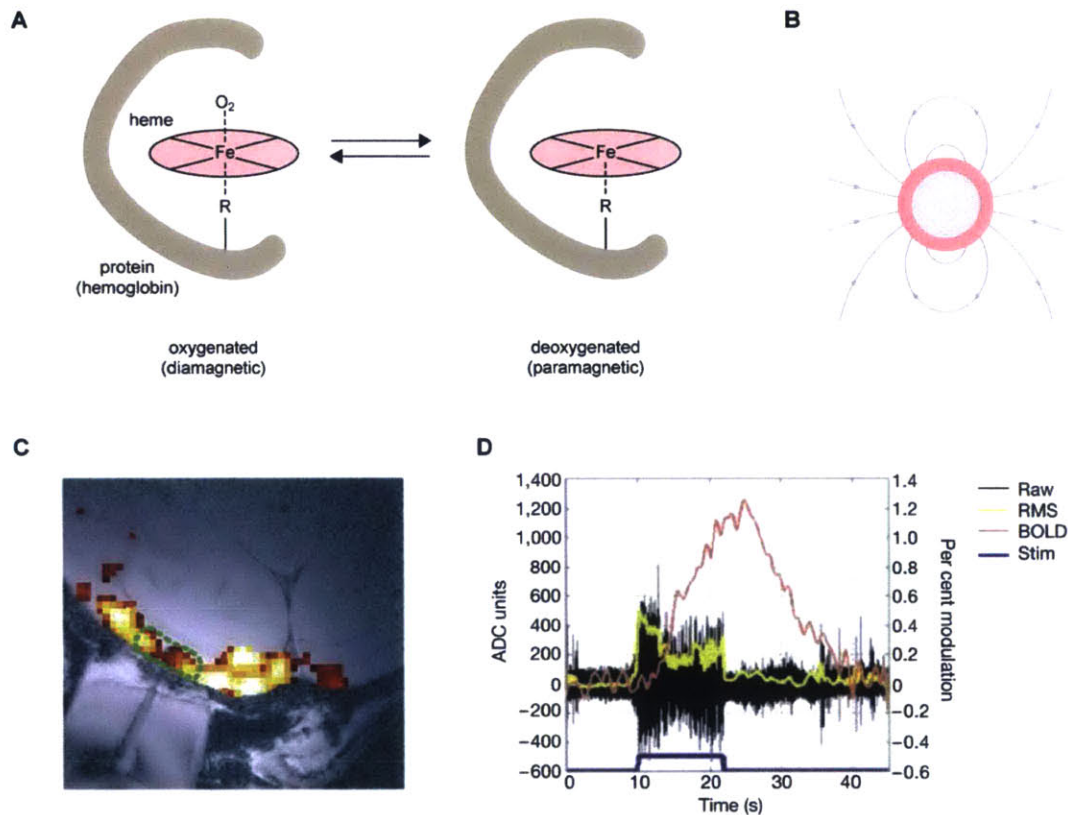


Fig. 1-2: Blood oxygenation level-dependent functional MRI.

- (A) Hemoglobin acts as an MRI contrast agent. Oxygenated hemoglobin, with molecular oxygen bound at the iron inside its heme group, is diamagnetic while deoxygenated hemoglobin is paramagnetic.
- (B) The paramagnetic iron in deoxyhemoglobin creates local distortions in the applied magnetic field around a blood vessel (shown in cross-section) which affects the relaxation of nearby water protons and can be visualized using T_2^* -weighted MRI.
- (C) BOLD MRI map in the visual cortex of monkeys during visual stimulation, overlaid on an anatomical image. In the anatomical image, the presence of a recording electrode can also be seen in the lower left corner.
- (D) Correlation between electrical neural activity and BOLD MRI signal changes during stimulation in the setup seen in (B). Electrical spiking activity (raw data in black, root mean square of 250 ms windows in yellow) can be seen commencing immediately upon stimulation and ending when the stimulation ends, and BOLD MRI signal changes beginning 2-3 seconds after the start of stimulation and peaking 10-20 seconds after the onset of stimulation. This illustrates the utility of BOLD MRI for functional neuroimaging, although molecular specificity is lacking.

(B) and (C) reproduced with permission from Logothetis et al. 2001⁴².

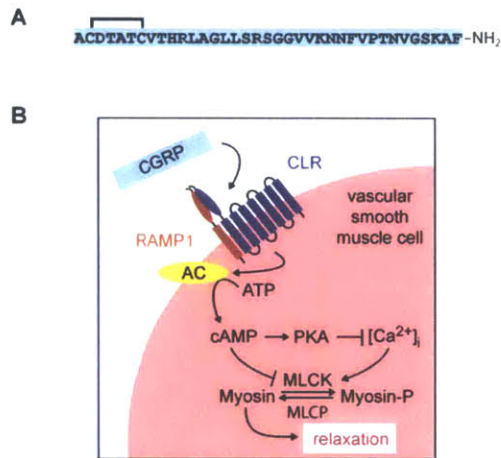


Fig. 1-3: CGRP is a potent vasoactive neuropeptide.

- (A) The primary sequence of the alpha isoform of human CGRP. Key features include the disulfide ring near the N-terminus, a region that is essential for receptor activation, and the C-terminal amide which is involved in making contact to the receptor.
- (B) The mechanism of CGRP-mediated vasodilation. CGRP activates its heterodimeric receptor, a Class B GPCR, on the surface of vascular smooth muscle cells. This activates adenylate cyclase to produce cAMP, and elevated cAMP levels cause dephosphorylation of myosin and relax the vascular muscle, allowing dilation of the blood vessel and an increase in bloodflow. This mechanism could be hijacked to engineer changes in bloodflow.

Caged neuropeptides as vasoactive molecular imaging probes for protease activity

Abstract

In vivo imaging techniques are powerful tools for evaluating brain biology. Relating image signals to precise molecular phenomena can be challenging, however, due to limitations of existing optical, magnetic, and radioactive imaging probes. We demonstrate a concept for molecular-level neuroimaging which bypasses the need for conventional imaging agents by selectively manipulating potent endogenous contrast afforded by the cerebral vasculature. Variants of the calcitonin gene-related peptide (CGRP)³⁸ artificially actuate vasodilation pathways and induce contrast changes that are readily measured by optical and magnetic resonance imaging. CGRP-based agents induce effects at nanomolar concentrations in deep tissue and can be engineered into switchable analyte-dependent forms suitable for molecular imaging. Such artificial physiological interventions therefore provide a versatile means for high sensitivity analysis of molecular events in living organisms.

Introduction

The combination of chemical probes with noninvasive imaging-based detection uniquely enables molecular and cellular phenomena to be mapped across large regions of the living brain. Molecular neuroimaging applications range from basic neurobiological investigations to clinical evaluation of neurological diseases, inflammation, and cancer. Current molecular imaging approaches are limited by the available forms of imaging probes, however. Radioactive probes are detected with subnanomolar sensitivity but generally poor spatial resolution by positron emission tomography (PET) and single photon computed tomography (SPECT). Radiotracers cannot be switched on and off, which increases their toxicity, rules out biosensing approaches, and limits most dynamic measurements to pharmacokinetic time scales on the order

of minutes. Existing probes for dynamic molecular magnetic resonance imaging (MRI) can be imaged in animal brains at submillimeter resolution²¹, but are difficult to detect with sensitivity appropriate for most biological targets of interest, in the nanomolar range¹⁷. Although techniques such as nuclear hyperpolarization³² have been proposed to boost the sensitivity of MRI probe detection, these approaches are complex and have so far proved limited for neuroimaging applications. Ultrasound and diffuse optical molecular neuroimaging techniques are in earlier stages of development, and also require effective probes for applications in brain tissue^{43,44}.

We sought to establish a molecular neuroimaging paradigm that bypasses limitations of existing imaging agents by manipulating a strong endogenous biological contrast source rather than employing exogenous agents that are themselves directly measured. The cerebral vasculature is one of the most potent endogenous contrast sources available to neuroimaging modalities. Changes in cerebral blood volume, flow, or oxygenation are robustly detectable by MRI, optical, and ultrasound-based noninvasive imaging, as well as by PET, SPECT, and X-ray imaging performed in conjunction with intravascular tracers. The vasculature permeates the entire brain, such that the mean distance from any point to a blood vessel in murine cortex is about 13 μm ³⁶. Vascular hemodynamic changes can be evoked by a variety of chemical species, many of which act at nanomolar concentrations. We therefore reasoned that a strategy for “hijacking” vascular physiology to report on specific molecular events of interest by means of engineered chemical messengers could provide a sensitive and minimally disruptive new platform for molecular neuroimaging.

To demonstrate this approach, we chose to engineer calcitonin gene-related peptide (CGRP), the most potent known human vasodilatory peptide³⁸. Endogenous CGRP occurs as two closely-related 37 residue isoforms that act on widely expressed RAMP1/CLR receptor hetero-dimers to induce dilation of intracerebral arterioles with a half-effective concentration (EC_{50}) below 10 nM^{38,40}. This suggests that CGRP variants should be capable of artificially inducing equivalents to the well-known blood oxygen level dependent (BOLD) MRI response¹⁹ that constitutes the basis of most functional brain imaging

experiments (Fig. 1A). Molecular imaging of arbitrary analytes could be possible if activation of an initially blocked or caged CGRP analog could be coupled to presence of the analyte (Fig. 1B).

Results

To determine the feasibility of imaging the action of CGRP, we first characterized *in vivo* vasodilation effects of wild-type human alpha-isoform CGRP (wtCGRP) in the rat brain using optical imaging and MRI. Optical imaging via a cranial window (Fig. 2A) permitted direct visualization of the dilation of rat cortical surface blood vessels upon topical infusion of wtCGRP (0.3 mL, 50 nM). Dilation of macroscopic vessels was quantified as percent change in vascular diameter (Fig. 2B red bar and Fig. 2C top panel), and apparent parenchymal microcapillary blood volume changes were tracked by optical signal intensity change in a region of interest (Fig. 2B black box and Fig. 2C bottom). Significant changes in macroscopic vessel diameter ($9.5 \pm 2.4\%$ dilation, *t*-test $p < 10^{-9}$, $n = 5$) and microcapillary bed reflectance ($8.0 \pm 2.8\%$ intensity change, $p < 10^{-11}$, $n = 5$) were observed (Fig. 2C), thus demonstrating that CGRP-induced responses are amenable to *in vivo* optical imaging.

We investigated the ability of wtCGRP to induce contrast detectable by noninvasive imaging in deep brain regions by acquiring MRI scans during intracranial infusion of 100 nM wtCGRP in artificial cerebrospinal fluid (aCSF). Injections of wtCGRP or vehicle control at 0.1 μ L/min were performed through cannulae bilaterally implanted in arbitrarily selected thalamic regions of live rat brains, and MRI data were acquired using weighting parameters suitable for detecting BOLD contrast (Fig. 2D). Voxels clustered around the sites of wtCGRP injection showed substantial signal changes that were significantly correlated with a 10 minute infusion epoch (corrected $p < 0.05$), whereas no voxels near control injection sites showed significant correlation. Data from six animals revealed mean peak MRI signal changes of $5.3 \pm 0.9\%$ during wtCGRP injection, compared with changes of $1.2 \pm 0.1\%$ during injection of aCSF alone; the difference between wtCGRP and vehicle was highly significant ($p = 0.001$). Time courses of mean MRI

signal changes observed during infusion were consistent with the optical imaging data and indicated that wtCGRP is not rapidly removed or degraded in brain tissue (Fig. S1A). Hemodynamic contrast provided sufficient resolution to monitor convective spread of the imaging agent from the site of infusion (Fig. S1B). To dissociate wtCGRP-induced image contrast from hemodynamic effects evoked via pathways associated with neural activity, we performed wtCGRP infusion in the presence or absence of neuronal nitric oxide synthase (nNOS) inhibition, which has previously been shown to reduce neural stimulation-evoked BOLD signals by over 60%⁴⁵. MRI response profiles and amplitudes (Fig. 2E) evoked by wtCGRP, before and after an intravenous injection of the nNOS inhibitor *N*-Nitro-*L*-Arginine Methyl Ester (L-NAME; 50 mg/kg)⁴⁶ were statistically indistinguishable ($p > 0.05$). These results demonstrate that wtCGRP can be used to engineer substantial and specific image contrast changes in deep brain, at concentrations about 1,000-fold lower than those at which conventional MRI contrast agents produce equivalent effects¹⁷.

To perform molecular imaging of biochemical targets using CGRP-mediated contrast, we developed an analyte-dependent uncaging scheme as shown in Fig. 1B. We focused on detection of proteases, which are important as drug targets, diagnostic biomarkers, and bases for biotechnological applications such as cell signaling and prodrug activation^{47,48}. Since proteases are subject to extensive posttranslational regulation, it is often important to measure their activity rather than their abundance⁴⁹, thus necessitating enzymatically-sensitive probes per se. To rapidly evaluate candidate CGRP-based protease activity sensors, we developed an in vitro bioassay for CGRP receptor activation in cultured cells (Fig. S2). Cells used for the bioassay were engineered to co-express the RAMP1/CLR complex in conjunction with a bioluminescent reporter sensitive to RAMP1/CLR-mediated cyclic adenosine monophosphate (cAMP) production, such that effective receptor activation leads to luminescence signals readily detected in a microtiter plate reader. Measurements using this system indicated an EC_{50} for receptor activation by wtCGRP of 48 pM [95% confidence interval (CI) 37-63 pM], which was 2.5- to 14-fold impaired by N-terminal extensions of one to three residues (Fig. S3). C-terminal extension of wtCGRP by addition of a glycine residue in contrast resulted in a much higher EC_{50} of 2.5 nM (CI 2.1-3.1 nM), and substitution of the C-terminal amide of wtCGRP by a carboxylate reduced potency of the peptide by a factor

of ~250. These findings are consistent with earlier studies of terminal modifications of CGRP⁵⁰. The relatively modest effects of N-terminal modifications to wtCGRP suggested that protease sensors might best be formed by fusing blocking domains via protease cleavage sites to the N-terminus of CGRP, so that cleavage products could recover vasodilation activity close to the wild type variant.

Guided by these findings, we designed candidate vasoactive sensors for a number of proteases relevant to biotechnology (Fig. 3A). Targets included fibroblast activation protein (FAP), a cell surface-bound collagenase and cancer biomarker⁵¹ which removes the dipeptide AP from the N-terminus of polypeptides; TEV protease and enterokinase (EK), both well-studied endopeptidases that are absent in the central nervous system and could therefore be used as bio-orthogonal markers for transgenesis or cell tracking^{52,53}; and caspase-3 (CASP3), another endopeptidase and cytosolic apoptosis actuator that can be released following apoptosis and secondary necrosis⁵⁴ and serve as a prognostic indicator during cancer treatments^{55,56}. FAP and CASP3 have been targeted by previous optical⁵⁷⁻⁵⁹ or MRI^{60,61} probes, but improvements in sensitivity for deep tis-sue detection would be valuable. CGRP constructs targeted toward these proteases and incorporating AP repeats, green fluorescent protein (GFP), or biotin as blocking domains were produced in *E. coli* or by solid phase peptide synthesis.

We used our in vitro bioassay to identify protease sensor candidates which displayed minimal activity prior to cleavage and high potency after enzyme treatment. We found that uncleaved recombinant sensors of the format GFP-(cleavable linker)-CGRP-G were completely inactive as CGRP receptor agonists even at concentrations of 10 μ M (Fig. 3B and Fig. S4). After 2 h incubation with their cognate proteases (TEV, EK, or CASP3), the constructs were largely cleaved and elicited bioluminescence in RAMP1/CLR reporter cells with apparent EC₅₀ values from ~0.4-1.0 μ M. Amidated synthetic CGRP-based substrates for FAP and CASP3 regained much higher levels of potency following cleavage, with EC₅₀ values for FAP of 16 pM (CI 13-20 pM) and for CASP3 of 42 pM (CI 38-46 pM). These constructs were less effectively inactivated by blocking domains prior to cleavage however, with EC₅₀ values of 114 pM (CI 112-116 pM) and 5.7 nM (CI 5.2-6.4 nM) for FAP and CASP3, respectively. Effective conditions for protease sensing by each of the CGRP constructs could be identified based on the shift in EC₅₀ values

measured in the bioassay upon cleavage, indicating that each of the candidates could potentially function as a molecular imaging probe for protease activity in vivo. Because the optimum protease sensitivity and post-cleavage potency was displayed by the biotin-(CASP3 site)-CGRP construct, this variant was selected for further studies in animals.

To demonstrate hemodynamic imaging-based detection of CASP3 probe activation, we again used the intracranial injection procedure of Fig. 2C. CASP3 sensor aliquots (100 nM) were injected at 0.1 $\mu\text{L}/\text{min}$ for 10 minutes in the presence or absence of CASP3 enzyme (2.3 $\text{ng}/\mu\text{L}$) in paired injections into rat thalamus. MRI scans acquired with BOLD contrast weighting revealed clusters of voxels for which significant correlation between the injected sensor and the image signal (corrected $p < 0.05$) was observed in the presence but not the absence of the co-injected protease. The mean MRI peak signal change observed during sensor/CASP3 coinjection was $7.0 \pm 0.9\%$, whereas the peak signal change observed in the absence of CASP3 was only $1.6 \pm 0.5\%$; this difference was highly significant, with t -test $p = 0.02$. These results demonstrate that CGRP-based molecular sensors can elicit analyte-dependent engineered hemodynamic contrast changes detectable by noninvasive imaging in deep brain regions. The volumes over which probe-dependent responses were observed, as well as experience with conventional MRI contrast agent injections²¹, suggest that CGRP variants were diluted approximately tenfold from 100 nM levels in the infusion cannulae to effective concentrations near 10 nM in the brain parenchyma. The magnitude of observed MRI changes elicited by these probe levels suggests that substantially lower CGRP concentrations would also be detectable in the brain.

Discussion

Our data show that engineered hemodynamic signals provide a sensitive, analyte-responsive alternative to established molecular imaging approaches. By manipulating an endogenous physiological property, this strategy avoids the need for directly detected imaging agents. Required concentrations of vasoactive molecules approach the low tracer doses used in nuclear imaging techniques

like fluorodeoxyglucose PET ⁶², and unlike radiotracers, CGRP derivatives are activatable by molecular targets, intrinsically less hazardous, detectable at higher spatiotemporal resolution, and compatible with multiple imaging modalities. The minimal amounts of CGRP-related species required for engineered hemodynamic imaging are likely to be conducive to noninvasive brain delivery strategies ⁶³, as well as to endogenous expression in genetically modified cells or organisms. A possible drawback of CGRP-based probes involves the action of CGRP in migraine ³⁹, but migraine-related effects seem to require interaction with the trigeminal nerve specifically ⁶⁴, and are unlikely to be exhibited by targeted probes prior to unblocking by analytes.

Engineered hemodynamic responses suitable for neuroimaging applications could also be elicited by alternatives to CGRP, such as molecular interventions in nitric oxide, cyclooxygenase, and norepinephrine-mediated vasodilation and vasoconstriction pathways. More broadly, the idea of engineering artificial physiological effects to report on latent molecular-level phenomena could generalize beyond the brain to many tissues and organs, as well as to biological variables in addition to control of blood flow, such as endothermia, secretion, or autonomic responses. Molecular imaging with engineered physiology therefore represents a versatile paradigm for biological experimentation and diagnostic medicine, as well as a basis for extension of synthetic biology concepts to organismic scale.

Materials and Methods

Animal procedures. All animal procedures were conducted in accordance with National Institutes of Health guidelines and with the approval of the MIT Committee on Animal Care.

Optical imaging of exposed cortex. Optical imaging experiments were performed using Sprague-Dawley rats (300–400 g; Charles River, Wilmington, MA). To probe the impact of wild-type α -isoform calcitonin gene related peptide (wtCGRP) on vascular diameter and parenchymal blood volume in vivo, we measured the effects of topical application to the primary somatosensory cortex (SI) of

rats. Animals ($n = 5$) were initially anesthetized with isoflurane (3% in 50:50 air:O₂ mixture for induction; 1% for maintenance). Breathing rate and end-tidal expired isoflurane (V9004 Capnograph Series, Surgivet, Waukesha, WI) were continuously monitored during the imaging experiment. The animals were positioned on the surgical stereotax and the isoflurane anesthesia was maintained at 1% during imaging. During the surgical and imaging procedures, animals were maintained at approximately 37 °C core temperature using a heating blanket.

The preparation for optical imaging is diagrammed in Fig. 2A. A craniotomy (diameter of ~5 mm in rats) and durotomy were performed over primary somatosensory cortex (SI) of each animal, and the cortex was protected with Kwik-Cast silicone elastomer sealant (WPI, Sarasota, FL). An imaging chamber was then attached with dental cement and the elastomer was removed. The imaging chamber was custom made using a 1 cm diameter plastic ring (McMaster-Carr, Elmhurst, IL) with a base cut to match the skull topography over each rat's SI region. To facilitate wtCGRP perfusion at a constant rate, holes for fluid inlet, outlet, and pressure regulation were drilled in the wall of this chamber, through which blunted 18-gauge stainless steel needles were attached and sealed using superglue. The pressure in the imaging chamber was regulated by a small vertical tube whose height could be adjusted. Inflow and outflow were controlled using two separate syringe pumps (Harvard Apparatus, Holliston, MA) that were operated at the same rate (1.8 mL/hr). The volume of the imaging chamber was approximately 0.3 mL, and this chamber was filled with artificial cerebral spinal fluid (aCSF; Harvard Apparatus, Holliston, MA) and sealed with a cover glass.

A charge-coupled device camera (Prosilica GC, Allied Vision, Newburyport, MA) attached to a dissection microscope (Stemi SV11 M2 Bio, Carl Zeiss AG, Oberkochen, Germany) was used to image the cortical surface at a frame rate of approximately 4 Hz. Illumination was regulated using a xenon arc lamp. A green band-pass filter (550 +/- 25 nm) was used to provide optimal vascular contrast. A 50 nM wtCGRP (human α -CGRP, Sigma-Aldrich, St. Louis, MO) solution was prepared in ACSF for each imaging experiment. To establish imaging baselines, aCSF alone was continuously infused (1.8 mL/hr) through the inlet port for 5 minutes prior to wtCGRP infusion; images were acquired continuously

throughout. Fluid was extracted from the imaging chamber through the outlet port at an equal rate, in order to maintain a constant pressure. A microfluidic switch designed to minimize propulsion impact and delay with 12 μ L dead space was used at the end of the baseline period to switch the infusion from aCSF to 50 nM wtCGRP in aCSF solution. 0.3 mL total of this material was perfused at the rate of 1.8 mL/hr. Impact of wtCGRP on the diameter of a cerebral artery (red bar, Fig 2B) and on parenchymal blood volume (black rectangle, Fig 2B) was quantified using ImageJ⁶⁵. Image signal intensity in a region without discernable blood vessels was used as an indicator of parenchymal volume changes. Statistical analysis of all measurements was performed in Matlab (Mathworks, Natick, MA).

Magnetic resonance imaging (MRI). Fourteen Sprague-Dawley rats were used for in vivo MRI experiments. Prior to MRI experiments, rats underwent surgery under isoflurane anesthesia, and bilateral cannula guides (22 gauge, Plastics One, Roanoke, VA) were implanted over an arbitrarily chosen deep brain target, the ventral posterolateral nucleus of the thalamus (VPL; 3 mm lateral to midline, 4 mm posterior to bregma, and a depth of 5 mm from the cortical surface). A head post was also attached atop their skulls using dental cement (C&B Metabond, Parkell, Inc., Edgewood, NY), during this surgery. Cannula guides were sealed with dummy cannulas to avoid exposure of brain tissue during the recovery period. Further experiments were performed after three or more days of post-operative care. Immediately prior to each experiment, two injection cannulae (28 gauge, Plastics One, Roanoke, VA) were attached to 25 μ L Hamilton glass syringes and prefilled with the appropriate intracranial injection solution (aCSF, wtCGRP, cleaved or uncleaved CGRP-based sensors). Cannulae were then lowered into the bilateral cannula guides previously implanted into VPL. The Hamilton syringes were then placed in a remote infuse/withdraw dual syringe pump (PHD 22/2000; Harvard Apparatus, Holliston, MA).

Animals were scanned by MRI to measure the changes in hemodynamic contrast following intracranial CGRP probe or control injections. Data were acquired on a 7 T 20 cm inner diameter, horizontal bore magnet (Bruker BioSpin MRI GmbH, Ettlingen, Germany). Home-built and commercial (Insight Neuroimaging Systems, Worcester, MA) radiofrequency (RF) coils designed for rat brain imaging were

used for excitation and detection. During imaging experiments, animals were anesthetized with isoflurane (3% in oxygen for induction; 1% for maintenance). Breathing rate and end-tidal expired isoflurane were continuously monitored. Anesthetized animals were attached via their head posts to a head holder designed to fit within the RF coil systems. Animals with their RF coils were inserted into the magnet bore and locked in a position such that the head of the animal was at the center of the magnet bore.

High resolution T_2 -weighted anatomical scans of each animal were obtained using a rapid acquisition with relaxation enhancement (RARE) pulse sequence with echo time (TE) = 44 ms, recycle time (TR) = 2500 ms, RARE factor = 8, spatial resolution = 100 μm x 100 μm x 500 μm , and matrix size = 128 x 128 with 7 slices. Hemodynamic contrast image series were acquired using a gradient echo echo planar imaging (EPI) pulse sequence with TE = 34 ms, TR = 4000 ms, spatial resolution = 300 μm x 300 μm x 500 μm , and matrix size = 64 x 64 with 7 slices. To parallel the optical imaging experiments, five minutes of baseline measurement with 4 s per image were acquired prior to probe infusion. Following this baseline period, while continuously collecting EPI images, infusion pumps were remotely turned on to commence intracranial injection of 1 μL aliquots of CGRP or control solutions at the rate of 0.1 $\mu\text{L}/\text{min}$ through the cannulae. For the experiments of Fig. 2D, aCSF (control) and 100 nM wtCGRP in aCSF were injected simultaneously through the bilaterally implanted cannulas. For the experiments of Fig. 3E, CGRP-based CASP3 sensors (100 nM) were co-injected simultaneously, either with or without comixed CASP3 enzyme (1.15 ng/ μL). For the neuronal nitric oxide synthase (nNOS) inhibition experiment of Fig. 2E, a bilateral simultaneous injection of wtCGRP and aCSF was performed as in Fig. 2D. Then 50 mg/kg of the nNOS inhibitor *N*-nitro-*L*-arginine methyl ester (L-NAME, Sigma-Aldrich, St. Louis, MO) was injected via the tail vein. After waiting roughly 5 minutes after L-NAME injection, wtCGRP and aCSF injection lines were switched, and another imaging experiment with bilateral injections was carried out to assess the effect of CGRP on hemodynamic contrast in the presence of nNOS inhibition.

MRI data was processed and analyzed using the AFNI software package⁶⁶. The AFNI 3dAllineate command was used to align each animal's EPI dataset to the corresponding RARE anatomical image. Each animal's image data were then aligned to a reference MRI rat atlas⁶⁷. To identify voxels with

significant increases or decreases in BOLD signal, we used the 3dDeconvolve routines in AFNI to correlate individual or group level voxel-level signal changes with the injection epochs. For correlation analysis, injection epochs were modeled by “box car” regressors with a single stimulus block synchronized with the onset and offset of infusion, without delays. Activation in a region was deemed significant if a cluster of at least four contiguous voxels displayed a raw p -value < 0.001 for positive or negative correlation between the voxel time courses and the regressors. No significant negative correlation was observed. The cluster size and p -value threshold were objectively chosen, based on AFNI’s AlphaSim routine, to provide a type I error rate of 5% after correction for multiple comparisons^{68,69}; this was appropriate for robust hypothesis testing on individual voxels throughout the entire imaging volume. For visualization, group statistical maps were overlaid on a reference anatomical image as in Fig. 2D. Time courses were obtained by averaging MRI signal over 1.5 x 1.5 mm square regions of interest (ROIs) defined around cannula tip locations in individual animals’ datasets. The peak percent signal change was determined by comparing signal values during baseline and infusion conditions. Additional statistical analysis was performed in Matlab.

Plasmids. A tabulated list and sequences for all plasmids used in this study are provided as Supplementary Information. Lentiviral helper plasmids pMD2.G (Addgene #12259, Cambridge, MA) and psPAX2 (Addgene #12260) were gifts from Didier Trono. Plasmids pEF-ENTR A (Addgene #17427) and pLenti X1 Zeo (Addgene #17299) were gifts from Eric Campeau⁷⁰. Bacterial expression plasmids Z503, Z507, and Z508 were cloned using the Golden Gate method⁷¹ by assembling synthetic DNA sequences (IDT, Coralville, IA) and PCR amplicons into the backbone of pEF-ENTR A. cfSGFP2 is a cysteine-free variant of the green fluorescent protein (GFP)⁷². CGRP is the alpha-isoform of human CGRP. Lentiviral plasmids were cloned using the Golden Gate method by assembling fragments for the polycistronic expression cassettes into a variant of the pLentiX1 Zeo plasmid with its kanamycin resistance replaced by the ampicillin resistance cassette from pUC18. Each lentiviral plasmid used in this study contains a gene of interest followed by an internal ribosome entry site (IRES) and a selection marker comprising a fluorescent protein, a 2A viral sequence⁷³, and an antibiotic resistance gene. The HA-tagged human calcitonin receptor-

like receptor (CLR) and myc-tagged human receptor activity-modifying protein 1 (RAMP1) sequences, together encoding the two components of human CGRP receptor, were previously functionally characterized ⁷⁴. The Glo22F gene encodes an engineered luciferase whose activity is modulated by cyclic AMP (Promega, Madison, WI) ⁷⁵.

Plasmids were assembled by one-pot restriction and ligation using an optimized Golden Gate protocol. DNA fragments were obtained as double-stranded synthetic DNA gBlocks (IDT), annealed oligonucleotides (IDT), or PCR products and either used directly or subcloned into a backbone with different antibiotic resistance. For each fragment, 40 fmol were added to a reaction containing 0.7 μ L highly concentrated (HC) T4 ligase (Promega), 1X ligase buffer, 0.3 μ L BsaI (NEB), and 1X bovine serum albumin (New England Biolabs, Ipswich, MA) in a final volume of 10 μ L. The reaction was performed in a thermocycler using the following program: 1 x (37 °C, 5 min); 25 x (37 °C, 2 min; 16 °C; 5 min); 1 x (50C, 5 min; 80 °C, 5 min); hold at 4 °C. The reaction product (2 μ L) was transformed into chemically competent *E. coli* (*E. cloni* 10G, Lucigen Corp.). DNA preparations from kanamycin-resistant clones were screened by restriction digest and verified by sequencing (Genewiz).

Lentiviral plasmids C504, C505, and C512 were cloned as above, verified, and then re-transformed into Stbl3 cells (New England Biolabs) for plasmid production. Liquid cultures were grown in 50 mL LB and DNA was extracted by midi-prep (Qiagen, Valencia, VA).

Mammalian cell culture. HEK293FT cells were purchased from Life Technologies (Grand Island, NY) and cultured in 90% DMEM medium, supplemented with 2 mM glutamine, 10% fetal bovine serum (FBS), 100 units/mL penicillin, and 100 μ g/mL streptomycin. Cells were frozen in freezing medium composed of 50% unsupplemented DMEM, 40% FBS, and 10% dimethylsulfoxide.

Lentivirus production. HEK293FT cells were seeded into 6-well plates at 1 million cells/well and transfected using Lipofectamine 2000 (Life Technologies, Grand Island, NY) according to instructions at sub-confluence. Co-transfection of 0.5 μ g pMD2.G, 1 μ g psPAX2, and 1 μ g of the lentiviral

plasmid of interest was performed with 6.25 uL Lipofectamine 2000 reagent. Virus-containing supernatant was collected after 48 and 72 hours, filtered through 0.45 µm filters, and used for infection without further concentration. Supernatants were stored at 4 °C for up to a week.

Lentiviral infection and cell line generation. HEK293FT cells were seeded into 24-well plates at 40,000 cells/well (final) in the presence of 4 µg/mL Polybrene in 50% fresh medium and 50% viral supernatants containing between one and three different viruses. The medium was replaced with fresh viral supernatants daily for two days (infection with single virus) or four days (triple infection). Selection was performed using both antibiotic resistance and fluorescent markers for each lentivirus. Beginning on day 3 after initial infection, appropriate antibiotics (blasticidin at 10 µg/mL, puromycin at 1 µg/mL, hygromycin at 250 µg/mL, or combinations; all from Life Technologies) were added to the medium for selection and selection was continued until all cells expressed the appropriate fluorescent markers. Selection was then discontinued, cells were expanded and aliquots were frozen down.

Luminescent cAMP assay for CGRP receptor activation. The GloSensor cAMP assay⁷⁵ (Promega) was used to measure cAMP generation upon CGRP receptor activation in real time. HEK293FT reporter cells were virally transduced with an engineered luciferase whose activity is subject to fast allosteric modulation by cytosolic cAMP. We generated one HEK293FT cell line carrying only the lentiviral construct encoding the engineered luciferase (negative control) and another cell line carrying three lentiviral expression constructs, encoding the engineered luciferase and the two components of the heterodimeric CGRP receptor (CGRP reporter cell line); see Fig. S2.

On day 0, 10,000 cells / well were seeded in 100 µL DMEM + 10% FBS in white opaque clear-bottom 96-well plates (Costar #3610, Coppel, TX). On day 1 or 2, the medium was removed from the wells and replaced with 90 µL/well of Gibco CO₂-independent medium (Life Technologies) + 10% FBS containing 1% v/v of cAMP GloSensor substrate stock solution (Promega). The cells were incubated in substrate-containing medium at 37 °C in 5% CO₂ for at least 2 h (maximally 8 h). Prior to the

luminescence bioassay, cells were removed from the cell culture incubator and equilibrated to room temperature and atmospheric CO₂ for 30 min. Then, a pre-addition read was performed for 10 min to establish a baseline for luminescence. Compounds and reaction products to be tested were quickly added in 10 µL volume per well at 10x of the desired final concentration using a multichannel pipet. A 30 min time resolved readout of luminescence was then performed post-addition with time points every 60 or 90 s, and the time course was examined to confirm a plateau in the signal after 10-15 min, persisting at least through the 25 min time point. All further data analysis was performed on the basis of the luminescence intensity at the 15 min post-addition time point.

Bioassay data analysis. Data analysis was performed with a custom Python program. Unless stated otherwise, luminescence intensities at minute 15 were normalized within each microplate to 0.0 = blank signal from reporter cells with buffer added and 1.0 = signal from reporter cells with 100 nM of wild-type synthetic human alpha CGRP (Sigma) added. Triplicate wells were grouped and the mean and standard deviation for each compound concentration were plotted and used for weighted least squares regression. Dose-response curves were fit to a four-parameter Hill equation of the following form:

$$y = a + \frac{(b-a)x^n}{x^n + (10^k)^n}$$

x is the concentration of CGRP or equivalent, y is the luminescence reading, a and b are baseline constants, k is the logarithm of the EC₅₀ value, and n is the effective Hill coefficient. Fitting was performed by weighted nonlinear least-squares regression with the Levenberg-Marquardt algorithm as implemented in the `leastsq` module from the Scientific Python library. For dose-response curves that did not reach a plateau over the examined concentration range, the values of the asymptotes were constrained to a = mean value of blank and b = mean value of 100 nM wtCGRP and only n and EC₅₀ were allowed to vary. For curves that never left the baseline (maximum activity < 10% of activity of 100 nM wtCGRP), no

attempt was made to determine an exact value of EC_{50} . Standard errors for $\log(EC_{50})$ values were computed using the delta method and converted to asymptotic 95% confidence intervals (CI values noted in the text) for EC_{50} and $\log(EC_{50})$.

Reporter validation. Forskolin, wtCGRP, and [8-37]CGRP were purchased from Sigma-Aldrich and used in bioassays as described above. To determine whether CGRP responses were specifically mediated by RAMP1 and CLR, two HEK293FT cell lines were used, one expressing the Glo22F cAMP-responsive luciferase only and the other also expressing the RAMP1:CLR CGRP receptor heterodimer. All luminescence values were normalized from zero to one using baseline values obtained from buffer only or addition of 100 μ M forskolin on the same respective cell line. In a separate experiment, CGRP dose-response curves were obtained in the presence of [8-37]CGRP on reporter cells expressing RAMP1 and CLR. [8-37]CGRP is an N-terminally truncated CGRP variant that acts as a competitive inhibitor of CGRP agonist activity and is expected to shift CGRP dose-response curves to the right. Here, luminescence data were normalized between values obtained for buffer only and 100 nM CGRP only.

Peptide synthesis. CGRP-like peptides were made by solid-state synthesis at the MIT Koch Institute Biopolymers lab, oxidatively cyclized, and purified by high performance liquid chromatography (HPLC). Identity and purity were confirmed by matrix-assisted laser desorption ionization-time of flight (MALDI-TOF) mass spectrometry and analytical HPLC. After lyophilization, the peptides were weighed, dissolved in water or 50% dimethylsulfoxide, and quantified rigorously using a fluorescent microplate assay (FluoroProfile, Sigma-Aldrich) with CGRP from Sigma-Aldrich as a concentration standard. The peptide solutions were then adjusted to a stock concentration of 100 μ M and stored at -20 °C.

Expression, refolding, and purification of GFP-CGRP fusions. GFP-CGRP fusions were expressed from a T7 promoter upon induction with 0.4 mM isopropyl β -D-1-thiogalactopyranoside in

E. coli BL21 cells (New England Biolabs). Cells were grown in 50 mL LB medium at 37 °C to an optical density at 600 nm of 0.4-0.6, induced, and expression was allowed to proceed for 3-5 h at 37 °C. Cell pellets were collected, lysed with BugBuster (EMD Millipore, Billerica, MA), and processed for inclusion body (IB) preparation according to the manufacturer's instructions. IBs were dissolved in 5 mL denaturation buffer (6 M guanidinium HCl, 20 mM dithiothreitol, 50 mM Tris-HCl, pH 7.5) overnight and the absorbance at 280 nm (A_{280}) was measured. Extinction coefficients at 280 nm (ϵ_{280}) and molar masses (MW) were computationally predicted from the amino acid sequence [sensor (2): $\epsilon_{280} = 26,980 \text{ cm}^{-1} \text{ M}^{-1}$, MW = 33,174 Da; sensor (3): $\epsilon_{280} = 25,700 \text{ cm}^{-1} \text{ M}^{-1}$, MW = 32,911 Da; sensor (4): $\epsilon_{280} = 25,700 \text{ cm}^{-1} \text{ M}^{-1}$, MW = 32,780 Da]. From these values and the measured 280 nm absorbances, concentrations were then calculated and adjusted to 0.5 mg/mL for refolding. Refolding was performed by dialysis of 40 mL denatured protein solution against refolding buffer (100 mM NaCl, 20 mM Tris-HCl, pH 7.5). Insoluble material was removed from the refolded solution by centrifugation (16,000g for 20 min) and the supernatant containing soluble protein was concentrated to a volume of 3-4 mL. The fusion protein was isolated by StrepII affinity purification using 1 mL StrepTactin agarose resin (Qiagen) with refolding buffer as wash buffer. Elution buffer additionally contained 2.5 mM desthiobiotin. Fractions containing the bulk of eluted protein (as judged by green color) were pooled, buffer exchanged into storage buffer (identical to refolding buffer) using NAP-10 size exclusion columns (GE Healthcare), and concentrated with spin columns. A_{280} values were determined and concentrations of the stock solutions were adjusted to 100 μM using predicted extinction coefficients and molar masses. Purity and identity of the proteins were verified by sodium dodecylsulfate polyacrylamide gel electrophoresis (SDS-PAGE) and MALDI-TOF mass spectrometry. Stock solutions were stored for up to two weeks at 4 °C.

Proteolytic cleavage reactions. Recombinant human fibroblast activation protein alpha (FAP) expressed in Sf21 cells (400-600 ng/ μL ; Sigma-Aldrich product F7182), recombinant human caspase-3 (CASP3) expressed in *E. coli* (230 ng/ μL ; Sigma-Aldrich product C1224), ProTEV Plus protease (5 U/ μL ; Promega product V6101) and enterokinase light chain (2 ng/ μL ; New England Biolabs product

P8070) were purchased from commercial sources and used at the final concentrations indicated for each experiment. Reactions were performed by combining varying concentrations of the relevant protease and the desired concentration of the sensor peptide or fusion protein (10x the highest desired final concentration in the bioassay) in reaction buffer (100 mM NaCl, 20 mM Tris-HCl, pH 7.5), and incubating the mixture at 37 °C for 2 h. These conditions permitted all investigated proteases to achieve near-complete cleavage, as indicated by our assays. For cleavage reactions followed by serial dilution and CGRP bioassays, 1% 3-[(3-cholamidopropyl)dimethylammonio]-1-propanesulfonate (CHAPS) was included in the reaction buffer to reduce adsorptive loss of free peptides. For cleavage mixtures used for in vivo injection, CHAPS was omitted. The extent of cleavage was assessed in each case by SDS-PAGE for fusion proteins and by MALDI-TOF mass spectrometry for small peptide substrates.

Figures and tables

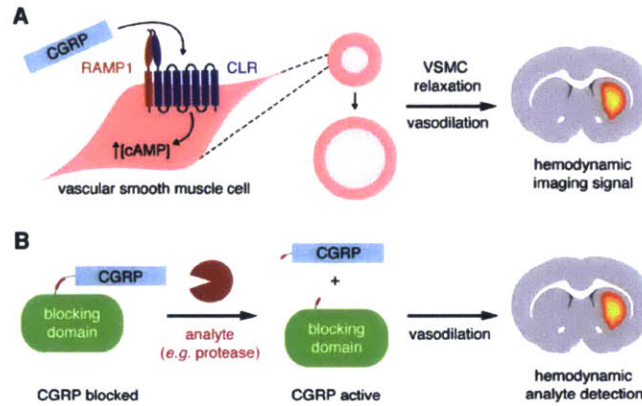


Fig. 2-1. Principle of molecular neuroimaging with CGRP-induced hemodynamic responses.

- (A) CGRP acts on the heterodimeric G-protein coupled receptor RAMP1/CLR (left) to induce intracellular cAMP production, resulting in relaxation of vascular smooth muscle cells (VSMCs) and consequent vasodilation (middle). Dilation of cerebral microvasculature induces hemodynamic effects visible by MRI and other imaging methods (right).
- (B) Design for analyte-sensitive vasoactive probes comprising CGRP fused to a labile blocking domain via an analyte-responsive linker. Such probes can be activated by analytes that act sterically on the sensor to unblock the CGRP moiety, e.g. by cleaving the blocking domain as shown here. This would induce an analyte-dependent hemodynamic response and enable molecular imaging with CGRP-based constructs.

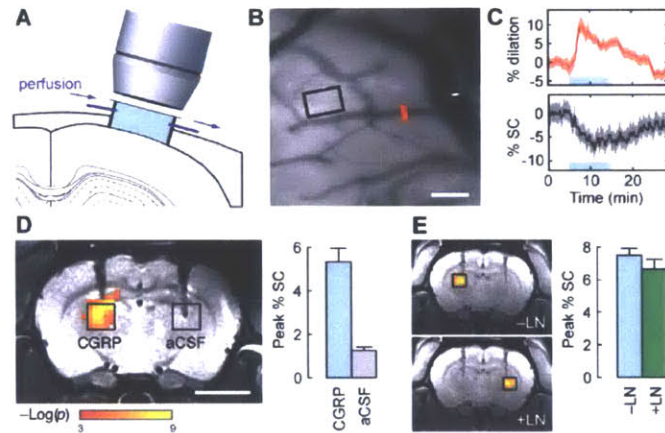


Fig. 2-2. Imaging artificial hemodynamic responses induced by CGRP probes *in vivo*.

- (A) Direct effects of perfused CGRP on cerebral vasculature are assessed by optical reflectance imaging of exposed cortex.
- (B) Cortical image of a representative rat, revealing discrete blood vessels (dark) and parenchymal tissue (light background). Scale bar = 100 μm .
- (C) Time course of CGRP-induced hemodynamic changes. The CGRP infusion period is denoted by the blue shaded lines. Top panel shows changes in the diameter of a vessel measured at the position of the red bar in (B). Bottom panel shows mean optical signal changes in the parenchymal region denoted by the black rectangle in (B).
- (D) MRI changes observed in conjunction with intracranial injection of CGRP (100 nM) or vehicle only (aCSF), both at 0.1 $\mu\text{L}/\text{min}$. for 10 min. Colored voxels overlaid on a grayscale anatomical image (left) indicate the correlation strength of observed signal changes with the injection period. Bar graph (right) indicates peak signal changes observed upon injection of CGRP or aCSF, each averaged over corresponding injection regions in multiple animals (black boxes at left, $n = 6$). Scale bar = 5 mm.
- (E) Dissociation of CGRP-induced artificial hemodynamic signals from nitric oxide-mediated signaling. Left, hemodynamic responses observed by imaging before (top) or after (bottom) intravenous infusion of the nNOS inhibitor L-NAME (50 mg/kg). Right, comparison of peak percent signal changes observed in regions as identified on the left, without and with L-NAME and showing no significant difference. Error bars denote SEM values ($n = 4$).

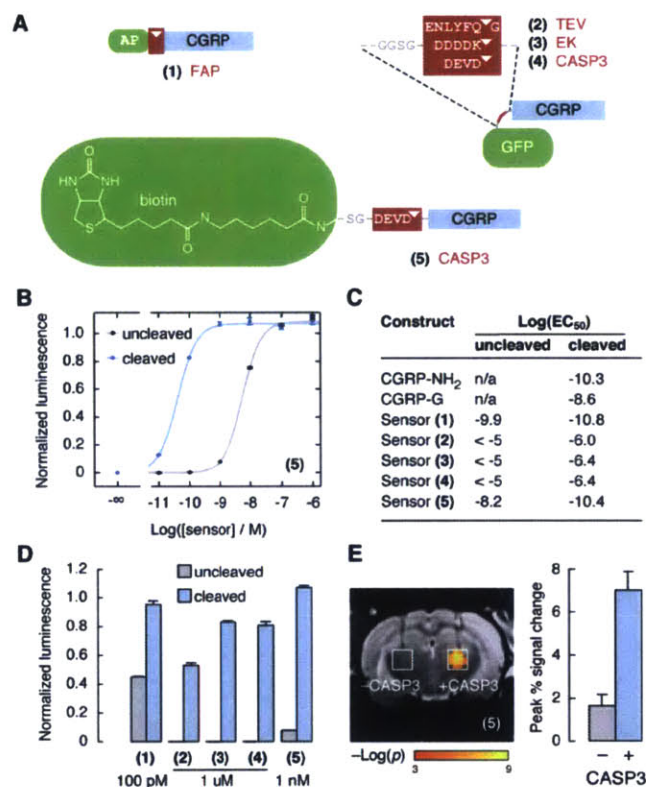


Fig. 2-3. Design and assessment of protease-activated imaging probes based on CGRP.

- (A) Protease sensor designs incorporate an N-terminal blocking moiety (green), a protease cleavage sequence (red, cleavage sites indicated by triangles), and a C-terminal CGRP moiety (blue). Structures of five protease sensors are shown, with cognate proteases labeled in red text: (1) The synthetic peptide AP-CGRP-amide detects dipeptidase activity of fibroblast activation protein (FAP). (2-4) Recombinant fusion proteins comprised of cysteine-free GFP, a short linker, a protease site, and non-amidated CGRP detect TEV protease (2), enterokinase (EK) (3), and caspase-3 (CASP3) (4). (5) The synthetic peptide (long-chain biotin)-SG-DEVD-CGRP-amide also detects CASP3 activity.
- (B) Dose response curve for sensor (5) measured using a cell-based bioassay (Fig. S2) following incubation with or without CASP3. Luminescence values were normalized, and error bars reflect SD from $n = 3$ replicates.
- (C) Log(EC₅₀) values obtained by dose response curve measurement from sensors (1-5) incubated with or without corresponding proteases: (1) with 5 ng/μL of human FAP; (2) with 0.1 U/μL of TEV protease; (3) with 2 pg/μL of EK light chain; (4) with 23 ng/uL and (5) with 11.5 ng/μL of human CASP3. Standard errors were all less than 0.1 ($n = 7$).
- (D) Protease sensing by CGRP-based probes measured *in vitro*, using probe concentrations indicated. Error bars represent SD of $n = 3$ replicates.

(E) Protease-dependent switching of 100 nM CGRP-based molecular imaging probe (5) induces contrast differences in MRI. Left, an image showing significant hemodynamic activation in the presence but not the absence of coadministered 1.15 ng/ μ L CASP3. Right, bar graph showing peak signal change induced by uncleaved vs. cleaved sensor (5). Error bars indicate SEM values over $n = 4$ animals.

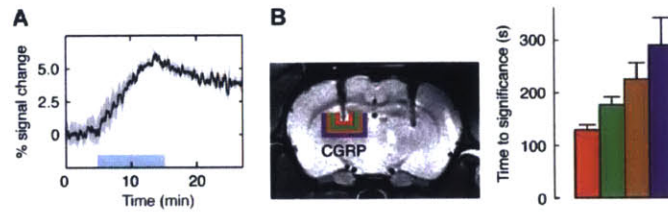


Fig. 2-S1. Time course of MRI signal during CGRP infusion in rat brain.

- (A) Time course of mean MRI signal change (black line) observed before, during (blue bar), and after 0.1 $\mu\text{L}/\text{min}$ infusion of 100 nM wtCGRP into rat thalamus. Signals were averaged over six animals in 1.5 mm square regions of interest (ROIs) positioned around the infusion cannulae tips in each animal (cf. Fig. 2D); gray shading denotes standard errors as a function of time.
- (B) Time courses from multiple approximately concentric ROIs (diagrammed at left) were analyzed to determine whether hemodynamic MRI has sufficient spatial resolution to monitor convection of CGRP from the infusion site. For each ROI, the delay between the start of infusion and the observation of statistically significant signal changes from baseline was measured (color coded bars at right). The onset of significant signal changes increases monotonically with distance from the cannula tip, consistent with the expected spread of the imaging agent during infusion. Times to significance observed in peripheral ROIs (green, brown, and purple) were all significantly longer than the time to significance observed for the innermost ROI (red, all t -tests $p < 0.05$).

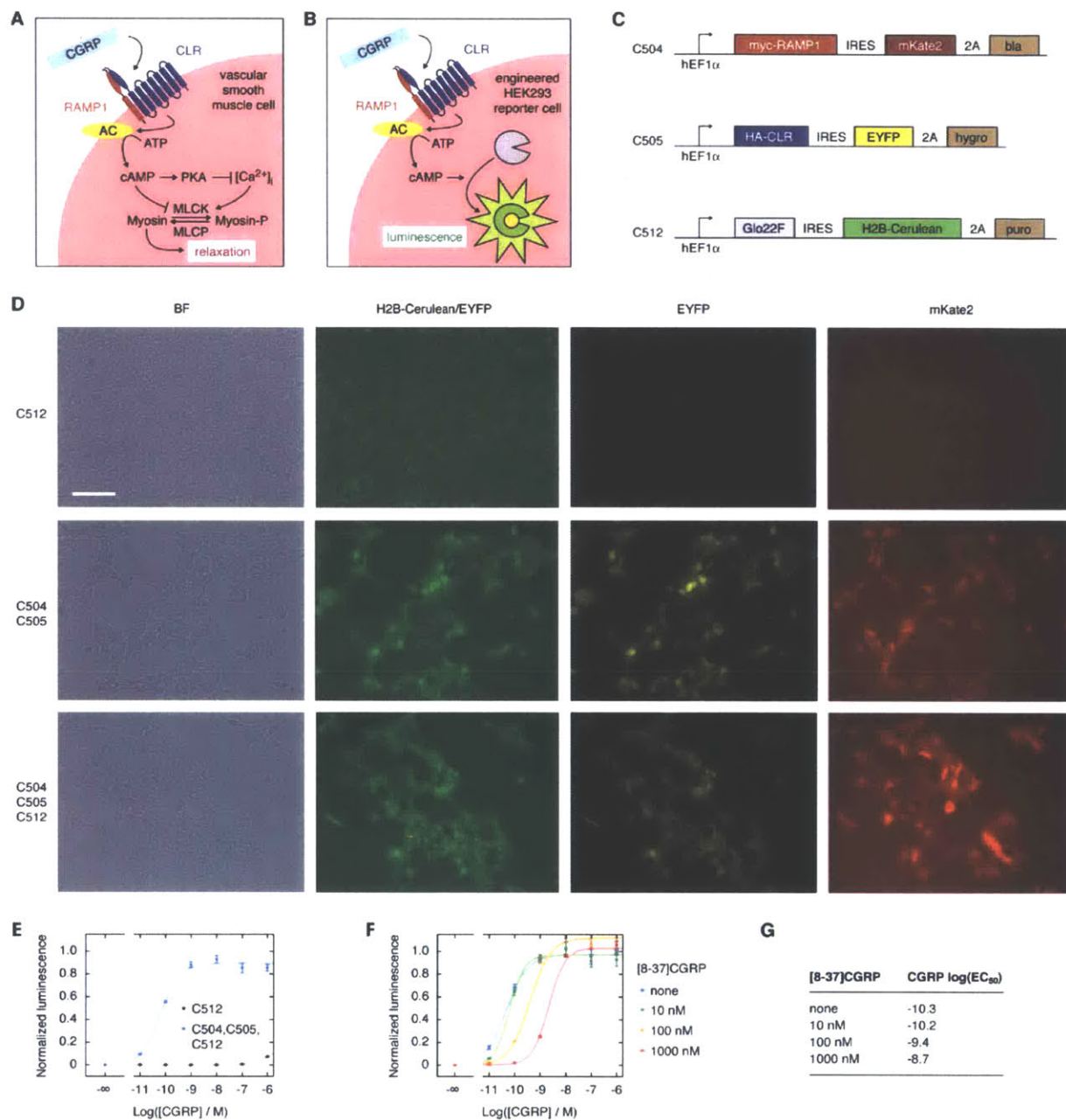


Fig. S2. Cell-based bioassay for CGRP activity.

(A) Mechanism of vasodilation by CGRP. CGRP peptide binds and activates the heterodimeric CGRP receptor (RAMP1:CLR) on vascular smooth muscle cells (VSMCs). Activation of adenylate cyclase (AC) results in cyclic adenosine monophosphate (cAMP) production that acts through protein kinase A (PKA)-dependent and independent pathways to inhibit myosin light chain kinase (MLCK), resulting in VSMC relaxation and blood vessel dilation.

- (B)** Engineered HEK293FT reporter cells provide a readout of cAMP accumulation upon activation of the CGRP receptor via a constitutively expressed, cAMP-responsive luciferase variant, Glo22F (Promega)⁷⁵.
- (C)** Lentiviral transgenes used to construct the CGRP reporter cell line. Full sequences provided in Supplementary Tables 2-S2 to 2-S6.
- (D)** Fluorescence micrographs verifying expression of fluorescent reporters expressed by vectors encoding the Glo22F luciferase (C512) and the heterodimeric CGRP receptor components (C504 and C505) in cell lines transfected with constructs as noted at left. Color channels (labeled at top) depict bright field (BF) images, H2B-Cerulean (nuclear) with bleed-through from EYFP (cytosolic), EYFP alone, and mKate2.
- (E-G)** Pharmacological validation of the reporter cell line.
- (E)** Dose-response curve for synthetic wild-type human alpha CGRP for reporter cell line infected with lentiviruses C504, C505, and C512 (blue) and for a cell line transfected with the cAMP reporter vector C512 but not the CGRP receptor vectors (gray). Luminescence values were normalized to the range evoked by buffer vs. 100 μ M forskolin for each cell line.
- (F)** Dose-reponse curves for CGRP in absence or presence of different concentrations of the competitive inhibitor [8-37]CGRP, a C-terminal fragment of CGRP. Luminescence values were normalized to the range obtained with buffer vs. 100 nM CGRP.
- (G)** Tabulated potencies for CGRP in the presence of different [8-37]CGRP concentrations. Standard errors were all less than 0.1 ($n = 7$).

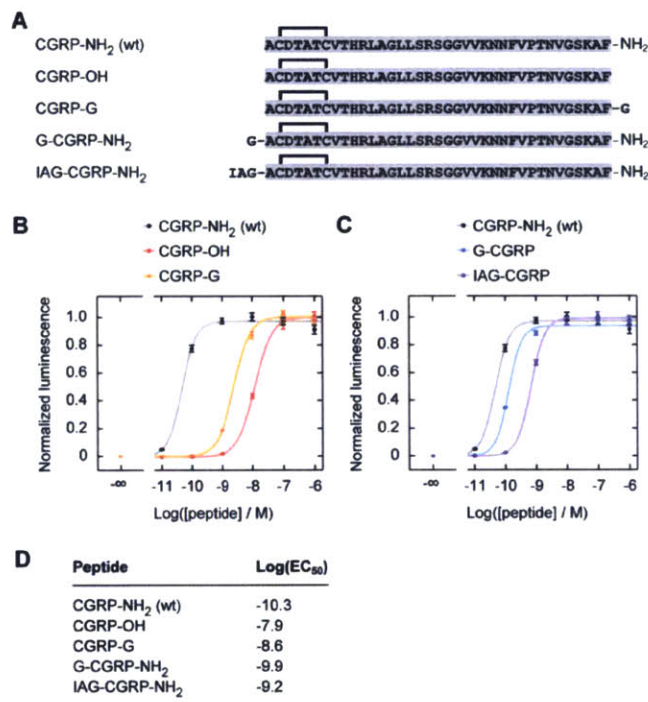


Fig. 2-S3. Impact of small terminal modifications on CGRP potency.

- (A) Sequence of peptide variants. -NH₂ denotes an amidated C-terminus; CGRP-OH and CGRP-G contain a regular C-terminal carboxylate. Bioassays were performed with peptides serially diluted into water plus 0.1% CHAPS from 100 μ M stock solutions in water or 50% DMSO.
- (B) Dose-response curves for C-terminally modified CGRP variants. Values normalized to the range obtained with buffer vs. 100 nM wtCGRP stimulation.
- (C) Dose-response curves for N-terminally modified CGRP variants.
- (D) Half maximal potencies, presented as log(EC₅₀), determined from the dose-response data in panels B and C. Standard errors were all less than 0.1 ($n = 7$).

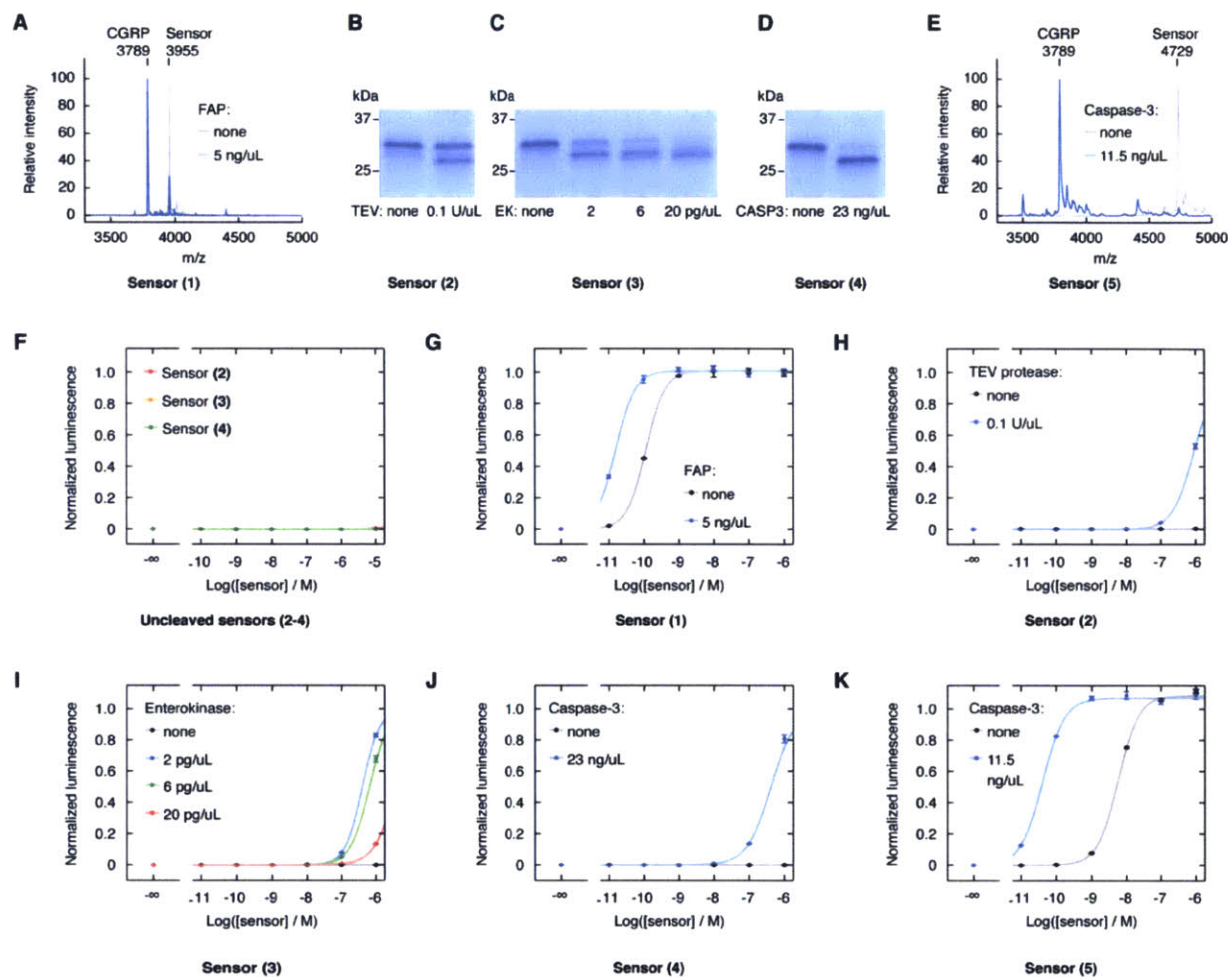


Fig. 2-S4. Proteolytic cleavage of candidate sensors and assessment by bioassay.

(A-E) Cleavage reaction products after incubation of 10 μ M sensor with or without enzyme for 2 h at 37 $^{\circ}$ C.

(A) MALDI mass spectrum of sensor (1) after incubation with or without FAP shows near-complete cleavage and liberation of free CGRP.

(B) SDS-PAGE analysis of sensor (2) after incubation with or without TEV protease shows substantial but not complete cleavage.

(C) SDS-PAGE analysis of sensor (3) after incubation with different concentrations of EK light chain shows increasing cleavage with increasing concentrations.

(D) SDS-PAGE analysis of sensor (4) after incubation with or without caspase-3 shows near-complete cleavage.

- (E)** MALDI mass spectrum of sensor (5) after incubation with or without caspase-3 shows complete cleavage and liberation of free CGRP.
- (F-K)** Dose-response curves of uncleaved and cleaved sensors in cell-based bioassay. All measurements were normalized to blank = 0 and 100 μM wtCGRP = 1.0.
- (F)** Dose-response curves for Sensors (2-4) at final assay concentrations up to 10 μM (addition of 10 μL of 100 μM solution to 90 μL medium per well in bioassay) show no receptor activation by uncleaved GFP-linker-CGRP-G sensors even at 10-fold higher concentrations than were used in cleavage assays (G-K).
- (G-K)** Dose-response curves for reaction products from (A-E).

Supplementary Table 2-S1: Catalog of plasmids used in this study

ID	Name	Source
Z503	pEXPR-T7-cfSGFP2-DEVD-CGRP-G	This study
Z507	pEXPR-T7-cfSGFP2-DDDDK-CGRP-G	This study
Z508	pEXPR-T7-cfSGFP2-ENLYFQG-CGRP-G	This study
C504	pLV-hEF1a-myc-RAMP1-IRES-mKate-2A-bla	This study
C505	pLV-hEF1a-HA-CALCRL-IRES-EYFP-2A-Hygro	This study
C512	pLV-hEF1a-Glo22F-IRES-H2B-Cerulean-2A-puro	This study
X106	pMD2.G	Addgene 12259
X107	psPAX2	Addgene 12260
X108	pLenti X1 Zeo DEST (668-1)	Addgene 17299
X109	pEF-ENTR A (696-6)	Addgene 17427

Supplementary Table 2-S2. Full sequence for bacterial expression plasmid Z503 (pEXPR-T7-cfSGFP2-DEVD-CGRP-G)

color coding key:

cfSGFP2: cysteine-free GFP variant (with N-terminal StrepII tag underlined)

Cleavable linker

haCGRP-Gly: Human alpha CGRP extended with one C-terminal glycine residue

Kanamycin resistance gene

pBR322 origin of replication

sequence:

```
GCTCAGAGGATCGAGATCTCGATCCCGCAAATTAATACGACTCACTATAGGGAGAGCCACAACGGTTTCCCTCTAGAAAATAATTT
TGTTTAACTTTAAGAAGGAGATATACATATGAGCGCGTGGAGCCATCCGCAGTTTGAAAAAGGTGCTGTATCCAAGGGCGAAGAGC
TGTTCACGGCGTAGTACCGATTTTGGTGGAGCTGGACGGCGATGTGAACGGCCATAAATTTAGTGTGAGCGGGGAAGGTGAGGGC
GATGCGACATATGGCAAACGACCTGAAATTTATTAGTACCACCGTAAACTGCCAGTGCCTTG6CCGACGCTGGTTACCACCCCT
GACCTACGGTGTGCAAATGTTCCGCTCGCTACCCCGACCATATGAAACAGCATGACTTCTTCAAGAGCGCAATGCCGGAAGGTACG
TGCAGGAGCGTACGATTTTTCAAAGATGATGGGAATTACAAGACACGTGCCGAAGTGAATTCGAGGGCGATACCGTGGTTAAT
CGCATCGAACTGAAAGGCATCGACTTCAAAGAAGATGGTAACATTTGGGTACAAAGCTTGAATACAACATAAAGTACATAACGT
ATATATCACAGCAGATAAGCAGAAGAATGGTATTAAGGCGAATTTCAAGATCCGTCACAATATGAGGATGGCGGTGTTCAGTTAG
CTGATCATATCAACAGAACACCCCTATTGGAGATGGCCAGTGTGCTGCCAGATAATCATTACCTGTCTACCCAGAGCAAAGT
AGCAAAGACCCCTAATGAGAAACGTGATCATATGGTCTTACTGGAGTTCGTACAGCGCGCGGCATTACGCTGGGTATGGATGAGCT
GTATAAGGGTGGCTCAGGTGATGAAGTAGATGCTTGTGACACAGCCACCTGTGTCACCCACCGCTGGCCGGTCTGCTGTCTCGCT
CGGGTGGCGTTGTTAAAAACAATTTGTGCGCAACCAATGTTGGTTCAAAGCGTTTGGCTAACAAAGCCCGAAAGGAAGCTGAGTT
GGCTGCTGCCACCGCTGAGCAATAACTAGCATAACCCCTTGGGGCTCTAAACGGGTCTTGGGGGTTTTTGTCTGAAAGGAGGAA
CTATATCCGGATATCCACAGGACGGAGGTAGCTCTGGCCCGTGTCTCAAATCTCTGATGTTACATTGCACAAGATAAAAAATATAT
CATCATGAACAATAAACTGTCTGCTTACATAAACAGTAAACAAGGGGTGTTTTCAGCCATATTCAGGGGAGGGTCCAGCCGCT
TCAGATTAATTCAGAAATCGATCGATCATTTATTTGGCTATTAAGGGTCCGGCATATGTCGCGCAATTCAGGTTCGGCAATTCGATC
TGTGATTCGGAGCGGAGCCGAGGTTGCTTGTGTAAGCATGGCAAGGTAGCCGCTTCCGCAATTCAGGTTCGGCAATTCGATC
GACTTAATTCGGGTGAGCGAATTTATGCTCTTCCGACCATCAGGATTTTATCCTACTCCTGTGATTCGATTCGATTCGATTC
GCGATTCGCGGAATACAGCCTTCAGCTATTAGAAGAAATTCGCTHATTCAGGTTCAGGATATTCGATTCAGGTCGATTCGATTC
GCGCGGTTGCGATTCGATTCGATTCGATTCGATTCGATTCGATTCGATTCGATTCGATTCGATTCGATTCGATTCGATTCGATTC
ATAACGGTTTGGTTCGATTCGATTCGATTCGATTCGATTCGATTCGATTCGATTCGATTCGATTCGATTCGATTCGATTCGATTC
TTCGATTCGATTCGATTCGATTCGATTCGATTCGATTCGATTCGATTCGATTCGATTCGATTCGATTCGATTCGATTCGATTC
TATTGATTCGATTCGATTCGATTCGATTCGATTCGATTCGATTCGATTCGATTCGATTCGATTCGATTCGATTCGATTCGATTC
TTCGATTCGATTCGATTCGATTCGATTCGATTCGATTCGATTCGATTCGATTCGATTCGATTCGATTCGATTCGATTCGATTC
TTCGATTCGATTCGATTCGATTCGATTCGATTCGATTCGATTCGATTCGATTCGATTCGATTCGATTCGATTCGATTCGATTC
TCAGAATTGGTTAATTTGGTTGTAACATTATTCAGATTGGGCCCCGTCCACTGAGCGTCAGACCCCGTAGAAAAGATCAAAGG
ATCTTCTTGAGATCCTTTTTTCTGCGCGTAATCTGCTGCTTGCACAAAAAACCACCGCTACCAGCGGTGGTTTGTGTTGCCGG
ATCAAGAGCTACCAACTCTTTTCCGAAGGTAAGTGGCTTCAGCAGAGCGCAGATACCAATACTGTTCTTCTAGTGTAGCCGTAG
TTAGGCCACCACTTCAAGAATCTGTAGCACCGCTACATACCTCGCTCTGCTAATCCTGTTACCAGTGGCTGCTGCCAGTGGCGA
TAAGTCGTGCTTACCAGGTTGGACTCAAGACGATAGTTACCAGGATAAGGCGCAGCGGTGGGGTGAACGGGGGGTTCGTGCACAC
AGCCCAGCTTGGAGCGAACGACCTACACCGAAGTACCTACAGCGTGGAGTATGAGAAAGCGCCACGCTTCCCGAAGGGGAGA
AAGGCGGACAGGTATCCGTAAGCGCGAGGGTCCGAACAGGAGAGCGCAGGAGGAGCTTCCAGGGGAAACGCTTGGTATCTTTA
TAGTCTGTGCGGGTTTCGCCACCTTGACTTGAGCGTCGATTTTGTGATGCTCGTCAGGGGGGGGAGCCATGAAAAACGCCA
GCAACGCGGCTTTTTACGTTTCTGCGCTTTTGTGCGCTTTTGTGCGCTTTTGTGCGCTTTTGTGCGCTTTTGTGCGCTTTTGTG
AACCCTATTACCGCTAGCATGGATCTCGGGGACGTCTAACTACTAAGCGAGAGTAGGAACTGCCAGGCATCAAATAAACGAAAG
GCCAGTCTTCCGACTGAGCCTTTCTGTTTTATCTGTTGTTTGTGCGGTGAACGCTCTCTGAGTAGGACAAATCCGCCGGGAGCGGA
TTTGAACGTTGTGAAGCAACGCGCGGAGGGTGGCGGGCAGGACGCCGCCATAAACTGCCAGGCATCAAATAAGCAGAAGGCCA
TCCTGACGGATGGCCTTTTTGCGTTTCTACAACTCTTCTGTTAGTTAGTTACTTAA
```

Supplementary Table 2-S3. DNA and amino acid sequence of cleavable linkers for all bacterial expression plasmids

Z503 (pEXPR-T7-cfSGFP2-DEVD-CGRP-G)	GGTGGCTCAGGTGATGAAGTAGAT G G S G D E V D
Z507 (pEXPR-T7-cfSGFP2-DDDDK-CGRP-G)	GGTGGCTCAGGTGACGATGATGACAAG G G S G D D D D K
Z508 (pEXPR-T7-cfSGFP2-ENLYFQG-CGRP-G)	GGTGGCTCAGGTGAAAACCTGTATTCCAGGGT G G S G E N L Y F Q G

Supplementary Table 2-S4. Full sequence of lentiviral plasmid C504 (pLV-hEF1a-myc-RAMP1-IRES-mKate-2A-bla)

color coding key:

hEF1a: Human elongation factor 1 alpha promoter
 Transgene cassette: myc-RAMP: Human receptor-activity modifying protein 1 preceded by the H. influenza hemagglutinin signal peptide and the c-myc epitope
 IRES: Internal ribosome entry site
 mKate2: Red fluorescent protein
 2A: Autoproteolytic viral amino acid sequence
 Bla: Blasticidin resistance gene
 delta_U3 / 3'LTR: HIV 3'LTR with deletion in the U3 region
 AmpR: Ampicillin resistance gene
 pUC origin of replication
 RSV / 5'LTR: Rous Sarcoma Virus / HIV 5'LTR hybrid promoter
 Psi: Lentiviral Psi packaging sequence
 RRE: Rev response element
 CPPT: Central polypurine tract

sequence:

CTTTGCAGCTAATGGACCTTCTAGGCTTTGAAAGGAGTGGGAATTGGCTCCGGTGCCCGTCAAGTGGGCGAGAGCGGCACATCGCCAC
 AGTCCCCGAGAAGTTGGGGGGAGGGGTCCGGCAATTGAACCGGTGCCCTAGAGAAGGTGGCGCGGGGTAAACTGGGAAAAGTGATGTCG
 TGTACTGGCTCCGCTTTTCCCGAGGGTGGGGGAGAACCGTATATAAGTGCAGTACTCGCCGTGAACGTTCTTTTCGCAACGGG
 TTTGCCCGCAGAACACAGGTAAGTGCCTGTGTGGTTCCCGCGGGCTGGCCTCTTTACGGSTTATGGCCCTTGCGTGCCTTGAAT
 TACTTCCACCTGGCTGCAGTACGTGATCTTGATCCCGAGCTTCGGGTGGAAAGTGGGTGGGAGAGTTCGAGGCCTTGCGCTTAAG
 GAGCCCTTCGCTCGTGTGAGTTGAGGCTGGCCTGGGGCGTGGGGCGCCGCTGCGAATCTGGTGGCACCTTCGCGCTGT
 CTGCTGCTTTCGATAAGTCTCTAGCCATTTAAAATTTTGTATGACCTGCTGCGACGCTTTTTTCTGGCAAGATAGTCTGTAAA
 TCGGGCCAAAGATCTGCACACTGGTATTTTCGGTTTTTGGGGCCCGGGCGCGACGGGGCCCGTGGTCCCAGCGCACATGTTCCG
 CGAGGCGGGGCTGCGAGCGCGGCCACCGAGAATCGGACGGGGTAGTCTCAAGCTGGCCGGCTGCTCTGGTGCCTGGCTCGCC
 CCGCGTGTATCGCCCCCGCTGGGCGGCAAGGCTGGCCCGGTGCGCACAGTTCGCTGAGCGGAAAAGATGGCCGCTTCCCGGCC
 TGCTGCAGGAGCTCAAATGGAGGACGCGCGCTCGGGAGAGCGGGCGGTGAGTCAACCCACACAAAGGAAAAGGGCCTTCCGT
 CCTCAGCCGTCGCTTCAATGTGACTCCAGGAGTACCGGGCGCCCTCCAGGCACCTCGATTAGTTCTCGAGCTTTTGGAGTACGTCG
 TCTTTAGGTTGGGGGGAGGGGTTTTATGCGATGGAGTTTCCCGACACTGAGTGGGTGGAGACTGAAGTGGCCAGCTTGGCACTT
 GATGTAATTCCTTGGAAATTGCCCCTTTTGAGTTGGATCTTGGTTCATTCTCAAGCCTCAGACAGTGGTTCAAAGTTTTTTTC
 TTCCATTTAGGTGTCGTGAGGAATTAGCTTGGTACTAATACGACTCACTATAGCCTGGCCACCATGAAGACCATCCTGGCCCTGA
 GCACCTACATCTTCTGCCTGGTGTTCGCGGAGCAGAAGCTGATCAGCGAGGAGGACCTGGCCTGCCAGGAGGCTAACTACGGTGCC
 CTCCTCCGGAGCTCTGCCTCACCCAGTTCAGGTAGACATGGAGGCCGTGGGGGAGACTCTGTGGTGTGACTGGGGCAGGACCAT
 CAGGAGCTACAGGGAGCTGGCCGACTGCACCTGGCACATGGCGGAGAAGCTGGGCTGCTTCTGGCCCAATGCAGAGGTGGACAGGT
 TCTTCTGGCAGTGCATGGCCGCTACTTCAGGAGCTGCCCATCTCAGGAGGGCCGTGGCGGACCCCGCCGCGCAGCATCTCTAC
 CCCTTCATCGTGGTCCCATCACGGTGACCCTGCTGGTGACGGCACTGGTGGTCTGGCAGAGCAAGCGCACTGAGGGCATTGTGTA
 GGACTGGGATCCGCCCCCTCTCCCTCCCCCCCCCTAACGTTACTGGCCGAAGCCGCTTGGAAATAGGCCGGTGTGCGTTTTGCTAT
 ATGTTATTTCCACCATATTGCCGCTTTTGGCAATGTGAGGGCCCGGAAACCTGGCCCTGTCTTCTTGACGAGCATTCCTAGGGG
 TCTTTCCCTCTCGCCAAAGGAATGCAAGGCTGTTGAAATGTCGTGAAGGAAGCAGTTCCTCTGGAAGCTTCTGAAGACAAACA
 CGTCTGTAGCACCCTTTGAGGCGAGCGGAACCCCACTGGCGACAGGTGCCTTGGCGCCAAAAGCCAGTGTATAAGATACA
 CCTGCAAAGGCGGCACAACCCAGTGCACGTTGTGAGTTGGATAGTTGTGAAAGAGTCAAATGGCTCTCCCAAGCGTATTCAA
 CAAGGGGCTGAAGGATGCCAGAAGTACCCCATTTGATGGGATCTGATCTGGGGCCTCGGTACACATGCTTTACATGTGTTTAGT
 CGAGGTTAAAAAACGTTAGGCCCCCCGAACCAGGGGACGTGGTTTTCTTTGAAAAACACGATGATAATATGGCCACAGCCAC
 CATGGTGAAGGAGCTGATTAAGGAGAACATGCACATGAAGCTGTACATGGAGGGCACCGTGAACAACCAACCACTCAAGTGCACAT
 CCGAGGGCCAAAGCCCTACGAGGGCACCCAGACCATGAGAATCAAGCCGTCGAGGGCGGCCCTCTCCCTTCGCTTCGAC
 ATCCTGGCTACCAGCTTCATGTAGCGCAGCAAAAACCTTCATCAACCCACACCCAGGGCATCCCCGACTTCTTTAAGCAGTCTTCCC
 CGAGGGCTTCACATGGGAGAGAGTCAACACATACGAAGATGGGGGGTGTGACCGCTACCCAGGACACCAGCTCCAGGACGGCT
 GCCTCATCTACAACGTCAGATCAGAGGGGTGAACCTCCCATCCAACCGCCCTGTGATGCAGAAGAAAACACTCGGCTGGGAGGCC
 TCCACCGAGACACTGTACCCCGCTGACGGCGGCTGGAAGGACAGCCGACATGGCCCTGAAGCTCGTGGGCGGGGGCCACTGAT
 CTGCAACCTTAAGACCACATACAGATCCAAGAAACCCGCTAAGAACCCTCAAGATGCCCGGCTTACTATGTGGACAGGACACTGG
 AAAGAATCAAGGAGGCCGACAAAAGACATACGTCGAGCAGCAGAGGTGGCTGTGGCCAGTACTGCGACCTCCCTAGCAAACCTG
 GGGCAAACTTAATTCCTGAGGGCGGCGCAGCCTGCTGACCTGGCGGCACTGGAGGAAAATCGAGGCCATGCGCTAAGCC

TTTGTCTCAAGAAGAATCCACCCTCATTGAAAGAGCAACGGCTACAATCAACAGCATCCCATCTCTGAAGACTACAGCGTCGCCA
GCGCAGCTCTCTCTAGCGACGGCCGCATCTTCACTGGTGTCAATGTATATCATTTTACTGGGGGACCTTGTGCAGAAGCTCGTGGT
CTGGGCACCTGCTGCTGCTGCGGCAGCTGGCAACCTGACTTGTATCGTCGCGATCGGAAATGAGAACAGGGGCATCTTGAGCCCTG
CGGACGGTGGCGACAGGTGCTTCTCGATCTGCATCCTGGGATCAAAGCCATAGTGAAAGGACAGTGATGGACAGCCGACGGCAGTTG
GGATTTCGTGAATTGCTGCCCTCTGGTTATGTGTGGGAGGGATAAGGGACAGGTGATATCCAGCACAGTGGCGGCCGCTCGACAATC
AACCTCTGGATTACAAAATTTGTGAAAGATTGACTGGTATTCTTAACATATGTTGCTCCTTTTACGCTATGTGGATACGCTGCTTTA
ATGCCTTTGTATCATGCTATTGCTTCCCGTATGGCTTTCATTTCTCCTCCTTGATAAAATCCTGGTTGCTGTCTCTTTATGAGGA
GTTGTGGCCCGTTGTCAGGCAACGTGGCGTGGTGTGACTGTGTTTGTGACGCAACCCCACTGGTTGGGGCATTGCCACCCT
GTCAGCTCCTTCCGGGACTTTCGCTTTCCTCCCTTATGCCACGGGGAACCTCATCGCCGCTGCTTGCCTGCTGTTGCCAC
GGGGCTCGGCTGTTGGGCACTGACAATTCGCTGGTGTGTGCGGGGAAAGTGTGACGTCCTTTCCATGGCTGCTCGCCTGTGTTGCCAC
CTGGATTCTGCGGGGACGCTTCTGCTACGTCCTTCCGCCCTCAATCCAGCGGACCTTCTTCCCGGGCTGCTGCCGGCTC
TGGCCCTCTCCCGCTTTCGCCCTTCGCCCTCAGACGAGTGGATCCTCCCTTTGGGCGCCTCCCGCTGGAATTTCTGAGATA
TCCGGTTAGTAATGAGTTTGAATTAATCTGTGGAATGTGTGTCAGTTAGGGTGTGAAAGTCCCAGGCTCCCAGGCAGGCAG
AAGTATGCAAAGCATGCATCTCAATTAGTCAGCAACCAGGTGTGAAAGTCCCAGGCTCCCAGCAGGCAGAAATGCAAAGCA
TGCATCTCAATTAGTCAGCAACCATAGTCCCGCCCTAATCCGCCCTAATCCCGCCCTAATCCCGCCAGTTCGCCCATTTCTCG
CCCCATGGCTGACTAATTTTTTTATTTATGTCAGAGCCGAGGCCGCTCTGCCTCTGAGCTATTCAGAAGTAGTGAGGAGGCTT
TTTTGGAGCCCTAGGCTTTTGCAAAAAGCTCCCTGTTGACAATTAATCATCGGCATAGTATATCGGCATAGTATAATACGACAA
GGTGAGGAACTAAACCATGGCCAAGTTGACCAGTGCCGTTCCGGTGTCTACCAGCGCGCAGCTCGCCGAGCGGTGAGTTCTGGA
CCGACCGGCTCGGGTCTCCCGGACTTCGTGGAGGACGACTTCGCCGTTGTTCCGGGACGACGTGACCTGTTTCATCAGCGG
GTCCAGGACAGGTGGTGGCGGACAACCCCTGGCCTGGGTGTGGGTGGCGGCCCTGGACGAGCTGTACGCCAGTGGTGGAGGT
CGTGTCCAGCAACTCCGGGACGCTCCGGCCGGCCATGACCAGAGTCCGGCAGCAGCCGTGGGGGGGGATTCGCCCTGCGCG
ACCCGGCCGCAACTGCTGACTCTGTGGCCGAGGAGCAGGACTGACAGCTGTACGAGATTTAAATGGTACTTTAAGACCAAT
GACTTACAAGCGAGCTGTAGACTCTTAGCCACTTTTTAAAAGAAAAGGGGGGACTGGAAAGGGCTAGCTCCTCCCAAGCAAG
ATCTGCTTTTTGCTTGTACTGGGTCTCTCTGGTTAGACCAGATCTGAGCCTGGGAGCTCTCTGGCTGCTAGGGAACCCACTGCTT
AAGCCTCAATAAAGCTTGCCTTGAAGTCTCAAGTAGTGTGTGCCCGCTCTGTTGTGTGACTCTGGTAACTAGAGATCCCTCAGACC
CTTTTAGTCACTGTGGAAAATCTCTAGCAAGTAGTAGTTTATGTCATCTTATTATTCAGTATTTATAAATTCGAAAGAAATGAATAT
CAGAGAGTGAGAGGAACCTGTTTATTGTCAGCTTATAATGGTTACAAATAAAGCAATAGCATCACAAATTTACAAATAAAGCATT
TTTTCACTGCATTCTAGTTGTGGTTTTGTCCAAACTCATCAATGTATCTTATCATGTCTGGCTCTAGCTATCCCGCCCTAATCCG
CCCAGTTCGGCCATTTCTCCGCCATGGCTGACTAATTTTTTTTATTTATGTCAGAGGCCGAGGCCGACGTGTGTTTCTTAGACGT
CAGGTGGCATTTCGGGGAAATGTGCGCGGAACCCCTATTTGTTTATTTTCTAAATACATTCAATATGTATCCGCTCATGAGA
CAATAACCCTGATAAATGCTTCAATAATATGAAAAAGGAAGAGTATGAGTATTCAACATTTCCGTGTGCCCTTATTCCCTTTTT
TGCGGCATTTGCTTCTGTTTTGCTCACCCAGAAACGCTGGTGAAGTAAAAGATGCTGAAGATCAGTTGGGTGCACGAGTGG
GTTACATCGAAGTGGATCTCAACAGCGGTAAGATCCTTGAGAGTTTTCCGCCCGAAGAACGTTTTTCCAATGATGAGCACTTTAAA
GTTCTGCTATGTGGCGCGTATTATCCCGTATTGACGCGGGCAAGAGCAACTCGGTGCCCGCATACTACTATTCTCAGAATGACTT
GGTTGAGTACTACCCAGTACAGAAAAGCATCTTACGGATGGCATGACAGTAAAGAAATATGTCAGTGTGCCATAAACCATGAGTG
ATAACACTGCGGCCAATTTACTTCTGACAACGATCGGAGGACCGAAGGAGCTAACCCTTTTTTGCAACAACATGGGGGATCATGTA
ACTCGCTTGATCGTTGGGAACCGGAGCTGAATGAAGCCATACCAACGACGAGCGTGACACCACGATGCCTGTAGCAATGGCAAC
AAGCTTCCGCAACTATTAACTGGCGAATCTTACTGACTCTCCTGCTCCTCCCGCAACAATTAATAGACTGGATGGAGCCGATAAAGT
CAGGACCACTTCTGCGCTCGGCCCTTCCGGCTGGCTGTTTTATTGCTGATAAATCTGGAGCCGGTGGAGCGTGGGTCTCGCGGTATC
ATTGACGACTGGGGCCAGATGGTAAGCCCTCCGCTATCGTAGTTATCTACACGACGGGGAGTCCAGGCAACTATGGATGACGAAA
TAGACAGATCCCTGAGATAGGTGCCCTACTGATTAAGCATTGGTAACTGTGACACCAAGTTTACTCATATATACTTTAGATTGATT
TAAAATCTATTTTTAATTTAAAAGGATCTAGGTGAAGATCCTTTTTGATAATCTCATGACCAAAATCCCTTAACGTGAGTTTTCG
TCCACTGAGCGTCCAGCCGTCAGAAAAGATCAAGGATCTCTTGAGATCCTTTTTTCTGCGGTAATCTGCTGTTGCAAC
AAAAAACCACCGCTACCAGCGGTGGTTTTGCTCCGGATCAAGACTACCAACTCTTTTTCCGAAAGTAACTGCTTCAGCAGAG
CGCAGATACCAAACTACTGTCTTCTAGTGTAGCCGTAGTTAGGCCACCCTCAAGAACTCTGTAGCACCGCCTACATACCTCGCT
CTGCTAATCCTGTTACCAGTGGCTGCTGCCAGTGGCGATAAGTCTGTGCTTACCAGGTTGGACTCAAGACGATAGTTACCAGGATAA
GGCGCAGCGGTGGGCTGAACGGGGGGTTCGTGCACACAGCCAGCTTGGAGCGAACGACCTACACCGAAGTGAATACCTACAGC
GTGAGCTATGAGAAAGCCACGCTTCCCGAAGGGAGAAGCGGACAGGTATCCGGTAAGCGGCAGGGTCGGAACAGGAGAGCGC
ACGAGGGAGCTTCCAGGGGGAAACGCTGGTATCTTTATAGTCTCTGCGGTTTTCCGCCACTCTGACTTGAGCGCTGATTTTTGTG
ATGCTCGTACAGGGGGCGGAGCCTATGAAAAACGCCAGCAACGCGGCCTTTTTACGGTTCTGCGCTTTTGTGCGCTTTTTGCTC
ACATGTTCTTTCTGCGTTATCCCTGATTCTGTGGATAACCGTATTACCCTTTGAGTGGCTGATACCGCTCGCCGACGCGA
ACGACCGAGCGCAGCGAGTCAAGTGGCGAGGAAGCGGAAGAGCGCCCAATACGCAAAACCGCTCTCCCGCGCGTTGGCCGATTCA
TTAATGCAGCTGGCAGCAGAGTTTCCGACTGGAAAGCGGGCAGTGGAGCGCAACGCAATTAATGTGAGTTAGCTCACTCATTAGG
CACCCAGGCTTTACACTTTATGCTTCCGGCTGTATGTTGTGGAATTTGTGAGCGGATAACAATTTACAGGAAACAGCTAT
GACCATGATTACGCCAAGCGCAATTAACCCCTACTAAAGGGAACAAAAGCTGGAGCTGCAAGCTTAATGTAGTCTTATGCAATA
CTCTTGTAGTCTTGCAACATGGTAACGATGAGTTAGCAACATGCCTTACAAGGAGAGAAAAGCACCGTGCATGCCGATTTGGTGA
AGTAAGGTGGTACGATCGTGCCTTATTAGGAAGCAACAGACGGGCTGACATGGATTGGACGAACCACTGAATTTGCCGATTTGCA
GAGATATTGATTAAAGTGCCTAGCTCGATAACAATAAAGGGTCTCTCTGGTTAGACCAGATCTGAGCCTGGGAGCTCTCTGGCTA
ACTAGGAACCCACTGCTTAAAGCTCAATAAAGCTTGCCTTGAGTGTCTCAAGTAGTGTGTGCCCGTCTGTTGTGTGACTCTGGTA
ACTAGGATCCCTCAGACCCTTTTACTGAGTGTGAAAAATCTTAGCAGTGGCGCCCGAACAGGACCTGAAAGCGAAAAGGGAAC
CAGAGCTCTCTGACGCGAGGACTCGGCTTGTGAAAGCGCGCACGGCAAGAGGCGAGGGGGCGGACTGGTGGTACGCCAAAAAT
TTGACTAGCGGAGGCTAGAAGGAGAGATGGGTGCGAGAGCGTCAATTAAGCGGGGGAGAATTAGATCGCGATGGGAAAAAT
TCGGTTAAGGCCAGGGGAAAGAAAAATATAAATTAACATATAGTATGGGCAACGAGGGAGCTAGAACGATTTCGAGTTAATC

CTGGCCTGTTAGAAACATCAGAAGGCTGTAGACAAATACTGGGACAGCTACAACCATCCCTTCAGACAGGATCAGAAGAAGCTTAGA
TCATTATATAATACAGTAGCAACCCCTCTATTGTGTGCATCAAAGGATAGAGATAAAAAGACACCAAGGAAGCTTTAGACAAGATAGA
GGAAGAGCAAAAACAAAAGTAAGACCACCGCACAGCAAGCGGCCGCTGATCTTCAGACCTGGAGGAGGAGATATGAGGGACAATTGG
AGAAGTGAATTATATAAAATATAAAGTAGTAAAAATTGAACCATTAGGAGTAGCACCCACCAAGGCAAAGAGAAGAGTGGTGCAGAG
AGAAAAAAGAGCAGTGGGAATAGGAGCTTTGTTCCCTTGGGTTCTTGGGAGCAGCAGGAAGCACTATGGGCGCAGCCTCAATGACGC
TGACGGTACAGGCCAGACAATTATTGTCTGGTATAGTGCAGCAGCAGACAATTGCTGAGGGCTATTGAGGCGCAACAGCATCTG
TTGCAACTCACAGTCTGGGGCATCAAGCAGCTCCAGGCAAGAATCCTGGCTGTGGAAAGATACCTAAAGGATCAACAGCTCCTGGG
GATTTGGGGTTGCTCTGGAAAACCTATTTGCACCCTGCTGTGCCTTGGAAATGCTAGTTGGAGTAATAAATCTCTGGAACAGATTG
GAATCACACGACCTGGATGGAGTGGGACAGAGAAATTAACAATTACACAAGCTTAATACACTCCTAATTGAAGAATCGCAAAACC
AGCAAGAAAAGAATGAACAAGAATTATTGGAATTAGATAAATGGGCAAGTTTGTGGAATTGGTTTAAACATAACAAATTGGCTGTGG
TATATAAAATTATTCATAATGATAGTAGGAGGCTTGGTAGGTTTAAAGAATAGTTTTTGTGCTGTACTTTCTATAGTGAATAGAGTTAG
GCAGGGATATTCACCATTTACGTTTTCAGACCCACCTCCCAACCCGAGGGGACCCGACAGGCCCGAAGGAATAGAAGAAGAGGTG
GAGAGAGAGACAGAGACAGATCCATTCGATTAGTGAACGGATCTCGACGGTTAACTTTTAAAAGAAAAGGGGGATTGGGGGTAC
AGTGCAGGGGAAAGAATAGTAGACATAATAGCAACAGACATACAACTAAAGAATTACAAAACAAATTACAAAATTCAAAATTT
TATTCCAGTGTGGTGAATCTGCAGTCTGC

Supplementary Table 2-S5. Sequence of transgene cassette for C505 (pLV-hEF1a-HA-CALCRL-IRES-EYFP-2A-Hygro)

color coding key:

HA-CALCRL: Human calcitonin receptor-like receptor preceded by the H. influenza hemagglutinin signal peptide and the influenza hemagglutinin antigen (HA) sequence

IRES: Internal ribosome entry site

EYFP: Enhanced yellow fluorescent protein

2A: Autoproteolytic viral amino acid sequence

Hygro: Hygromycin resistance gene

sequence:

```
ATGAAGACCCTCTGGCCCTGAGCACCTACATCTTCTGCCTGGTGTTCGCCTACCCCTACGACGTGCCCGTGTACGCCGCAGAATT
AGAAGAGAGTCCTGAGGACTCAATTCAGTTGGGAGTTACTAGAAATAAAAATCATGACAGCTCAATATGAATGTTACCAAAAGATTA
TGCAAGACCCCATTCACAAGCAGAAGGCGTTTACTGCAACAGAACCCTGGGATGGATGGCTCTGCTGGAACGATGTTGCAGCAGGA
ACTGAATCAATGCAGCTCTGCCCTGATTAATTTTCCAGGACTTTGATCCATCAGAAAAAGTTACAAAAGATCTGTGACCAAGATGGAAA
CTGGTTTAGACATCCAGCAAGCAACAGAACATGGACAAAATTTATACCCAGTGTAAATGTTAACACCCACGAGAAAAGTGAAGACTGCAC
TAAATTTGTTTTACCTGACCAATAATGGACACGGATTGTCTATTGCATCAGCTGCTTATCTCGCTTGGCATATTTCTTTATTTCAAG
AGCTTAAGTTGCCAAAGGATTAACCTTACACAAAAATCTGTTCTTCTCATTTGTTTGTAACTCTGTTGTAACAATCATTACCTGAC
TGCAAGTGGCCAAACAACCAGGCTTAGTAGCCACAATCCTGTAGTTGCAAAAGTGTCCAGTTTATTTCATCTTTACCTGATGGCT
GTAATTAATTTTGGATGCTCTGTGAAGGCATTTACCTACACACTCATTTGGTGGCCGTGTTTGCAGAGAAGCAACATTTAATG
TGGTATATTTTCTTGGCTGGGATTTCCACTGATTCCTGCTGTATACATGCCATTGCTAGAAGCTTATATTACAATGACAATTG
CTGGATCAGTCTGATACCCATCTCCTCTACATTAATCCATGGCCCAATTTGTGCTGCTTACTGGTGAATCTTTTCTTGTAA
ATATTGTACGGCTTCTCATACCAAGTAAAAGTTACACACCAAGCGGAATCCAATCTGTACATGAAAGCTGTGAGAGTACTCTT
ATCTTGGTGCCATTGCTTGGCATTGAATTTGTGCTGATTCATGGCGACCTGAAGGAAAAGATTGCAGAGGAGGTATATGACTACAT
CATGCACATCCTTATGCACTTCCAGGGTCTTTTGGTGTCTACCATTTCTGCTTCTTAAATGGAGAGGTTCAAGCAATCTGAGAA
GAAACTGGAATCAATACAAAATCCAATTTGGAAAACAGCTTTTCCAACCTCAGAAGCTCTCGGTAGTGGCTCTTACACAGTGTCAACA
ATCAGTGATGGTCCAGGTTATAGTCATGACTGTCTAGTGAACAATTAATGGAAAAAGCATCCATGATATTGAAAATGTTCTCTT
AAAACCCAGAAAAATTTATATAATTTGAGACTGGGATCCGCCCTCTCCCTCCCCCCCCCTAACGTTACTGGCCGAAGCCGCTTGAA
TAAGGCCGGTGTGCGTTTGTCTATATGTTATTTTCCACCATATTGCCGCTTTTGGCAATGTGAGGGCCCGGAAACCTGGCCCTGT
CTTCTTGACGAGCATTCTAGGGGTCTTCCCTCTCGCCAAAGGAATGCAAGGTCTGTTGAATGTCGTGAAGGAAGCAGTTCTCTC
TGGAAAGCTTCTTGAAGACAACAACGCTGTGTAGCGACCCTTTCAGGCAGCGGAACCCCCACCTGGCGACAGGTGCCCTGCGGGC
CAAAGCCACGTTGATATAAGATACACCTGCAAAAGGCGGCACAACCCAGTCCACGTTGTGAGTTGGATAGTTGTGGAAAGAGTCAA
ATGGCTCTCCTCAAGCGTATTCAACAAGGGGTGAAGGATGCCAGAAGTACCCCATTTGATGGGATCTGATCTGGGCTCGGT
ACACATGCTTTACATGTGTTTAGTCCAGGTTAAAAAACGCTTAGGCCCCCGAACCACGGGGACCTGGTTTTCTTTGAAAAACA
CGATGATAATATGGCCACAGCCACCATGGTGAAGCAAGGGCGAGGAGCTGTTACCAGGGTGGTGGCCATCCTGGTCGAGCTGGACG
GCGACGTAACGGCCACAAGTTCAGCGTGTCCGGCGAGGGCGAGGGCGATGCCACCTACGGCAAGCTGACCCCTGAAGTTCATCTGC
ACCACCGGAAGCTGCCCGTGCCTGGCCACCCTCGTGACCACCTTCGGCTACGGCTGCAGTGTCTCGCCCGCTACCCCGACCA
CATGAAGCAGCAGACTTCTCAAGTCCGCCATGCCGAAGGCTACGTCCAGGAGCGCACCATCTTCTTCAAGGACGACGGCAACT
ACAAGACCCGCGCCGAGGTGAAGTTCGAGGGCGACACCCTGGTGAACCGCATCGAGCTGAAGGGCATCGACTTCAAGGAGGACGGC
AACATCCTGGGGCACAAGCTGGAGTACAACATAACAGCCACAACGCTCTATATCATGGCCGACAAGCAGAAGAAGCGGCATCAAGGT
GAACCTCAAGATCCGCCACAACATCGAGGACGGCAGCGTGCAGCTCGCCGACCCTACCAGCAGAACACCCCATCGGGCAGCGCC
CCGTGCTGCTGCCCGACAACCACTACCTGAGCTACCAGTCCAAGCTGAGCAAAAGACCCCAACGAGAAGCGCGATACATGGTCTG
CTGGAGTTCGTGACCGCCCGGGATCACTCTCGGCATGGACGAGCTGTACAAGTAATGGAGGGTCCGGGTCAGCTGCTTGCCTG
CGGCCACTGGAGGAAAAGTCCGGGCTATGAAAAAGCCTGAACTCACCGCGACGCTCTGTGAGAAAGTTCCTGATCGAAAAGTTCG
ACAGCGTGTCCGACCTGATGCAGCTCTCGGAGGGCGAAGAACTCTGCTGCTTTCAGCTTCGATGTAGGAGGGCGTGGATATGCTCTG
CGGGTAAATAGCTGCGCCGATGGTTTCTACAAAAGATCGTTATGTTTATCGGCACCTTTCATCGGCCCGGCTCCCGATTCCGGAAAGT
GCTTGACATTTGGGGAATTCAGCGAGAGCCTGACCTATTGCATCTCCCGCGTGCACAGGGTGTGACGTTGCAAGACCTGCCTGAAA
CCGAACTGCCCGCTGTTCTGCAGCCGGTCCGCGGAGGCATGGATGCGATCGCTGCGGCCGATCTTAGCCAGACGAGCGGGTTCCGG
CCATTCGGACCCGAAGGAATCGGTCAATACACTACATGGCGTATTTCATATGCGCGATGCTGATCCCCATGTGATACCTCTCTG
GCAAACTGTGATGGACGACACCGTCACTGCCTCCGTCGCGCAGGCTCTCGATGAGCTGATGCTTTGGCCGAGGACTGCCCGAAG
TCCGGCACCTCGTGCACGGGATTTCCGCTCCAACAATGTCTGACGGACAATGGCCGATAACAGCGGTCAATGACTGGAGCGAG
GCGATGTTCCGGGATTTCCCAATACGAGGTCGCCAACATCTTCTTCTGGAGGCGGTGGTTGGCTTGTATGGAGCAGCAGACGCGCTA
CTTCGAGCGGAGGCATCCGGAGCTTGCAGGATCCCGCGGCTCCGGGCTATATGCTCCGATTTGGTCTTGACCAACTCTATCAGA
GCTTGGTTGACGGCAATTTGATGATGCAGCTTGGGCGCAGGGTTCGATGCGACGCAATCGTCCGATCCGGAGCCGGGACTGTCCGG
CGTACACAAATCGCCCGCAGAAGCGCGCCGCTCTGGACCGATGGCTGTGTAGAAGTACTCGCCGATAGTGGAAACCGACGCCCCAG
CACTCGTCCGATCCGGAGATGGGGGAGGCTAACTGA
```

Supplementary Table 2-S6. Sequence of transgene cassette for C512: pLV-hEF1a-Glo22F-IRES-H2B-Cerulean-2A-puro

color coding key:

Glo22F: Engineered cAMP-responsive luciferase (Promega Corp.)

IRES: Internal ribosome entry site

H2B-Cerulean: DNA binding domain of histone 2B fused to Cerulean

2A: Autoproteolytic viral amino acid sequence

Puro: Puromycin resistance gene

sequence:

ATGCCTGGCGCAGTAGGCAAGGTGGTGCCTTCATCGAGGCTAAGGTGGTGGACTTGGACACTGGTAAGACACTGGGTGTGAACCA
 GCGGGCGAGCTGTGCGTCCGTGGCCCATGATCATGAGCGGTACGTTAACACCCCGAGGCTACAAACGCTTCATCGACAAGG
 ACGGCTGGCTGCACAGCGCGACATCGCCTACTGGGACGAGGACGAGCACTTCTTCATCGTGGACCGGCTGAAGAGCCTGATCAAA
 TACAAGGGCTACCAGGTAGCCCCAGCCGAACCTGGAGAGCATCCTGCTGCAACACCCCAACATCTTCGACGCCGGGGTCGCCGCCCT
 GCCCGACGACGATGCCGGCGAGCTGCCCGCCGAGTCTGCTGCTGGAACACGGTAAAACCATGACCGAGAAGGAGATCGTGGACT
 ATGTGGCCAGCCAGGTTACAACCGCCAAGAAGCTGCGCGGTGGTGTGTGTAGTGGACGAGGTGCCTAAAGGACTGACCCGGCAAG
 TTGGACGCCCGCAAGATCCGCGAGATTCTCATTAAGGCCAAGAAGGGATCCAATTGGGATTCTGGGTGCTCCAGAGAAGGTATGTA
 TGAAGCTTTATTGAGTCACTGCCATTCCTTAAATCTTTGGAGTTTTCTGCACGCTGAAAGTAGTAGATGTGATAGGCCACCAAG
 TATAACAACGATGGAGAACAATCATTTGCTCAGGGAGATTCCGGCTGATTTCTTTTTTTCATTATTGAATCTGGAGAAGTGAATTTACT
 ATGAAAAGAAAGGGTAAATCAGAAGTGAAGAGAAATGGTGCAGTAGAAATCGCTCGATGCTCGCGGGGACAGTACTTTGGAGAGCT
 TGCCCTGGTAACTAACAACCTCGAGCAGCTTCTGCCACGCCATTGGGACTGTCAAATGTTTAGCAATGGATGTGCAAGCATTG
 AAAGGCTTCTGGGACCTTGCATGGAATATGAAAAGGAACATCGCTACCTATGAAGAACAGTTAGTTGCCCTGTATGGAACGAAC
 ATGGATATTGTAGCAAAAACATTAAGAAGGGCCAGCGCCATTCTACCCACTCGAAGACGGGACCCTCGGGCAGCAGCTGCACAA
 AGCCATGAAGCGCTACGCCCTGGTGCCCGGCACCATCGCCTTTACCGACGCACATATCGAGGTGGACATTACCTACGCCGAGTACT
 TCGAGATGAGCGTTTCGGCTGGCAGAAGCTATGAAGCGCTATGGGCTGAATACAAACCATCGGATCGTGGTGTGACGCGAGATAGC
 TTGCAGTTCTTCATGCCCGTGTGGGTGCCCTGTTTCATCGGTGTGGCTGTGGCCCCAGCTAACGACATCTACACGAGCGCGGAGCT
 GCTGAACAGCATGGGCATCAGCCAGCCACCGTTCGATTCGTGAGCAAGAAAGGGCTGCAAAAGATCCTCAACGTGCAAAAGAAGC
 TACCGATCATACAAAAGATCATCATCGGATAGCAAGACCGACTACCAGGGCTTCCAAAGCATGTACACCTTCGTGACTTCCCAT
 TTGCCACCCGGCTTCAACGAGTACGACTTCGTGCCGAGAGCTTCGACCGGGACAAAACCATCGCCCTGATCATGAACAGTAGTGG
 CAGTACCGGATTGCCCAAGGGCGTAGCCCTACCGCACCACCGCTTGTGTCCGATTAGTTCATGCCCGCAGCCCATCTTCGGCA
 ACCAGATCATCCCCGACACCGCTATCCTCAGCGTGGTGCATTTTACCACGGCTTCGGCATGTTACCACGCTGGGCTACTTGATC
 TGCGGCTTTCGGGCTCGTGCATGTACCGCTTCGAGGAGGAGCTATTCTTGCGCAGCTTGAAGACTATAAGATTCAATCTGCCCT
 GCTGGTGGCCACACTATTAGCTTCTTCGCTAAGAGCACTCTCATCGACAAGTACGACCTAAGCAACTTGCACGAGATCGCCAGCG
 GCGGGCGCCGCTCAGCAAGGAGGTAGGTGAGGCCGTGGCCAAACGCTTCCACCTACCAGGCATCCGCCAGGGCTACGGCTGACA
 GAAACAACCAGCGCCATTCGTATCACTCCAGAAGGGGTTAAACTGGGATCGGCCCTCTCCCTCCCCCCCCCTAACGTTACTG
 GCCGAAGCCGCTTGGAAATAAGGCCGGTGTGCGTTTGTCTATATGTTATTTTCCACCATATTGCCGCTTTTGGCAATGTGAGGGCC
 CGAAACCTGGCCCTGTCTTCTTGACGAGCATTCTAGGGGTCTTTCCCTCTCGCCAAAGGAATGCAAGGTCTGTTGAATGTGCT
 GAAGGAAGCAGTTCCTCTGAAGCTTCTTGAAGACAACAACGCTGTAGGACCCCTTTCGAGGACCCCTTTCGAGGACGCCAACCCACCTGGCG
 ACAGGTGCCCTTCGCGCCAAAAGCCAGCTGTATAAGATACACCTGCAAAAGCGGCGACAACCCAGTGCACGTTGTGAGTTGGATA
 GTTGTGGAAGAGTCAAATGGCTCTCTCAAGCGTATTCAACAAGGGGCTGAAGGATGCCAGAAGGTACCCCATTTGATGGGATC
 TGATCTGGGGCTCGGTACACATGCTTTACATGTGTTAGTTCGAGGTTAAAAAACGTTCTAGGCCCCCGAACCACGGGGACGTGG
 TTTTCTTTGAAAAACAGCATGATAATATGGCCACAGCCACATGCCAGAGCCAGCGAAGTCTGCTCCCGCCCCGAAAAAGGGCTC
 CAAGAAGCGGCTGACTAAGGCGCAGAAGAAAGCGGCAAGAAGCGCAAGCGCAGCCGAAGGAGAGCTATTCATCTATGTGTACA
 AGGTTCTGAAGCAGGTCCACCTTGACACCGGCATTTCTGTCAAAGCCATGGGCATCATGAATTCGTTTGTGAACGACATTTTCGAG
 CGCATCGCAGGTGAGGCTTCCCGCTGGCGCATTAACAACAGCGCTCGACCATCACCTCCAGGGAGATCCAGACGGCCGTGCGCCT
 GCTGCTGCCCTGGGAGTTGGCCAAGCAGCCGTGTCGGAGGTAATAAGGCATCACCAAGTACACCAGCGCTAAGGATCCCGGG
 TACCGGTTCGCCACCATGGTGAAGGCGAGGAGCTGTTACCGGGGTGGTGCCTATCCTGGTTCGAGCTGGACGGCGACGTAAC
 GGCCACAAGTTCAGCGTGTCCGGCGAGGGCGAGGGCGATGCCACCTACGGCAAGCTGACCTGAAGTTTCATCTGCACCACCGGCA
 GCTGCCCTGCCCTGGCCACCTCGTGACCACCTGACCTGGGGCGTGCAGTGTCTTCGCCGCTACCCCGACCACATGAAGCAGC
 ACGATTCTTCAAGTCCGCCATGCCGAAGGCTACGTCAGGAGCGACCATCTTCTTCAAGGACGACGGCAACTACAAGACCCGC
 GCCGAGGTGAAGTTCGAGGGCGACACCTGGTGAACCGCATCGAGCTGAAGGGCATCGACTTCAAGGAGGACGGCAACATCCTGGG
 GCACAAGCTGGAGTACAACGCCATCAGCGACAACGCTATATACCCGCGACAAGCAGAAGAACGGCATCAAGGCCAACTTCAAGA
 TCCGCCACAACATCGAGGACGGCAGCGTGCAGCTCGCCGACCCTACCCAGCAGAACACCCCATCGCGCAGCCCGCCGCTGCTGT
 CCGGACAACCACTACCTGAGCACCAGTCCAAGCTGAGCAAAAGACACCCCAACGAGAAGCGCATCACATGGTCTGCTGAGTTCGT
 GACCCCGCCGGGATCACTCTCGGCATGGACGAGCTGTACAAGGAGGGCCGGCAGCTGACTGACCTGCGGGCAGCTGGAGGAAA
 ACCCGGCCCCATGACCGAGTACAAGCCACGGTGCGCCCTCGCCACCCCGCAGCAGCTCCCCGGGGCGTACGCACCCTCGCGCC
 GCTTCGCCGACTACCCCGCCACGGCCACACCGTTCGACCCGGACCGCCACATCGAGCGGGTCCCGAGCTGCAGAAGTCTTCTCT
 CACGCGCGTCCGGCTCGACATCGGCAAGGTGTGGTTCGCGGACGACGGCCCGCGGTGGCGGTCTGGACCACGCCGGAGAGCTCG
 AAGCGGGGGCGGTTCGCGGAGATCGGCCCGCATGGCCGAGTTGAGCGGTTCCCGGTGGCCCGCAGCAACAGATGGAAGGC

CTCCTGGCGCCGCACCGGCCAAGGAGCCCGCTGGTTCCCTGGCCACCCTCGGGCTGTCGCCCGACCACCAGGGCAAGGGTCTGGG
CAGCGCCGTCGTGCTCCCGGAGTGGAGCGGCCGAGCGCCCGGGTGCCTGCTTCCCTGGAGACCTCCGCGCCCGCAACCTCC
CCTTCTACGAGCGGCTCGGCTTACCGTCACCGCCGACGTGGAGGTGCCGAAGGACCGCGCACCTGGTGCATGACCCGCAAGCCC
GGTGCCTGA

Vasoactive probes as genetic reporters for cell tracking by MRI

Abstract

Genetically encodable imaging agents could be used for molecular imaging in intact animals without the need for invasive probe delivery, but previously reported genetically encodable molecular MRI contrast agents have required too high concentrations to be useful for imaging after expression and secretion *in situ*. Here we implement MRI imaging of vasoactive peptidic probes secreted by genetically modified cells implanted in rat brains. We take advantage of the low nanomolar sensitivity of the vasoactive imaging approach we demonstrated previously to achieve MRI tracking of xenografted cells *in vivo* without exogenous contrast agents. Beyond the utility of vasoactive imaging probes as genetic reporters for cell tracking per se, our results suggest that analyte-switchable forms of such probes could potentially be expressed at sufficient concentrations in the brains of transgenic animals to obviate the need for probe delivery across the blood-brain barrier and enable noninvasive longitudinal molecular imaging studies.

Introduction

Increasing probe sensitivity and enabling delivery across the blood-brain barrier have been identified as the two most central, related but distinct, challenges for molecular MRI in intact animals¹⁷. In our previous work (Chapter 2), we have demonstrated that imaging the action of engineered vasoactive neuropeptides requires only low nanomolar probe concentrations, or 3-4 orders of magnitude less than previously reported protein-based molecular MRI probes²¹, while retaining the advantages of polypeptides as probes. These advantages include ease of iterative engineering by established protein engineering methods and versatility with respect to different modes of modulation by analytes which have been widely

implemented, for example, in switchable optical probes based on fluorescent proteins – and also the possibility of genetic encoding and expression *in situ*.

Vasoactive neuropeptides such as CGRP are naturally secreted to exert their action at their physiologically relevant concentrations, raising the possibility that the concentration needed for activity and the concentration achievable by expression and secretion *in vivo* have already been brought into harmony by evolutionary processes. Furthermore, we have previously shown that direct intracranial injection of 100 nM solutions of CGRP (which after accounting for dilution post-injection we estimated to correspond to effective concentrations *in vivo* on the order of 10 nM) elicits a strong signal change in T_2 -weighted MRI, which lies within the low-to-high nanomolar concentration range typical for secreted signaling proteins. Thus, we hypothesized that we should be able to image CGRP produced *in situ*.

The conceptually and experimentally simplest test of this hypothesis is the application of CGRP as a genetic reporter for cell tracking by MRI. Radioactive probes have been used for cell tracking and offer high sensitivity but low resolution and higher toxicity. Cell tracking *in vivo* by noninvasive MRI is a promising research tool in areas such as regenerative medicine (where the descendants of engrafted stem cells are tracked), tumor biology (where brain metastases formed from distal tumors could be assessed early), or immunology (where homing immune cells are traced), given an imaging probe and strategy appropriate for the specific task at hand^{28,52}. MRI cell tracking has been used in human patients clinically to trace implanted cells loaded exogenously with iron-rich nanoparticles²⁸, but such “pre-loading” is limited by loss of signal due to dilution as cells divide and by false positives from nanoparticle uptake by other cells after the death of the engrafted cells⁷⁶. Several kinds of reporter genes for cell tracking by MRI have been reported⁵². Some such reporter genes are simply cell surface epitopes or enzymes which rely on an externally administered conventional contrast agent, limiting their utility in the brain. Others achieve iron accumulation inside the cell by overexpression of iron transporters such as TfR or of iron storage proteins such as ferritin. However, at sufficient concentrations for facile imaging, such strategies can severely perturb iron metabolism and cellular phenotypes^{76,77}. Finally, lysine-rich proteins (LRPs) can serve as CEST

agents, but these are in an early stage of development and likely lack the flexibility and versatility to engineer responsive probes beyond passive tracers⁷⁸.

We therefore endeavored to validate genetic reporters based on the vasoactive peptide CGRP for cell tracking by MRI to extend the available repertoire of MRI reporter genes and to open up the future possibility of *in situ* expression of analyte-responsive MRI probes.

Results

As an initial test of this idea, we sought to determine whether xenografted cells genetically modified to constitutively secrete CGRP could be visualized by imaging in the rat brain, as schematized in Fig. 3-1. Endogenous CGRP is produced by proteolytic processing of a prepro peptide and exported by machinery common to mammalian cells. To exploit this mechanism artificially, we constructed a bicistronic vector encoding prepro-CGRP as well as the fluorescent protein mKate linked to the ampicillin resistance gene *Bla* via a self-cleaving 2A peptide (Fig. 3-2a). HEK293FT cells were transfected with this construct or with a control vector encoding only mKate-2A-*Bla* and cultured on selective medium to obtain stable lines. CGRP production was assessed by washing the cells and then performing the RAMP1/CLR activation bioassay described previously (Chapter 2) on aliquots of growth medium withdrawn at defined time intervals following the wash. Results were compared with a standard curve obtained with known amounts of synthetic CGRP and demonstrated that cells expressing prepro-CGRP release an average of between 10^{-19} and 10^{-18} mol CGRP per cell over a 24 hour period. Given the detection limit for CGRP below 10 nM by MRI in rat brains, we predicted that cell densities between 10^4 and 10^5 cells/ μ L should be easily detectable over analogous time periods *in vivo*. This is competitive with existing genetic MRI reporters for cell tracing¹⁷ and could be further optimized if desired.

Cells expressing the prepro-CGRP/mKate-2A-*Bla* vector or the control vector were injected intracranially into rat striatum and imaged at time points immediately before and one day after implantation. Signal brightening consistent with vasodilation in the neighborhood of the CGRP cell injection, but not the

control injection, was discernable by simple visual inspection of T_2 -weighted MRI scans obtained at the 24 hour time point (Fig. 3-2b). Quantitative analysis of the signal change observed between day 0 and day 1 (Fig. 3-2c) revealed an average of $23 \pm 3\%$ signal change induced in the region of CGRP-expressing cells and an average of $7 \pm 2\%$ signal change induced near control cells; this difference was highly significant (t -test $p = 0.01$, $n = 5$), demonstrated specific detection of the CGRP expression construct. The larger magnitude of observed signal change, compared with effects of acute CGRP injection (Chapter 2), may reflect a greater extent of affected tissue. Importantly, the region of MRI signal enhancement observed in individual animals corresponded closely to the distribution of transplanted prepro-CGRP-expressing cells, as indicated by post-mortem histological analysis of mKate fluorescence after MRI procedures (Fig. 3-3). Injected control cells displayed robust mKate expression in the absence of MRI enhancements, and neither test nor control injections resulted in gross tissue disruption or evidence of toxicity (Fig. 3-3).

Discussion

Our results allow us to confirm the utility of CGRP as a genetic tool for cell monitoring in the brain. Importantly, applications can be envisioned which combine genetic control of vasoprobe with analyte-switchable behavior to probe both internal cell state and the extracellular biochemical context of genetically specified cell populations, a key problem in the field²⁷. Depending on the needs of the specific experimental applications, one can envision the use of constitutively expressing, cell-type specific, or inducible promoters, and of constitutively active, ligand-responsive, or otherwise biologically modulated vasoactive peptides.

Important caveats include the need for further evaluation of safety and possible crosstalk with endogenous signaling. While we saw no evidence of histological abnormalities or other pathologies in rats implanted with CGRP-expressing cells, longer studies and examination of biological functions immediately relevant to a particular class of research problem (e.g. regenerative therapy, immunology, cancer, etc.) will be required to validate the routine use of such reporters. Potential crosstalk with

endogenous signaling includes both the misidentification of endogenous changes in vascular tone as tracked cells, and the perturbation of endogenous neuropeptide signaling by secretion of the probe. Both toxicity and crosstalk could be mitigated by either using an inducible promoter so that the reporter gene would lie dormant until activated or by use of an analyte-switchable form of the reporter gene, which would be constitutively expressed and secreted but only become active in the presence of a biorthogonal, BBB-permeable small molecule.

Furthermore, it must be noted that RARE MRI is not commonly used for imaging hemodynamics, and is not as strongly T_2^* -weighted as the more typical EPI protocol. Therefore, it will be necessary to investigate more carefully what the basis for the CGRP-dependent signal change which we observed really is. Beside blood oxygenation and blood volume, it is possible that fluid accumulation could lead to a brightening of the RARE signal. While histology did not indicate any tissue abnormalities, a more extensive investigation into possible edema could be warranted.

Despite these objectives for future work, we have validated with our results to date the utility of CGRP as an MRI reporter gene for cell tracking in principle and open up the possibility of endogenous expression of switchable probes based on CGRP without the need of trans-BBB delivery.

Materials and methods

Most general laboratory methods including cloning, cell culture, and animal care were performed as in Chapter 2. The following methods are new or different in the study in this chapter.

MRI of implanted cells

High resolution T_2 -weighted anatomical scans of each of animal ($n = 5$) were obtained using a RARE pulse sequence with $TE = 44$ ms, recycle time (TR) = 2500 ms, RARE factor = 8, spatial resolution = $100 \mu\text{m} \times 100 \mu\text{m} \times 1000 \mu\text{m}$, and matrix size = 128×128 with 7 slices before injecting

HEK293FT cells (day 0). After an initial scan, 3 μL of the cell suspension solution ($\sim 100,000$ cells/ μL) was intracranially injected in CPu (CGRP-expressing cells in left hemisphere and control cells in the right hemisphere) at the rate of 0.1 $\mu\text{L}/\text{min}$. Animals were taken out from the scanner, recovered from anesthesia, and returned to their home cages.

Animals were reimaged 24 hours after the cell injection (day 1) using the same scan parameters as applied before the cell injection. To quantify the signal change in the T_2 -weighted MRI images, day 0 and day 1 datasets were registered with each other using the 3dAllineate routine in AFNI. For visualization, maps of percent signal change on day 1 compared to day 0 were then arithmetically computed and a map of average changes was overlaid in color over a grayscale anatomical image. Thresholds for display were chosen based on signal changes observed outside the regions of cell injection. Quantification of the percent signal change on day 1 compared to day 0 was performed within 1.5 x 1.5 mm square regions of interest (white squares in Fig. 3-2d) defined around the sites of CGRP or control cell injection.

Histology

After MRI cell tracking experiments, animals were transcardially perfused with phosphate buffered saline (PBS) followed by 4% formaldehyde in PBS. Brains were extracted, post-fixed overnight at 4 $^{\circ}\text{C}$, and then cryoprotected in 30% sucrose for 24-48 h before sectioning. Free-floating sections (50 μm) were cut using a vibratome (Leica VT1200 S, Leica Microsystems GmbH, Wetzlar, Germany), mounted on glass slides with Vectashield mounting medium with DAPI (Vector Laboratories, Burlingame, CA) and protected with a coverslip. The distribution of injected HEK293FT cells was indicated by red fluorescence due to mKate2 reporter expression in both CGRP-producing and control cells.

In vitro bioassay for CGRP secretion

Gelatin-coated 6-well tissue culture plates were seeded with 10^6 HEK293FT cells per well carrying a lentiviral transgene (either C503 prepro-CGRP or C501 control) on day 1. On day 2, each well

was covered by approximately 2×10^6 confluent, contact-inhibited cells. The medium was aspirated, the cell layers were washed twice with fresh medium, and 2 mL fresh medium were added. Aliquots of the culture supernatant (100 μ L) were taken immediately and again after 24 hours (on day 3). To quantify the CGRP-like bioactivity in the culture supernatants, 10 μ L of each sample was added to bioassay wells containing 90 μ L CO₂-independent medium, in triplicate. As a positive control and reference standard, known dilutions of synthetic wtCGRP (Sigma) were prepared in culture medium + 0.1 % CHAPS and added at the same 1:10 dilution. Culture medium alone served as the buffer-only control.

CGRP secretion (in mol per cell per day) was calculated from the CGRP bioactivity in the culture supernatant (in nM) by assuming 2×10^6 in 2 mL medium, or 10^9 cells/L and therefore multiplying the measured concentration by 10^9 (nM/M) \times 10^9 (cells/L). The required concentration of cells (in cells/ μ L) for *in vivo* detection was calculated by assuming a need for 10 nM CGRP (10^{-8} mol/L = 10^{-14} mol/ μ L) per day by the quantity of secreted CGRP (in mol per day) per cell.

Preparation of cells for *in vivo* implantation

HEK293FT cells carrying a C503 prepro-CGRP or a C501 control lentiviral expression cassette were seeded at 50% confluence (7.5×10^6 cells per plate) in 10 cm cell culture plates and grown to confluence overnight. The next day, the cell layer was washed twice with fresh medium, aspirated, and scraped. The total volume was adjusted to 150 μ L with fresh medium for a density of 10^5 cells/ μ L and pipetted up and down to break up clumps until a homogenous cell suspension was obtained. Dispersion and integrity of cells was confirmed by brightfield microscopy.

Figures and tables

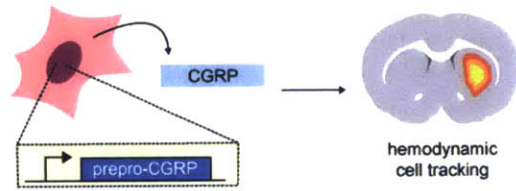


Fig. 3-1: Concept for using CGRP as a genetic reporter for cell tracking.

A genetic construct encoding prepro-CGRP is introduced into cells of interest, and the amino acid sequence it encodes fully directs the posttranslational processing and constitutive secretion of mature CGRP peptide. The constant release of CGRP from such cells after implantation into the brain then allows for cell tracking by imaging vasodilation without administration of an exogenous imaging agent.

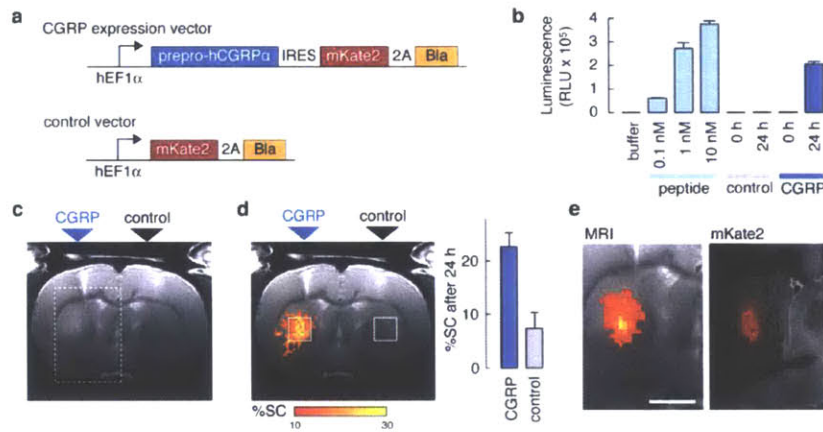


Fig. 3-2: Application of CGRP as a genetically expressed vasoactive reporter.

- (a) Lentiviral vectors were used for expression of prepro-CGRP or a control construct. Top: probe vector controlled by the hEF1 α promoter, encoding human prepro-CGRP (prepro-hCGRP α), an internal ribosome entry site (IRES), and the red fluorescent protein mKate2 joined by a self-cleaving viral 2A peptide to the blasticidin selection marker (Bla). Bottom: control vector lacking prepro-hCGRP α and the IRES sequence. Full sequences are given in the Supplementary Tables.
- (b) *In vitro* demonstration of substantial CGRP release from transfected HEK293FT cells. RAMP1/CLR activation by aliquots of purified CGRP peptide (light blue) or supernatants from cultured cells expressing control (gray) and prepro-CGRP (dark blue) lentiviral constructs was measured using the bioassay of Supplementary Fig. 2. Cell supernatants were assayed at 0 h and 24 h after an initial washing, and all samples were assayed at 10-fold dilution.
- (c) *In vivo* detection of implanted HEK293FT cells producing CGRP in rat brains. A representative T_2 weighted MRI scan obtained 24 h after striatal injection of 3×10^5 CGRP-producing or control cells (labels above) shows discernable signal enhancement consistent with probe-induced vasodilation in the CGRP injection region (dashed box) but not near the control injection site opposite.
- (d) Left: group-averaged map (left) displaying percent signal change (%SC, color scale) observed between 0 h and 24 h after cell implantation, averaged over five animals. Right: mean %SC in the square regions of interest superimposed on the image.
- (e) Correspondence of MRI signal change (left, color scale as in d) measured *in vivo* and mKate expression (right, red superimposed over a bright field image) visualized postmortem in a representative animal. The field of view corresponds to the rectangular box in panel c. Scale bar = 2 mm.

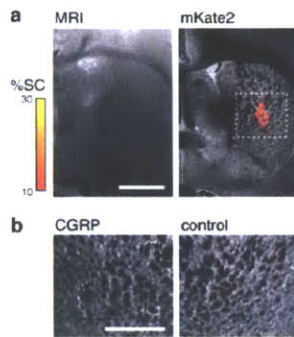


Fig. 3-3. MRI and histological signals from injected control cells.

- (a) Comparison of MRI (left) and optical microscopy (right) images of a field of view near injection of control HEK293FT cells in an individual animal, paralleling the data in main text Fig. 3-2e. The MRI scan shows no colored voxels overlaid on the grayscale anatomical image because MRI signal changes over 10% were not observed within a day of control cell implantation; this is in contrast to MRI results from CGRP-expressing cells in Fig. 3-2e. The histological image shows a bright field grayscale image, with mKate fluorescence in red overlaid to indicate the distribution of injected cells. Scale bar = 2 mm.
- (b) Close-ups of bright field images in the neighborhood of cell implantation on CGRP-expressing (left) and control cell (right) injection sites in a representative animal, showing normal patch-matrix striatal structural organization on both sides. The field of view corresponds to the rectangular box in panel a (right). Scale bar = 1 mm.

Table 3-S1: Catalog of plasmids used in this study

ID	Name	Source
C504	pLV-hEF1a-myc-RAMP1-IRES-mKate-2A-bla	Chapter 2
C505	pLV-hEF1a-HA-CALCRL-IRES-EYFP-2A-Hygro	Chapter 2
C512	pLV-hEF1a-Glo22F-IRES-H2B-Cerulean-2A-puro	Chapter 2
C501	pLV-hEF1a-mKate-2A-bla	This study
C503	pLV-hEF1a-prepro-CGRP-IRES-mKate-2A-bla	This study
X106	pMD2.G	Addgene 12259
X107	psPAX2	Addgene 12260
X108	pLenti X1 Zeo DEST (668-1)	Addgene 17299
X109	pEF-ENTR A (696-6)	Addgene 17427

Supplementary Table 3-S2. Full sequence of lentiviral plasmid C501 (pLV-hEF1a- mKate-2A-bla)

color coding key:

hEF1a: Human elongation factor 1 alpha promoter

Transgene cassette: mKate2: Red fluorescent protein

2A: Autoproteolytic viral amino acid sequence

Bla: Blastidicin resistance gene

delta_U3 / 3'LTR: HIV 3'LTR with deletion in the U3 region

AmpR: Ampicillin resistance gene

pUC origin of replication

RSV / 5'LTR: Rous Sarcoma Virus / HIV 5'LTR hybrid promoter

Psi: Lentiviral Psi packaging sequence

RRE: Rev response element

CPPT: Central polypurine tract

sequence:

CTTTGCAGCTAATGGACCTTCTAGGCTTGAAAGGAGTGGSAATTGGCTCCGGTGCCTCAGTGGGCAGAGCCACATCGCCAC
 AGTCCCGGAGAAGTTGGGGGAGGGCTCGGCAATTGAACCGTGCCTAGAGAAGGTGGCGGGGTAACCTGGGAAAGTGAITGCG
 TGTACTGGCTCCGCTTTTTCCCGAGGGTGGGGGAGAACCCTATATAAGTGCAGTAGTCGCCGTGAACGTTCTTTTCGCAACGGG
 TTTGCCGCCAGAACACAGGTAAGTGCCTGTGTGGTTCCCGCGGCCTGGCCTCTTTACGGGTTATGGCCCTTGGCGTGCCTGAAT
 TACTPCCACCTGGCTGCAGTACGTGATCTTGTATCCCGAGCTTCGGGTTGGAAGTGGTGGGAGAGTTCGAGGCCTTGGCCTTAAG
 GAGCCCTTCGCTCCTGCTTGAAGTGGAGCCTGGCCTGGGGCCTGGGGCCGCGCTGCCAATCTGGTGGCACCTTCGCGCCTGT
 CTCGCTGCTTTCGATAAGTCTCTAGCCATTTAAAATTTTGTATGACCTGCTGCCACGCTTTTTTCTGGCAAGATAGTCTGTAAA
 TCGGGCCAAGATCTGCACACTGGTATTTCCGTTTGGGGCCGCGGGCCGCGCACGGGGCCCGTGGTCCCAGCGCACATGTCGG
 CGAGGCGGGGCTGCGAGCCGCGCCACCGAGAATCGGACGGGGTAACTCAAGCTGGCCGGCTCTGCTGGTGCCTGGCCGCGC
 CCGCGTGTATCGCCCGCCTGGGGCGCAAGGCTGGCCCGTGGCCACAGTTGCGTGGCGGAAAGATGGCCGCTTCCCGGCC
 TGCCTGAGGGAGCTCAAAATGGAGGACCGGGCCTCGGGAGAGCGGGCGGTGAGTCAACCACACAAGGAAAAGGGCCTTCCCGT
 CCTCAGCCGCTCGCTTCATGTGACTCCACGGAGTACCGGGCGCGCTCCAGGCACCTCGATTAGTTCGAGCTTTGGAGTACGTCG
 TCTTTAGGTTGGGGGAGGGGTTTTATGCGATGGAGTTTCCCCACACTGAGTGGGTGGAGACTGAAGTTAGGCCAGCTTGGCACTT
 GATGTAATTCTCCTTGGAAATTGCCCTTTTGGATTTGGATCTTGGTTCATTCTCAAGCCTCAGACAGTGGTTCAAAGTTTTTTTC
 TTCCATTTAGGTGTCGTGAGGAATTAGCTTGGTACTAATACGACTCACTATAGCCTGGCCACCATGGTGGAGCTGATTAAGG
 AGAACATGCACATGAAGCTTACATGGAGGGCACCGTGAACAAACCACCTTCAAGTGCACATCCGAGGGCGGAAGGCAAGCCCTAC
 GAGGGCACCCAGACCATGAGAATCAAGGCGGTGAGGGCGGGCCTCTCCCTTCGCTTCGACATCCTGGCTACCAGCTTCATGTA
 CGGCAGCAAAACCTTCATCAACCACACCCAGGGCATCCCGACTTCTTTAAGCAGTCTTCCCGAGGGCTTACATGGGAGAGAG
 TCACCACATACGAAGATGGGGCGTGTGACCGCTACCAGGACACCCAGCCTCCAGGACGGCTGCCTCATCAACGCTCAAGATC
 AGAGGGGTGAACCTCCCATCAACGGCCGTGTGATGCAGAAGAAAACACTCGGCTGGGAGGCTCCACCCGAGACACTGTACCCCGC
 TGACGGCGGGCTGGAAGGCAGAGCCGACATGGCCCTGAAGCTCGTGGGGGGGGCCACCTGATCTGCAACCTTAAGACCAATACA
 GATCCAAGAAAACCGCTAAGAACCTCAAGATGCCCGCGCTTACTATGTGGACAGGAGACTGGAAGAATCAAGGAGGGCCGACAAA
 GAGACATAGCTGACGACGACGAGGTGGCTGTGGCCAGATACTGGCAGCTCCCTAGCAAACTGGGGCACAACTTAATTC
 GGGTATGTTGGGAGGGATTAAGGCTGATGAGGCTATGGCTAAGGCTATGGCTAAGCCTTTGTCCTCAAGAAGAATCCACCC
 TCATTGAAAGAGCAACGGCTACAATCAACAGCATCCCCATCTCTGAAGACTACAGCGTCGCCAGCGCAGCTCTCTAGCCAGGGC
 CGCATCTTCACTGGTGTCAATGTATATCATTTTTACTGGGGGACCTTGTGCAGAACTCGTGGTGTGGGCACTGCTGCTGCTGGGGC
 AGCTGGCAACCTGACTTGTATCGTCCGATCGGAAATGAGAACAGGGGCATCTTGAGCCCTGCGGACGGTCCGACAGGTGCTTC
 TCGATCTGCATCCTGGGATCAAAGCCATAGTGAAGGACAGTATGGACAGCCGACGGCAGTTGGGATTCGTGAATTGCTGCCCTCT
 GGTATGTTGGGAGGGATTAAGGACAGGTGATATCCAGCACAGTGGCGGGCCTCGACAATCAACCTCTGGATTACAAAATTTGT
 GAAAGATTGACTGGTATTTCTAACTATGTTGCTCCTTTTACGCTATGTGATACGCTGCTTTAATGCCCTTTGTATCATGCTATTGC
 TTCCCGTATGGCTTTCATTTCTCCTCCTTGTATAAATCCTGGTGTGCTCTTTATGAGGAGTTGTGGCCGTTGTGAGGCAAC
 GTGGCGTGGTGTGACTGTGTTGCTGACGCAACCCCACTGGTGGGGCATTGCCACCACCTGTGAGTCTTTCCGGGACTTTC
 GCTTTCCCTCCCTATTGCCACGGCGGAACCTCATCGCCGCTGCTTCCCGCTGCTGGACAGGGGCTCGGCTGTTGGGCACTGA
 CAATCCGTGGTGTGTCGGGAAGCTGACGTCCTTCCATGGCTGCTGCCTGTGTTGCCACCTGGATTCTGCGCGGGACGTCCT
 TCTGCTACGTCCTTCCGGCCTCAATCCAGCGGACCTTCCCTCCCGCGCTGCTGCCGCTCTGCGCCCTTCCGCTCTCGC
 CTTCGCCCTCAGACGAGTCGGATCTCCCTTTGGGGCCTCCCGCCTGGAATTCGAGATATCCGGTTAGTAATGAGTTGGAA
 TTAATTCGTGGAATGTGTGTCAGTTAGGGTGTGAAAGTCCCAGGCTCCCAGGCAGGCAGAGATGCAAAGCATGCATCTCA
 ATTAGTCAGCAACCAGGTGGAAGTCCCAGGCTCCCAGCAGGCAGAGATGCAAAGCATGCATCTCAATTAGTCAGCAACC
 ATAGTCCCGCCCTAACCCGCCCCAATCCGCCCCAATCCGCCCCAGTCCGCCCCATTCGCCCCATGGCTGACTAATTTTTTT
 TATTTATGCAGAGCCGAGCCGCTCTGCCTGACTATTCAGAGTATTCAGAGTGTGAGGAGCTTTTTGGAGGCTTAGCTTTTGCA
 AAAAGCTCCCGCTGTTGACAATTAATCATCGGCATAGTATATCGGCATAGTATAATACGACAAGGTGAGGAATAAACCATGGCCA
 AGTTGACCAGTGCCGTTCCGGTGTCCACCGCGCGACGTCGCCGGAGCGGTGAGTTCTGGACCGACCGGCTCGGGTCTCCCGG

GACTTCGTGGAGGACGACTTCGCCGGTGTGGTCCGGGACGACGTGACCTGTTTCATCAGCGCGGTCCAGGACCAGGTGGTGCCGGA
CAACACCTGGCCTGGGTGTGGGTGCGCGGCTGGACGAGCTGTACGCCGAGTGGTTCGGAGGTCGTGTCCACGAACCTCCGGGACG
CCTCCGGGCCGGCCATGACCGAGATCGCGGAGCAGCCGTGGGGCGGGAGTTCGCCCTGCGCGACCCGGCCGCAACTGCGTGCAC
TTCGTGGCCGAGGAGCAGGACTGACACGTCTACGAGATTTAAATGGTACCTTTAAGACCAATGACTTACAAGGCAGCTGTAGATC
TTAGCCACTTTTTAAAAAGAAAAGGGGGAC TGAAGGGCTAGCTCACTCCCAACGAAGACAGATCTGCTTTTTGCTTGTACTGGG
TCTCTCTGGTTAGACCAGATCTGAGCCTGGGAGCTCTCTGGCTGCTAGGGAAACCCACTGCTTAAGCCCTCAATAAAGCTTGCCTTG
AGTGCTTCAAGTAGTGTGTGCCCGTCTGTTGTGTGACTCTGGTAACTAGAGATCCCTCAGACCCCTTTTAGTCAGTGTGGAAAATCT
CTAGCA GTAGTAGTTCATGTCTATCTTATTATTCAGTATTTATAACTTGCAAAGAAATGAATATCAGAGAGTGAGAGGAACCTGT
ATTGCAGCTTATAATGGTTACAAATAAAGCAATAGCATCACAAATTCACAAATAAAGCATTTTTTTCACTGCATTCTAGTTGTGG
TTTGTCCAAACTCATCAATGTATCTTATCATGTCTGGCTCTAGCTATCCCGCCCTAACTCCGCCAGTTCGCCCATTTCTCCGCC
CCATGGCTGACTAATTTTTTTTATTTATGTCAGAGGCCGAGGCCAGCTGTGTCTTCTAGACGTGAGGTGGCACTTTTTCCGGGAAAT
GTCCGGGAACCCCTATTTGTTATTTTTCTAAATACATTTCAAATATGTATCCGCTCATGAGACAATAACCCGTGATAAATGCTTCA
ATAATATTGAAAAAGGAAGAGTATGAGTATTCAACATTTCCGTGTCGCCCTTATCCCTTTTTTTCGGGCAATTTGCTGTT
TTGCTCACCCAGAAACGCTGGTGAAGTAAAGATGCTGAAGATCAGTTGGGTGCACGAGTGGGTTACATCGAACTGGATCTCAAC
AGCGGTAAGATCCTTGAGAGTTTTTCGCCCGAAGAAGCTTTTCCATGATGAGCACTTTTAAAGTCTGCTATGTGGCGCGGTAT
ATCCCGTATTGACGCCGGCAAGAGCAACTCGGTGCGCGCATACACTATTCTCAGAATGACTTGGTTGAGTACTCACCAGTCACAG
AAAGCATCTTACGGATGGCATGACAGTAAGAGAATTATGCAGTGTGCCATAACCATGAGTGATAACACTGCGGCCAACTTACTT
CTGACACGATCGGAGGACCGAAGGAGCTAACCGCTTTTTGCACAACATGGGGGATCATGTAACCTCGCTTGATCGTTGGGAAC
GGAGCTGAATGAAGCCATACCAAACGACGAGCGTGACACCACGATGCCGTGTAGCAATGGCAACAACGTTGCGCAAACCTATTA
GCGAACTACTTACTCTAGCTTCCCGGCAACAATTAATAGACTGGATGGAGCGGATAAAGTTGCAGGACCCTTCTGCGCTCGGC
CTTCCGGCTGGCTGGTTTATTGCTGATAAATCTGGAGCCGGTGAAGCGTGGGTCTGCGGTTATCATTGACGCACTGGGGCCAGATGG
TAAGCCCTCCGCTATCGTATCTTACACGACGGGAGTCAGGCAACTATGGATGAACGAAATAGACAGATCGCTGAGATAGGTG
CCTCACTGATTAAGCATTTGGTAACTGTGACACCAAGTTACTCATATATACTTTAGATTGATTTAAACTTCATTTTTAATTTAAA
AGGATCTAGGTGAAGATCCTTTTTGATAATCTCATGACCAAAATCCCTAACGTGAGTTTTCGTTCCTGAGCGTACAGCCCGT
AGAAAAGATCAAAGGATCTTCTTGAGATCCTTTTTTCTGCGGTAATCTGCTGCTTGCAAAACAAAAAACCCGCTACCAGCGG
TGTTTGTGTTGCCGGATCAAGAGCTACCACTCTTTTTCCGAAGTAAGTGGCTTACGACAGCGCAGATACCAATACTGTCCTT
CTAGTGTAGCCGTAGTTAGGCCACCCTCAAGAATCTGTAGCACCGCTACATACTCGCTCTGTAATCCTGTTACCAGTGGC
TGCTGCCAGTGGCGATAAGTCTGTCTTACCGGGTTGACTCAAGACGATGTTACCAGGATAAGGCGCAGCGGTCGGGCTGAACGG
GGGTTGCTGCACACAGCCAGCTTGGAGCGAACGACCTACCCGAACGATGATACCTACAGCTGAGCTATGAGAAAGCCACAG
CTTCCGAAGGGGAGAAAGGCGGACAGGTATCCGGTAAGCGGCAGGGTCGGAACAGGAGAGCGCACAGGGGAGCTTCCAGGGGAA
CGCTGGTATCTTTATAGTCTGTCCGGTTTCGCCACTCTGACTTGAGCGTGCATTTTTGTGATGCTCGTCAGGGGGCGGAGCC
TATGGAAAACGCCAGCAACGCGCCTTTTTACGGTCTCTGGCTTTTTGCTGGCCTTTTTGCTCACATGTTCTTTCTGCGTTATCC
CCTGATCTGTGGATAACCGTATTACCGCCTTTGAGTGAAGTATACCGCTGATACCGCTGCGCGCAGCCGAACGACCGGAGCGCAGT
GAGCGAGGAAGCGGAAGAGCGCCCAATACGCAACCGCTCTCCCCGCGGTTGGCCGATTCATTAATGACAGTGGCACAGGTT
TTCCGACTGGAAAGCGGCGAGTGAAGCGCAACGCAATTAATGTGAGTTAGCTCACTCATTAGGCACCCAGGCTTTACACTTTATG
CTTCCGGCTCGTATGTTGTGTGGAATTGTGAGCGGATAACAATTTACACAGGAAACAGCTATGACCATGATTACGCCAAGCGCGC
AATTAACCTCACTAAAGGGAACAAAAGCTGGAGCTGAAGCTTAATGTAGTCTTATGCAATACTCTTGTAGTCTTGCAACATGGT
AAGATGAGTTAGCAACATCCCTTACAAGGAGAGAAAAAGCACCGTGCATGCCGATTTGGTGAAGTAAGGTGGTACGATCGTGCCT
TATTAGGAAGGCAACAGACGGTCTGACATGGATTGGACGAACCACTGAATGCCGATTCGAGAGATATGTAATTAAGTGCCTA
GCTCGATAACAATAAACGGGCTCTCTGTTAGACCAGATCTGAGCCTGGGAGCTCTCTGGCTAACTAGGGAACCCACTGCTTAAGC
CTCAATAAAGCTTGCTTGAAGTCTCAAGTAGTGTGTGCCCGTCTGTTGTGTGACTCTGGTAACTAGAGATCCCTCAGACCCCTT
TAGTCAGTGTGGAAAATCTCTAGCAGTGCAGCCCGAACAGGGACCTGAAAGCGAAAGGAAACAGAGCTCTCTCGACGACGAGGACT
CGGCTGCTGAAGCGGCACGGCAAGAGGCGAGGGCGGCGACTGGT GAGTACGCCAAAAATTTTACTAGCGGAGGCTAGAAGGA
GAGAGATGGGTGCGAGAGCCTCAGTATTAAGCGGGGAGAAATAGATCGCGATGGGAAAAAATTCGGTTAAGGCCAGGGGAAAGA
AAAAATATAAATTAACAATATAGTATGGGCAAGCAGGGAGCTAGAACGATTCGCAGTAACTCCTGGCCTGTTAGAAACATCAGAA
GGCTGTAGACAAATACTGGGACAGCTACAACCATCCCTTCAGACAGGATCAGAAGAACTTAGATCATTATATAATACAGTAGCAAC
CCTCTATTGTGTGCATCAAAGGATAGAGATAAAAGACACCAAGGAAGCTTTAGACAAGATAGAGGAAGAGCAAAACAAAAGTAA
CCACCGCACAGCAAGCGGCGCTGATCTTCAGACCTGGAGGAGGAGATATGAGGGACAATGGAGAAGTGAATATATAAATATAA
AGTAGTAAAAATGAACCATTAGGAGTAGCACCCACCAAGGCAAGAGAAAGTGGTGCAGAGAGAAAAAGAGCAGTGGGAATAG
GAGCTTTGTTCCCTTGGGTTCTTGGGAGCAGCAGGAAGCACTATGGGCGCAGCCTCAATGACGCTGACGGTACAGGCCAGACAATTA
TTGCTGGTATAGTGCAGCAGCAGAACAATTTGCTGAGGGCTATTGAGGCGCAACAGCATCTGTTGCAACTCACAGTCTGGGGCAT
CAAGCAGCTCCAGGCAAGAATCCTGGCTGTGGAAAGATACCTAAAGGATCAACAGCTCCTGGGGATTGGGGTTGCTCTGGAAAC
TCATTTGCACCACTGCTGTGCCTTGGAAATGCTAGTTGGAGTAATAAATCTCTGGAACAGATTGGAATCACACGACCTGGATGGAGT
GGGACAGAGAAATTAACAATTAACAAGCTTAATACTCCTTAATTAAGAATCGCAAAACAGCAAGAAAGAAATGAACAAGAA
TTATTGGAATTAGATAAATGGCAAGTTGTGGAATGGTTTAAACATAACAATTTGGCTGTGGTATATAAATTTATTCATAATGAT
AGTAGGAGGCTTGGTAGGTTAAGAATAGTTTTTGTGTACTTTCTATAGTGAATAGAGTTAGGCAGGGATTTACCATTATCGT
TTCAGACCCACCTCCAACCCGAGGGGACCCGACAGGCCGAGGAATAGAAGAAGAGGTGGAGAGAGACAGAGACAGATCC
ATTCGATTAGTGAACGGATCTCGACGGTTAAC TTTTAAAAAGAAAAGGGGGGATGGGGGGTACAGTGCAGGGGAAAGAATAGTAGA
CATAATAGCAACAGACATACAACTAAAGAATTACAAAACAATTAACAAAATTCAAAATTTTATTCCAGTGTGGTGAATTTCTG
CAGTCTGC

Supplementary Table 3-S3. Sequence of transgene cassette for C503 (pLV-hEF1a-prepro-CGRP-IRES-mKate2-2A-bla)

color coding key:

prepro-CGRP: human prepro-CGRP alpha

IRES: Internal ribosome entry site

mKate2: Red fluorescent protein

2A: Autoproteolytic viral amino acid sequence

Bla: Blasticidin resistance gene

sequence:

```
ATGGGCTTCCAAAAGTTCTCCCCCTTCCTGGCTCTCAGCATCTTGGTCTGTTGCAGGCAGGCAGCCTCCATGCAGCACCATTTCAG
GTCTGCCCTGGAGAGCAGCCAGCAGACCCGGCCACGCTCAGTGAGGACGAAGCGCGCCTCCTGCTGGCTGCACTGGTGCAGGACT
ATGTGCAGATGAAGGCCAGTGAGCTGGAGCAGGAGCAAGAGAGAGAGGGCTCCAGAATCATTGCCAGAAGAGAGCCTGTGACACT
GCCACCTGTGTACTCATCGGCTGGCAGGCTTGCTGAGCAGATCAGGGGCTGTTGGTGAAGAACAACCTTGTGCCACCAATGTGGG
TTCCAAAGCCTTTGGCAGGCGCCGACGGACCTTCAAGCCTGAGACTGGGATCCGCCCTCTCCCTCCCCCCCCCTAACGTTACT
GGCCGAAGCCGCTTGGAAATAAGGCCGGTGTGCGTTTGTCTATATGTTATTTTCCACCATATTGCCGCTCTTTTGGCAATGTGAGGGC
CCGAAACCTGGCCCTGTCTTCTTGACGAGCATTCTAGGGGCTTTTCCCTCTCGCCAAAGGAATGCAAGGTCTGTTGAATGTCCG
TGAAGGAAGCAGTTCCTCTGGAAGCTTCTTGAAGACAAACAACGCTGTAGCGACCTTTGCAGGCAGCGGAACCCCCACCTGGC
GACAGGTGCCCTCTGCGGCCAAAAGCCACGTGTATAAGTACACCTGCAAAGGCGGCACAACCCAGTGCCACGTTGTGAGTTGGAT
AGTTGTGGAAAGAGTCAAATGGCTCTCCTCAAGCGTATCAACAAGGGGCTGAAGGATGCCAGAAAGGTACCCCATTTGTATGGGAT
CTGATCTGGGGCCTCGGTACACATGCTTTACATGTGTTTAGTCGAGGTTAAAAAACGCTCTAGGCCCCCGAACCCAGGGGACGTG
GTTTTCCCTTGAAAAACACGATGATAATATGGCCACAGCCACCATGCTGAGCGAGCTGATTAAGGAGAACATGCACATGAAGCTGT
ACATGGAGGGCACCGTGAACAACCCACTTCAAGTGCACATCCGAGGGCGAAGGCAAGCCCTACGAGGGGCACCCAGACCATGAGA
ATCAAGGCGGTTCGAGGGCGGCCCTCTCCCTTCGCCTTCGACATCCTGGCTACCAGCTTCATGTACGGCAGCAAAACCTTCATCAA
CCACACCCAGGGCATCCCCGACTTCTTTAAGCAGTCTTCCCCGAGGGCTTCACATGGGAGAGAGTCACCACATACGAAGATGGGG
GGTGTGACCGCTACCCAGGACACCCAGCCTCCAGGACGGCTGCCTCATCTACAACGTCAGATCAGAGGGGTGAACTTCCCATCC
AACGGCCCTGTGATGCAGAAGAAAACACTCGGCTGGGAGGCTCCACCGAGACACTGTACCCCGCTGACGGCGGCCTGGAGGCAG
AGCCGACATGGCCCTGAAGCTCGTGGGCGGGGGCCACCTGATCTGCAACCTTAAGACCACATACAGATCCAAGAAAACCCGCTAAGA
ACCTCAAGATGCCCGCGTCTACTATGTGGACAGGAGACTGGAAGAATCAAGGAGGCCGACAAGAGACATACGTCGAGCAGCAG
GAGGTGGCTGTGGCCAGATACTGCGACCTCCCTAGCAAACCTGGGGCACAAACTTAATTCCCTCGGGCCCGGGGAGGCTTCCATCA
TTGGGGCGACGTGGAGGAAAACCCNSGCRS ATGGCTAAGCCTTTGTCTCAAGAAGAATCCACCCTCATTGAAAAGAGCAACGGCTA
CAATCAACAGCATCCCCATCTCTGAAGACTACAGCGTCGCCAGCGCAGCTCTCTCTAGCGACGGCCGCATCTTCACTGGTGTCAAT
GTATATCATTTTACTGGGGACCTTGTGCAGAACTCGTGGTGTGGGCACTGCTGCTGCTGCGGCAGCTGGCAACCTGACTTGTAT
CGTCGCGATCGGAAATGAGAACAGGGGCATCTTGAAGCCCTGCGGACGGTGGCCACAGGTGCTTCTCGATCTGCATCCTGGGATCA
AAGCCATAGTGAAGGACAGTGATGGACAGCCGACGGCAGTTGGGATTGCTGAATTGCTGCCCTCTGGTTATGTGTGGGAGGGATAA
```

A protein engineering platform for BBB-crossing vasoactive imaging probes

Abstract

Molecular neuroimaging holds tremendous promise for basic research and for biomedicine, but its utility has been limited by a lack of effective means for delivering imaging probes across the blood-brain barrier (BBB). BBB-crossing antibodies, which use receptor-mediated transcytosis (RMT) to deliver a fused protein or peptide across the BBB, are a rapidly maturing delivery platform that can be used to achieve nanomolar concentrations inside the brain. We sought to establish and validate a fusion protein architecture for highly potent molecular MRI probes based on vasoactive peptides, recently developed by us, for brain delivery using RMT shuttles. Here, we report that maxadilan, a vasoactive peptide from sand flies, retains low nanomolar potency when fused to several known BBB-crossing antibodies without impairing RMT receptor binding, raising the intriguing possibility that this fusion architecture could be used for molecular brain imaging with engineered vascular responses following minimally invasive peripheral injection.

Introduction

The BBB presents a formidable obstacle for the delivery of therapeutic and diagnostic agents to the brain, impeding progress in basic neuroscience and complicating drug development for CNS disorders^{79,80}. Delivery across the BBB is among the most important bottlenecks for widespread application of molecular MRI probes for neuroimaging¹⁷. Almost all large molecule drugs (and large imaging agents), and 98% of small molecule drugs, are unable to cross the BBB⁷⁹.

Two recent developments together raise the possibility of implementing an effective and experimentally simple strategy for the brain delivery of molecular MRI probes. Firstly, we have recently

demonstrated molecular imaging with engineered hemodynamic responses at nanomolar probe concentrations (see Chapter 2), thus substantially lowering the concentration required for probe delivery compared to previous molecular MRI probes. Secondly, rapid recent progress in the optimization, mechanistic understanding, and application of BBB-crossing antibodies^{63,81}, including the progress of several such constructs into human clinical trials⁸¹, suggests that brain delivery of vasoactive imaging probes could be feasible at the required concentrations.

Brain delivery of fusion proteins by receptor-mediated transcytosis

Some large molecules naturally cross the BBB via receptor-mediated transcytosis (RMT). Examples include peptide hormones such as insulin or the iron transport protein transferrin. They enter the brain by binding a specific receptor (here, the insulin receptor and the transferrin receptor (TfR), respectively), followed by endocytosis into brain vascular endothelial cells, vesicular transport to the basolateral membrane, and release into the brain parenchyma via exocytosis.

This process can be hijacked for the brain delivery of macromolecules using a strategy largely pioneered by William Pardridge and co-workers^{63,79,81}, referred to in the literature as “molecular Trojan horse”, “RMT shuttle”, or “BBB shuttle” (see Fig. 4-1A). In this strategy, a large moiety of interest – typically a biologic drug such as a monoclonal antibody or a replacement enzyme, or a peptide, oligonucleotide, or even liposome – is attached to an RMT ligand, such as an anti-TfR antibody. While this technology has been under development since at least the early 1990s, it is only recently that several key challenges were understood and overcome, facilitating broader adoption⁸¹. First, RMT requires fine-tuned kinetics. The RMT ligand needs to have high enough affinity for its receptor to achieve binding and endocytosis, but low enough affinity to allow for brain-side exocytosis and release. If affinity and avidity are not correctly tuned, RMT shuttles may remain associated with vascular endothelial cells and often are targeted for lysosomal degradation rather than endosomal transport. Second, early RMT studies relied on

analytical methods for quantifying brain delivery that tend to confound successful parenchymal release and sequestration inside the vascular endothelium. Autoradiography and PET /SPECT are fundamentally unsuitable for distinguishing release and sequestration due to their insufficient spatial resolution. Capillary depletion⁸² is a technique that uses density gradient centrifugation to remove the endothelial fraction from brain homogenates, but its efficiency is variable and often insufficient as evidenced by the detection of vascular markers inside the supposed brain fraction⁸³. Finally, microdialysis is notoriously challenging for large protein analytes. As a consequence, for many years, the kinetic requirements for efficient RMT were not fully appreciated; highly effective apparent brain delivery was reported in proof-of-concept studies; but doubts were cast on the attainable delivered quantities follow-on investigations⁸³.

Recently, several groups have shed light on the kinetic requirements for RMT, produced improved shuttles, and measured brain delivery carefully using multiple methods. Niewoehner and colleagues found that a monovalent RMT ligand was more effective than a bivalent ligand at facilitating brain delivery of an anti-beta-amyloid therapeutic mAb in the mouse⁸⁴. They showed efficient extravasation of the monovalent construct and amyloid plaque binding by immunohistochemistry and further saw improved pharmacodynamic efficacy in a mouse model of Alzheimer's. The bivalent construct was sequestered to lysosomes. In parallel, Yu and colleagues^{85,86} showed that for an already monovalent, bispecific anti-TfR antibody, decreasing affinity increased brain entry and pharmacological efficiency. Stanimirovic, Farrington, and colleagues have reported efficient brain delivery of a bivalent, low-affinity camelid single-domain antibody (sdAb) Fc fusion construct in the rat, quantifying the achieved brain concentration in the low nM range and showing pharmacological efficacy of an attached analgesic peptide⁸⁷. Together, these developments suggest that delivering protein agents to the brain at nanomolar concentrations is feasible, raising the possibility of delivering vasoactive imaging probes at effective concentrations.

It should moreover be noted that the consensus “gold standard” for measuring brain delivery by RMT is the quantitation of pharmacodynamic responses, such as decrease of circulating beta-amyloid in Alzheimer’s⁸⁶ or changes in paw withdrawal following a pain stimulus when given an analgesic peptide⁸⁷. These measurements, while convincing, are idiosyncratic, indirect, and often experimentally cumbersome and lengthy, suggesting that vasoactive imaging probes could not only benefit from RMT-mediated brain delivery but could also be used to characterize and improve RMT shuttles (since vasoprobe act on vascular smooth muscle cells and therefore only exert their action after release inside the brain).

Maxadilan as a potential new scaffold for vasoactive imaging probes

We originally demonstrated the principle of imaging with engineered hemodynamics using probes on the human vasodilatory peptide CGRP (Chapter 2), but this peptide would be challenging to use as part of an antibody fusion protein. Firstly, for maximal potency, CGRP must be amidated at the C-terminus, which can be done synthetically and happens naturally during posttranslational processing in dense core vesicles. However, the secretory path for antibodies is different, suggesting that correct processing could be problematic. Secondly, N-terminal extensions to CGRP reduce its potency. While it might be conceivable to work around these limitations by chemically amidating CGRP and by chemically linking it to RMT shuttles of interest by means other than a terminal fusion, this would be cumbersome both for the initial proof-of-concept for delivery and for routine engineering of a variety of BBB-crossing molecular sensors in the future. Our goal was instead to establish a relatively simple architecture for a fusion of RMT shuttle and vasoprobe that would be uncomplicated to engineer and to express recombinantly (see example in Fig. 4-1B).

Thus, we chose the large and highly potent vasoactive peptide Maxadilan as the vasoprobe for this study. Found in the saliva of sand flies, Maxadilan activates the PAC1 receptor^{88,89} on vascular smooth muscle, resulting in elevation of cAMP and dilation of the microvasculature⁹⁰. Upon injection into

the skin, Maxadilan causes erythema⁹⁰. It is even more potent than CGRP, activating its receptor at subnanomolar concentrations, and requires no amidation. Substantial variation in the Maxadilan sequence has been observed in fly populations in the wild⁹¹, and studies of sequence-activity relationships indicate a relatively small number of critical residues, as well as the requirement for the central disulfide loop to be intact, while many residues can be modified without substantial reduction in potency⁹²⁻⁹⁴. Since the receptor-binding residues of Maxadilan seem clustered within its central disulfide loop (Fig.4-1C), we conjectured that Maxadilan should be less sensitive than CGRP to the addition of terminal fusion proteins.

Results

Cell-based assay for PAC1 activation and bioactivity of Maxadilan fusions

We first developed a cell-based bioassay for PAC1 receptor activation by Maxadilan variants, in analogy to the bioassay for CGRP activity in Chapter 2. Since PAC1 also acts through adenylyl cyclase, we used the same allosteric luciferase reporter as previously (Chapter 2, lentiviral plasmid C512) and in conjunction cloned a lentiviral constructs expressing rat PAC1 (plasmid C525). As HEK293 cells express the VIP1/2 receptors at low but functional levels and Maxadilan cross-activates VIP receptors (albeit with lower potency), we chose CHO K1 cells as reporter cells and derived CHO cell lines transduced with either C512 alone or C512 and also C525. We validated a modified bioassay protocol that ensures no luciferase substrate depletion despite the higher substrate levels required for CHO cells, in which 2,500 reporter cells are seeded per microplate well (compared to 10,000 cells for HEK293 cells) and 6% Glo substrate are used (compared to 1% for HEK293 cells). We found that human PACAP-38 (Sigma) stimulates cAMP production in the PAC1 reporter cells fully at 0.1 nM final concentration, and we subsequently normalized all PAC1 bioassay luminescence data to the range spanned by buffer only and 1 nM PACAP-38 peptide.

Next, we cloned and expressed a fusion protein comprising cysteine-free GFP with an N-terminal StrepII tag (identical to the GFP sequence used in Chapter 2 for CGRP fusions) and a previously

reported⁹⁴ linker-Maxadilan construct. Expression in *E. coli* resulted in a mixture of inclusion bodies and soluble protein, with some C-terminal truncation observed in the soluble fraction. We therefore purified the inclusion bodies, refolded them using the same protocol as was used in Chapter 2 for GFP-CGRP fusions, and purified the refolded protein using Strep purification. SDS-PAGE gel electrophoresis and MALDI-TOF mass spectrometry confirmed highly pure, full-length protein (data not shown). The PAC1 bioassay results (Fig. 4-2) show a $\log(\text{EC}_{50})$ of -9.5, indicating subnanomolar potency. This is more than 4 orders of magnitude better than uncleaved GFP-CGRP-Gly fusions (Chapter 2) and compatible with the putative low nanomolar potency requirement for detection upon BBB delivery, prompting us to explore the potential of Maxadilan fusions to known BBB-crossing antibodies.

Bioactivity and Tfr binding of OX26-Maxadilan fusions

We conjectured that BBB-crossing antibodies well-characterized for delivery to the rat brain could serve as a useful starting point for brain delivery of vasoactive imaging probes. OX26 is a mouse anti-rat Tfr IgG2a antibody and has been widely characterized for brain delivery in the rat. Intriguingly, in one particular early study, OX26 was chemically conjugated to the vasointestinal peptide (VIP), a vasodilator. OX26-VIP was shown to cause an increase in cerebral bloodflow upon peripheral administration⁹⁵. Despite concerns that a significant fraction of brain-delivered OX26 conjugates remains inside the endothelium⁸³, this evidence of pharmacological activity inside the brain renders OX26 a strong candidate for BBB delivery of vasoactive imaging probes.

To characterize OX26 for Maxadilan delivery, we designed and produced several constructs (Fig. 4-3A). First, we cloned a simple OX26 IgG from published variable domain sequences of an OX26-derived scFv⁹⁶ and commercially available mouse IgG2a heavy chain and kappa light chain sequences. We also created variants with GSIL-Maxadilan attached to the C-terminus of the light chain via a $(\text{Gly}_4\text{Ser})_2$ linker with or without a thrombin (Th) site. For in vivo applications, we ultimately desire a

construct without a thrombin site, but having the ability to cleave off maxadilan will facilitate evaluating the effect of the large IgG fusion moiety on maxadilan potency. Finally, in order to be able to evaluate constructs with varying avidity, we created an OX26 Fab. All constructs were expressed and secreted correctly in the Freestyle mammalian expression system (Fig. 4-3B,C), and thrombin cleavage of OX26-IgG-Th-Max was highly efficient (Fig. 4-3D).

Next, we evaluated the bioactivity of the OX26-maxadilan fusions against the PAC1 receptor (Fig 4-3 E-G). Both OX26-IgG-Max and OX26-IgG-Th-Max activated the receptor with nanomolar potency ($\log(\text{EC}_{50})$ of -8.5 and -8.7, respectively; see Supplementary Table 4-18 for a list of all measured potencies and 95% confidence intervals). However, this is an order of magnitude less potent than the GFP-Max fusion with a $\log(\text{EC}_{50})$ of -9.5 (Fig. 4-2) and more than two orders of magnitude worse than free maxadilan after thrombin cleavage ($\log(\text{EC}_{50})$ of -11.0), suggesting that a longer linker or different fusion topology could be beneficial.

Finally, we evaluated the ability of our constructs to bind to TfR. To this end, we established a cell-based competition binding assay in which 9L rat glioma cells, which express TfR, are co-incubated with biotinylated wild-type OX26 from hybridoma culture and varying concentrations of our recombinant OX26 constructs of interest, stained with streptavidin-phycoerythrin, and assayed by flow cytometry. Both OX26-IgG-Max and the OX26-Fab effectively competed against biotinylated OX26 for TfR binding, and the avidity effect shifted the binding curve for the bivalent IgG by approximately two orders of magnitude to the left (Fig. 4-3H), as expected. Thus, our fusion constructs retain TfR affinity as well as maxadilan bioactivity.

Effect of fusion topology and linker length on maxadilan potency

As noted above, the potency of maxadilan was substantially reduced in the initial IgG fusions. Since literature reports of brain delivery by BBB-crossing antibodies indicate attainable brain concentrations in the low nanomolar range (based on both quantitation in brain homogenates and on

pharmacological effects), it would be desirable to achieve subnanomolar potency *in vitro*, and our results with GFP-maxadilan (Fig. 4-2) lead us to believe that this should be possible. We therefore chose to vary linker length and fusion topology in an effort to improve the potency of antibody-maxadilan fusions.

We constructed fusions as Fabs and as IgGs, with short (Gly₄Ser)₂ and long (Gly₄Ser)₄ linkers, and additionally examined a fusion of maxadilan to the C-terminus of the IgG heavy chain via a long linker (Fig. 4-4A). All fusions were expressed well and were efficiently cleaved by thrombin (Fig. 4-4 B,C).

We performed PAC1 bioassays and found improved potency for all of our new constructs (Fig. 4-4 D,E). Both Fab constructs exhibit log(EC₅₀) values of -9.5, irrespective of linker length and identical to that of GFP-maxadilan. For the maxadilan fusion to the light chain of the IgG, lengthening the linker by 10 amino acids shifted the log(EC₅₀) value from -8.7 to -9.5, a more than 6-fold improvement in potency. More potent still was the fusion of maxadilan to the C-terminus of the IgG heavy chain, giving a log(EC₅₀) of -9.7. Note that the potencies for IgG constructs were computed on a per-IgG basis; since each IgG contains two maxadilan moieties, the log(EC₅₀) of -9.7 for the heavy chain fusion is in close agreement with the value of -9.5 for the Fab or for GFP-Max, indicating minimal interference with receptor access.

Finally, we investigated the SDS-PAGE band broadening observed for maxadilan fusions of all antibody constructs in Fig. 4-3 and 4-4. This band broadening occurred toward higher-than-predicted molecular masses and hence could not result from cleavage or truncation. After thrombin cleavage, we observed bands with the usual sharp, narrow width, indicating that maxadilan is implicated in the broadening. We therefore performed MALDI-TOF mass spectrometry on the cleaved samples for two representative constructs (one Fab and one IgG) to accurately determine the mass of the maxadilan moiety (Fig. 4-4F). We saw a clean sharp peak at precisely the predicted molecular mass, indicating that the SDS-PAGE band broadening is likely due to conformational effects or non-covalent interactions but not due to any covalent modification or irregularity of maxadilan.

FC5-Fc-maxadilan fusions

In order to be able to evaluate brain entry by multiple different BBB-crossing antibodies, we next proceeded to construct fusions of maxadilan to FC5-Fc. FC5 is a brain-penetrating camelid antibody⁹⁷ found to accumulate to nanomolar brain concentrations when used as a bivalent Fc fusion⁸⁷. FC5 was derived by functional selection and was found effective for delivery of neuropeptides at nanomolar levels into the rat brain as confirmed by pharmacological effects as well as by post-mortem quantitation. The bivalent fusion of FC5 to a human Fc sequence was found to work best, and we used this construct^{87,98} as our starting point.

We constructed and expressed FC5-Fc alone and FC5-Fc fusions to maxadilan via a long linker to the C-terminus of the heavy chain (Fig. 4-5A). All constructs expressed well (Fig. 4-5B) and, in agreement with our previous results, the maxadilan fusions displayed subnanomolar potencies with log(EC50) values of -9.8 and -9.9 (Fig. 4-5 D,E). For the thrombin-cleavable variant, we confirmed the correct mass for the maxadilan moiety post-cleavage by MALDI-TOF mass spectrometry (Fig. 4-5F).

Thus, we now have both FC5 and OX26-based maxadilan fusions ready for evaluation of brain entry *in vivo*.

Conclusions and future work

In sum, as shown in this chapter, we have developed a protein engineering platform for the creation of vasoactive imaging probes which can potentially be delivered across the BBB. We have established and validated cell-based bioassay for maxadilan activity, demonstrated that maxadilan can retain sub-nanomolar potency when fused to large globular proteins including BBB-crossing antibodies, and determined an optimal fusion topology and linker length. We now have constructs, based on both OX26 and FC5, ready to be evaluated *in vivo*.

The next logical steps beyond the scope of this dissertation will be as follows. First, imaging of maxadilan-mediated vasodilation should be performed following intracranial injection. Second, brain delivery of maxadilan fusions should be attempted at high peripheral concentrations (on the order of 6 mg/kg in the rat). Since the kinetics of BBB crossing, accumulation in the brain, and receptor activation do not allow precise prediction of the expected time course of vasodilation, MRI imaging sequences and data normalization methods may need to be optimized to best capture the expected effect. Finally, if and when detection of brain entry by MRI has been successful in principle, the shuttles should be characterized with respect to kinetics, dose-response relationships upon peripheral injection, and any adverse effects. In particular attention, should be paid to any possible effects of maxadilan in the periphery.

While our fusion constructs functioned well *in vitro*, a major challenge to be addressed by these *in vivo* experiments will be to determine whether vasoactive imaging as described here can indeed be a robust, simple, reliable, and hence practically useful method for assessing brain entry by BBB shuttles. One essential aspect of this will be the comparative evaluation of our method against the current gold standard for determining brain entry, which includes a combination of immunohistology to show extravasation, quantitation of constructs in brain homogenates, and minimally invasive measurement of pharmacological effects. The hope for vasoactive imaging of brain entry is to provide a facile, general, and relatively direct pharmacological measurement of brain entry.

Materials and methods

Plasmids. A tabulated list and sequences for all plasmids used in this study are provided as Supplementary Information. Lentiviral helper plasmids pMD2.G (Addgene #12259, Cambridge, MA) and psPAX2 (Addgene #12260) were gifts from Didier Trono. Plasmids pEF-ENTR A (Addgene #17427) and pLenti X1 Zeo (Addgene #17299) were gifts from Eric Campeau⁷⁰. Plasmid gWiz Blank was purchased

from Genlantis (San Diego, CA). Plasmids pFUSE-CHlg-mG2a and pFUSE2-CLlg-mk were purchased from Invivogen (San Diego, CA). Plasmid C512 was re-used from Chapter 2.

DNA encoding the rat PAC1 receptor was synthesized (IDT, Coralville, IA) and plasmid C525 was cloned using the GoldenGate method into the same backbone as C512, as described in Chapter 2. The bacterial expression plasmid Z644 was cloned as in Chapter 2, using a sequence for LVPR-GSIL-maxadilan reported by Moro and colleagues⁹⁴. Mammalian expression plasmids were cloned using GoldenGate assembly into the gWiz Blank backbone. The sequences encoding the OX26 VL and VH domains were taken from Li and colleagues⁹⁶. The murine IgG2a constant heavy and murine Ckappa light sequences were from plasmids pFUSE-CHlg-mG2a and pFUSE2-CLlg-mk. Synthetic DNA encoding FC5-Fc was ordered based on a patent by Farrington and Sisk⁹⁸, and FC5-Fc plasmids were cloned using GoldenGate.

Expression, refolding, and purification of GFP-maxadilan. GFP-maxadilan was expressed, refolded from inclusion bodies, and Strep purified following the same protocol as GFP-CGRP fusions in Chapter 2, and stored at 10 μ M in 20 mM Tris-HCl pH 7.5, 100 mM NaCl. Purity and identity were verified by SDS-PAGE and MALDI-TOF mass spectrometry.

Mammalian cell culture. HEK293FT cells (for lentivirus production) were cultured as described in Chapter 2. CHO K1 cells were purchased from Sigma (St. Louis, MO) and cultured in 90% F10 medium supplemented with 10% FBS, 100 units/mL penicillin, and 100 μ g/mL streptomycin. Frozen stocks were prepared in 95% culture medium supplemented with 5% DMSO. 9L rat glioma cells (ATCC CRL-2200) were obtained from ATCC (Manassas, VA), cultured in 90% DMEM with 10% FBS, 100 units/mL penicillin, and 100 μ g/mL streptomycin and frozen in 95% culture medium with 5% DMSO. Freestyle 293 suspension cells were purchased from Life Technologies (Carlsbad, CA) and cultured according to instructions.

Antibody expression and purification. Antibody constructs were expressed in Freestyle 293 cells. For small-scale expressions (30 to 100 mL), transfections were performed with 293fectin (Life Technologies, Carlsbad, CA) according to instructions, using 1 μ g total DNA (1:1 heavy:light chain where appropriate) and 2 μ L transfection agent per 1 mL cell suspension at a density of 1 million cells per mL. Large-scale expressions (500 mL) were performed in 2L roller bottles at 1 million cells/mL using polyethylene imine (PEI). Per 500 mL cell culture, 1 mL pre-warmed PEI stock (1 mg/mL) was added to 9 mL OptiPRO medium, gently mixed, and incubated for 15 min at room temperature. DNA (500 μ g total) was mixed with 10 mL OptiPRO and likewise incubated. The PEI solution was added to the DNA solution and incubated for a further 15 min, then allowed to drip into the cell suspension while swirling. Both small-scale and large-scale expression cultures were incubated at 37°C for 8 days.

After 8 days, cultures were collected into containers and centrifuged at 10,000 g for 30 min. The supernatants were filtered using Nalgene Rapid-Flow Sterile Disposable Filter Units with PES membrane (Thermo Fisher Scientific, Waltham, MA). IgG and Fc fusion constructs were then purified by Protein A purification. Fab constructs were purified by His purification.

For Protein A purification, Protein A agarose and IgG elution buffer pH 2.8 (both from Pierce, Rockford, IL) were used according to instructions for column purification in Poly-Prep 2 mL chromatography columns (Bio-Rad, Hercules, CA). Supernatants were supplemented with 10% v/v 10X PBS pH 7.4 before passing them through the columns. Elution was performed in 250 μ L fractions into tubes pre-filled with 25 μ L 1M Tris-HCl pH 8.5 to immediately neutralize the eluate.

For His purification, Ni-NTA resin (Qiagen, Valencia, CA) was used according to instructions, using 50 mM sodium phosphate pH 8.0, 300 mM NaCl, 20 mM as wash buffer and the same with 250 mM imidazole as elution buffer.

After elution, protein-containing fractions were identified by absorbance at 280 nm, pooled, and buffer exchanged into 1X PBS pH 7.4 using NAP10 columns (GE Healthcare, Chicago, IL). Concentrations were determined by absorption at 280 nm using predicted values for molecular masses and extinction coefficients, listed in Supplementary Table 4-17. Protein solutions were stored at 4°C at 10 μ M.

Lentiviral infection and cell line generation. CHO K1 cell lines were generated as described for HEK293 cell lines in Chapter, with the following modification: Lentiviral supernatants were produced in 15 cm dishes of HEK293 cells and concentrated 100-fold using Centricon Plus-20 (20 mL) centrifugal filter units (Millipore, Billerica, MA) with a 100 kDa cutoff for 30 min at 3,000g. CHO cells were infected with 80 μ L titers of each virus per well in 24-well plates, then selected using appropriate antibiotics (blastidicin at 10 μ g/mL, puromycin at 10 μ g/mL, or combinations; all from Life Technologies).

Luminescent cAMP assay for PAC1 receptor activation. Bioassays using CHO K1 reporter cells for PAC1 were performed as described for HEK293 reporter cells for the CGRP receptor in Chapter 2, with the following modifications: 2,500 cells were seeded per well the previous day. CO₂-independent medium containing 6% Glo substrate was used. All serial dilutions of samples were made with 0.1% CHAPS added.

Bioassay data analysis. Data were analyzed as describes in Chapter 2. Luminescence intensities were normalized to the range spanned by buffer only and 1 nM human PACAP-38 peptide (Sigma, St. Louis, MO).

Reporter validation. CHO K1 cells carrying the allosteric cAMP C512 only and CHO K1 cells also carrying the lentiviral transgene C525 encoding rat PAC1 receptor were both evaluated with synthetic PACAP-38 to ensure specificity of the PACAP-38 response in the reporter cell line. The same was done with recombinant GFP-Max instead of PACAP-38.

Thrombin cleavage reactions. Antibody constructs stored at 10 μ M in 1X PBS pH 7.4 were subjected to thrombin cleavage by adding 1 μ L of a 0.2 U/ μ L aqueous stock solution of thrombin from bovine plasma (cat. no. T7513, Sigma, St. Louis, MO) to 50 μ L antibody for a final thrombin

concentration of 0.004 U/ μ L. Reactions were incubated at 37°C for 3 h and then further assayed by bioassay, MALDI-TOF mass spectrometry, and SDS-PAGE. Near-complete cleavage was generally achieved.

Cell-based TfR binding assay. To measure antibody binding to TfR, a competitive binding assay using 9L rat glioma cells and flow cytometry was used. A suspension of 9L cells was prepared using Non-Enzymatic Cell Dissociation Solution (Sigma, St. Louis, MO), counted, pelleted at 500 g for 5 min, and resuspended at 5 million cells / mL in FACS buffer (PBS pH 7.5, 5% FBS, 0.1% sodium azide). 250 or 500 thousand cells were combined with 10 nM biotinylated OX26 (Anti-CD71 antibody MRC OX-26 (Biotin), ab112215, Abcam, Cambridge, MA) and varying concentrations of non-biotinylated recombinant OX26 antibody variants in FACS buffer. Cell numbers and volumes were chosen to ensure at least 10-fold ligand excess under the conservative assumption of 1 million TfR surface receptors per cell. To reach equilibrium, competition binding was allowed to proceed for 3h at 37°C while nutating. Cell suspensions were then placed on ice and washed twice (spin for 5 min at 500g; aspirate; wash with 1 mL ice-cold FACS buffer). The cells were then stained with 1:100 streptavidin-phycoerythrin (Life Technologies, Carlsbad, CA) for 20 min at 4°C while nutating. The staining solution was removed, cells were washed one more time, pelleted, and the pellets were kept on ice until analysis by flow cytometry.

The pellets were resuspended in 0.5 mL FACS buffer and fluorescence per cell was measured by flow cytometry using an LSR HTS-1 analyzer (Becton Dickinson, Franklin Lakes, NJ) with 4 lasers and 10 color capability at the MIT Koch Institute Flow Cytometry Core. Using the machine's FACS-DIVA software, the relevant events were selected based on side and forward scatter of the cell population. Fluorescence was measured in the phycoerythrin channel and mean values from 10,000 events were plotted.

Figures and tables

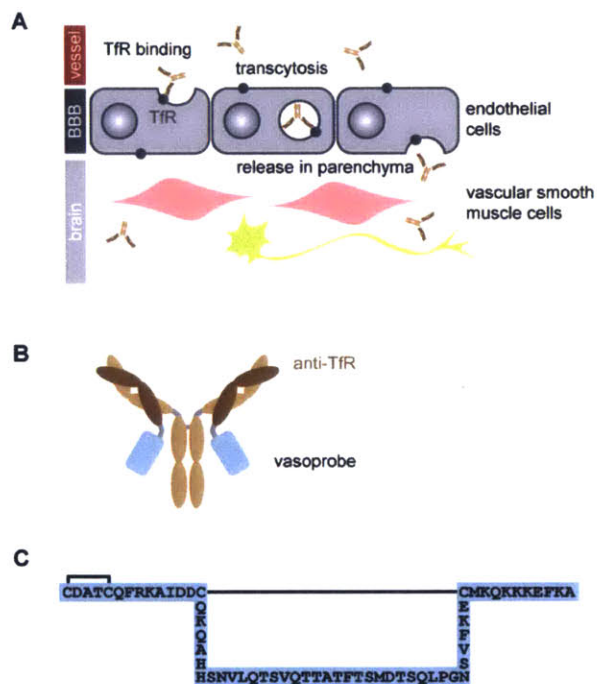


Fig. 4-1: Toward delivery of vasoactive imaging probes across the BBB.

- (A) Principle of brain delivery of biologics by receptor-mediated transcytosis. An anti-TfR antibody is injected intravenously on the periphery. Inside the brain vasculature, it binds to TfR expressed abundantly on the luminal (apical) surface of brain vascular endothelial cells and is endocytosed. Following vesicular transport to the opposite (basolateral) side of the endothelial cell, the TfR antibody is exocytosed and released into the brain parenchyma.
- (B) Schematic concept for a brain delivery vehicle for vasoactive probes. The vasoprobe is covalently fused to a BBB-crossing anti-TfR antibody (here, shown as a fusion to the C-terminus of the antibody light chain in dark brown).
- (C) Primary sequence of maxadilan, with disulfide bonds indicated as lines. This vasoactive peptide from sandflies causes vasodilation and erythema in mammalian skin by activating the PAC1 receptor with subnanomolar potency. The sequence shown, preceded by GSIL, was recombinantly expressed and characterized by Moro and colleagues⁹⁴.

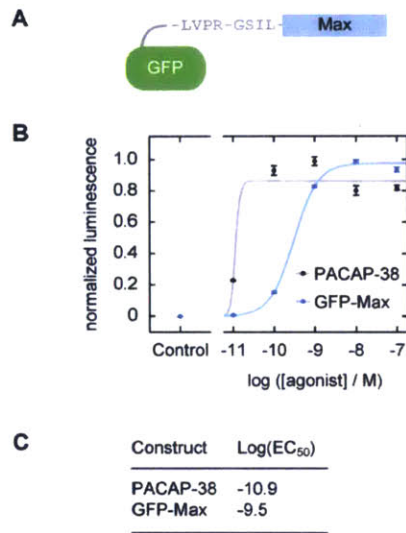


Fig. 4-2: Expression, refolding, and *in vitro* evaluation of a recombinant maxadilan fusion.

- (A) Design: The N-terminus of maxadilan was fused to the C-terminus of GFP via a previously reported⁹⁴ linker.
- (B) Results of CHO K1 cell-based *in vitro* bioassay for PAC1 agonist activity for synthetic rat PACAP-38 (Sigma) and recombinantly expressed GFP-maxadilan. The assay was performed under optimized conditions (6% Glo substrate, 2500 cells per well seeded 24 h prior). Luminescence intensities were normalized to the range evoked by buffer alone and 1 nM PACAP-38.
- (C) Fitted potencies for PACAP-38 and GFP-maxadilan. 95% confidence intervals are listed in Supplementary Table 4-18.

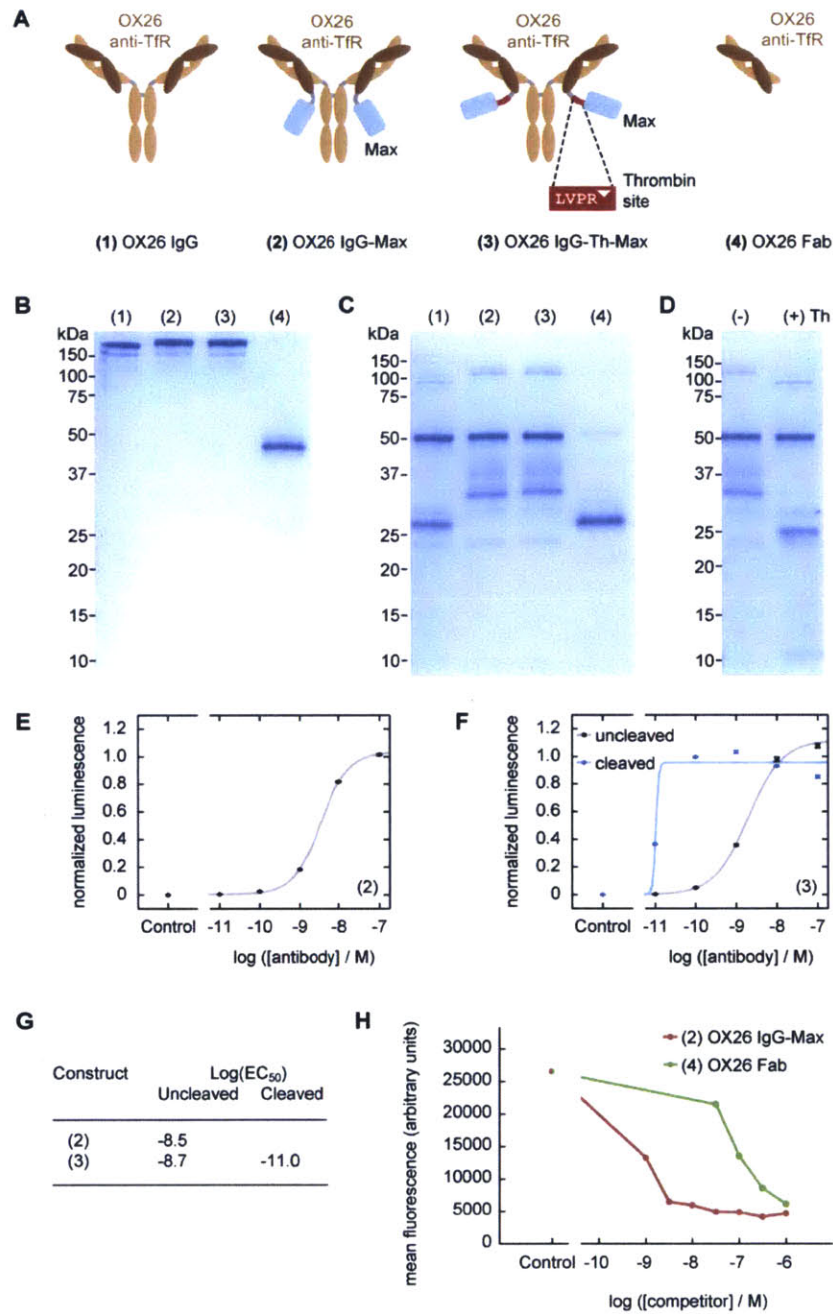


Fig. 4-3: Expression and characterization of OX26 brain shuttle variants.

(A) Schematic designs of recombinant OX26 constructs and fusions.

(B) Nonreducing SDS-PAGE gel of constructs (1) to (4) after expression and purification.

(C) The same as in (B) but under reducing conditions (100 mM DTT, samples boiled for 10 min).

- (D)** Reducing SDS-PAGE of construct (3) after incubation at 37C for 3h without or with addition of 2% v/v thrombin.
- (E)** PAC1 bioassay results for construct (2). Luminescence intensities were normalized to the range evoked by buffer alone and 1 nM PACAP-38.
- (F)** PAC1 bioassay results for construct (3) with or without thrombin. Luminescence intensities were normalized to the range evoked by buffer alone and 1 nM PACAP-38.
- (G)** Fitted potencies for (E) and (F). 95% confidence intervals are listed in Supplementary Table 4-18.
- (H)** Cell-based TfR competition binding assay results for IgG (2) and Fab (4). 9L rat glioma cells, which express TfR, were incubated with 10 nM biotinylated OX26 and varying concentrations of the construct of interest for 3h at 37C, washed, stained with SAPE, and analyzed by flow cytometry. Lower mean fluorescence values indicate more effective competition of the construct of interest against biotinylated OX26 IgG. Control indicates 10 nM biotinylated OX26 alone. Lines represent simple linear interpolation between data points.

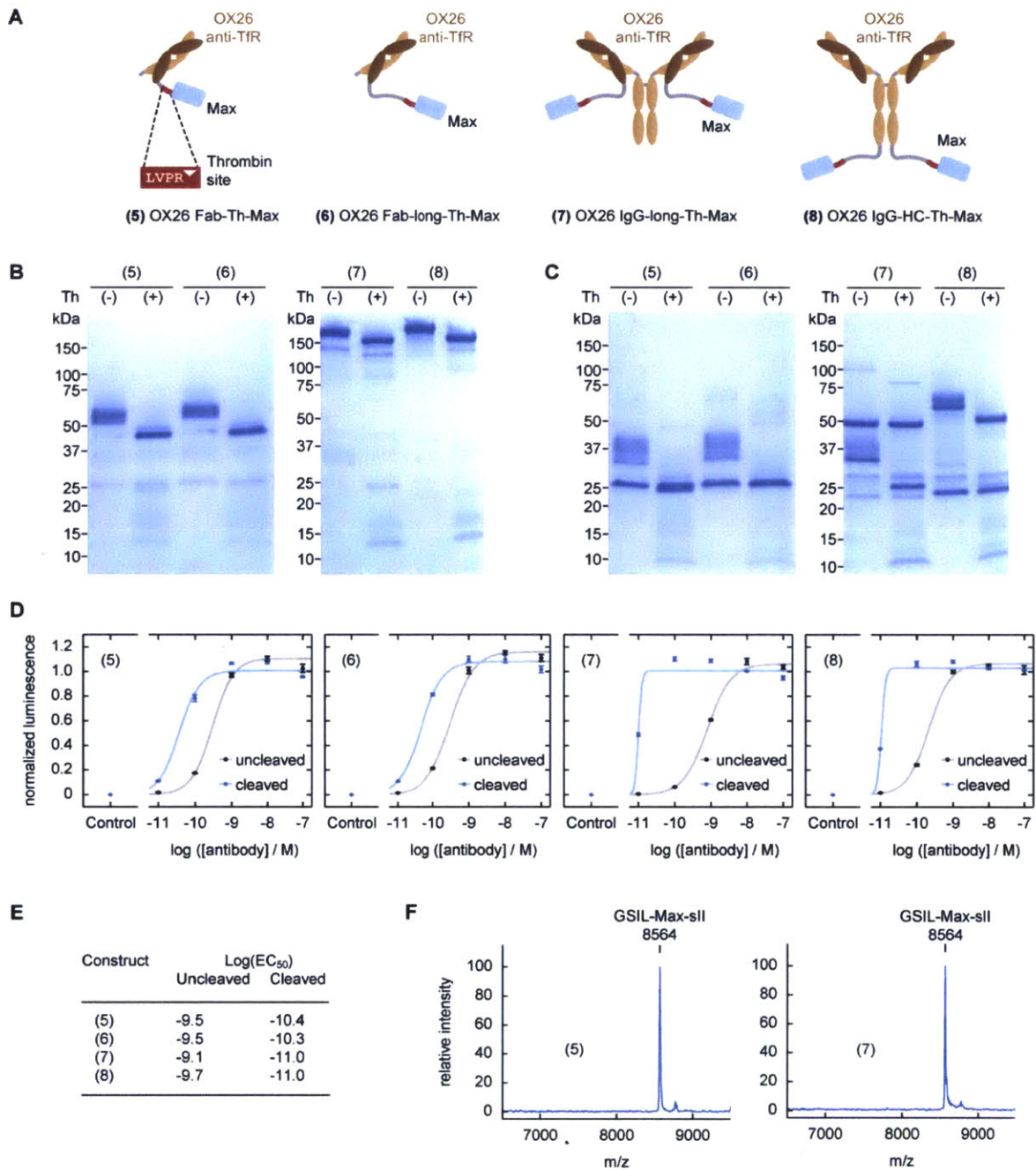


Fig. 4-4: Evaluation of revised OX26 brain shuttle variants.

- (A) Schematic designs of revised recombinant OX26 constructs and fusions.
- (B) Nonreducing SDS-PAGE of constructs (5) to (8) after incubation at 37C for 3h without or with addition of 2% v/v thrombin.

- (C)** Reducing gel of the samples in (B). Note the broadening of bands (toward higher, not lower, apparent mass) that correspond to chains fused to maxadilan, and the disappearance of the broadening effect after thrombin cleavage, indicating it is related to the maxadilan moiety.
- (D)** PAC1 bioassay results for constructs (5) through (8) with or without thrombin cleavage.
- (E)** Fitted potencies for (D). 95% confidence intervals are listed in Supplementary Table 4-18.
- (F)** MALDI mass spectra for constructs (5) and (7) after thrombin cleavage confirm a sharp peak at the precise expected mass/charge value for the cleaved maxadilan moiety.

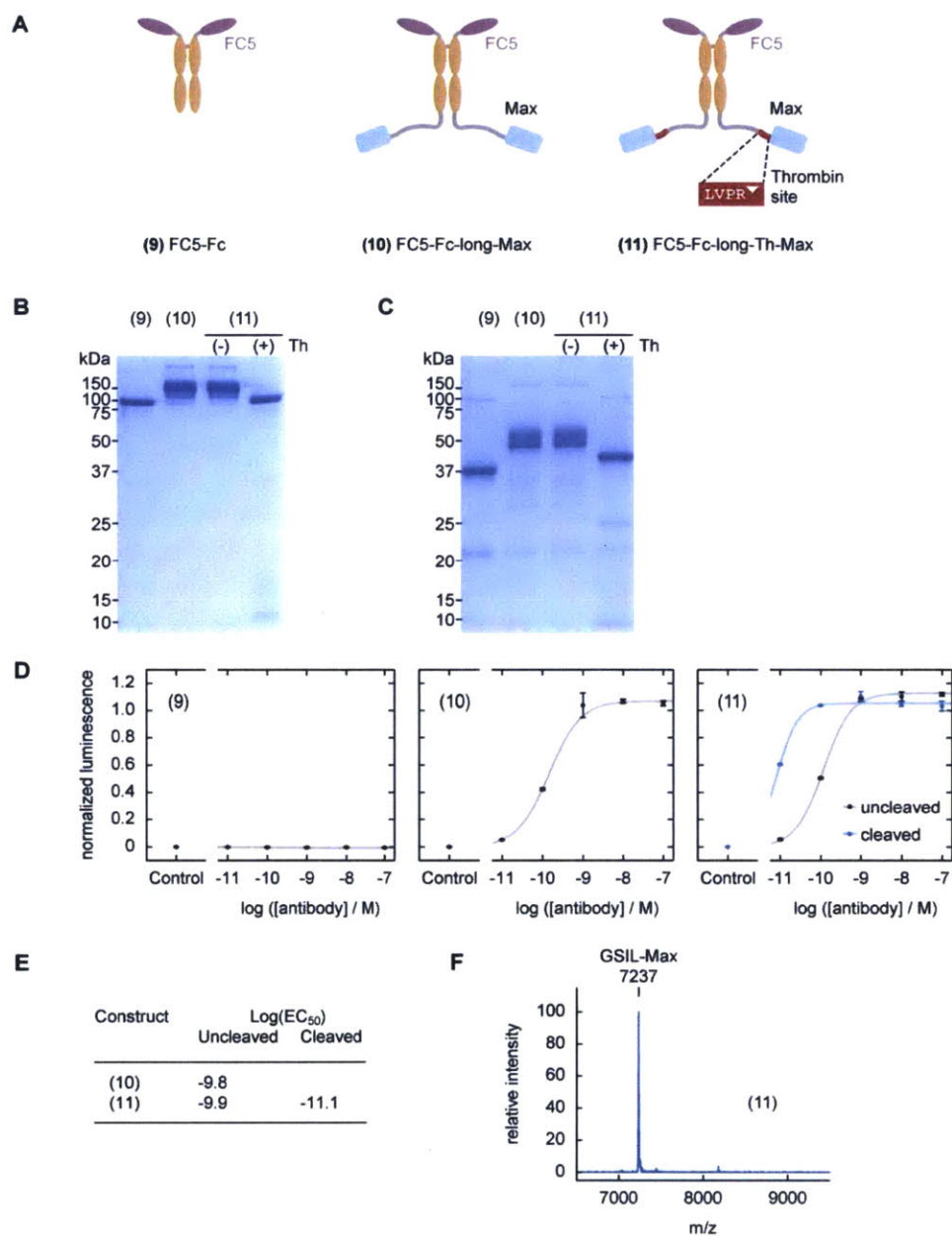


Fig. 4-5: FC5-Fc fusion brain shuttles.

- (A) Schematic designs of revised recombinant FC5-Fc constructs and fusions.
- (B) Nonreducing SDS-PAGE of constructs (9) to (11), in the case of (11) after incubation at 37C for 3h without or with addition of 2% v/v thrombin.
- (C) Reducing SDS-PAGE gel of the same samples as in (B). Note the band broadening for (10) and (11), fused to maxadilan. After thrombin cleavage, the (11) appears as a sharp band.

- (D)** PAC1 bioassay results for the indicated constructs.
- (E)** Fitted potencies for (D). 95% confidence intervals are listed in Supplementary Table 4-18.
- (F)** MALDI mass spectra for construct (11) after thrombin cleavage confirms a sharp peak at the precise expected mass/charge value for the cleaved maxadilan moiety.

Supplementary Table 4-S1: Catalog of plasmids used in this study

ID	Name	Source
Z544	pEXPR-T7-cfSGFP2-LVPR-GSIL-maxadilan	This study
C512	pLV-hEF1a-Glo22F-IRES-H2B-Cerulean-2A-puro	Chapter 2
C525	pLV-hEF1a-PACAP-R-IRES-mKate2-2A-bla	This study
C705	gWiz-OX26-LC	This study
C707	gWiz-OX26-LC-Th-Max-sll	This study
C708	gWiz-OX26-LC-Max-sll	This study
C709	gWiz-OX26-LC-His6	This study
C710	gWiz-OX26-HC	This study
C711	gWix-OX26-Fab-HC-His6	This study
C712	gWix-OX26-Fab-HC-sll	This study
C714	gWiz-OX26-LC-long-Th-Max-sll	This study
C715	gWiz-OX26-HC-long-Th-Max-sll	This study
C722	gWiz-FC5-Fc	This study
C723	gWiz-FC5-Fc-long-Max	This study
C724	gWiz-FC5-Fc-long-Th-Max	This study
X106	pMD2.G	Addgene 12259
X107	psPAX2	Addgene 12260
X108	pLenti X1 Zeo DEST (668-1)	Addgene 17299
X109	pEF-ENTR A (696-6)	Addgene 17427
	gWiz Blank	Genlantis (San Diego, CA)
	pFUSE2-CLlg-mk	Invivogen (San Diego, CA)
	pFUSE2-CHlg-mG2a	Invivogen (San Diego, CA)

Supplementary Table 4-S2. Full sequence for bacterial expression plasmid Z544 (pEXPR-T7-cfSGFP2-LVPR-GSIL-maxadilan)

color coding key:

cfSGFP2: cysteine-free GFP variant (with N-terminal StrepII tag underlined)

Linker: LVPR-GSIL

Maxadilan

Kanamycin resistance gene

pBR322 origin of replication

sequence:

```
GCTCAGAGGATCGAGATCTCGATCCCAGCAAAATTAATACGACTCACTATAGGGAGAGCCACAACGGTTTCCCTCTAGAAAATAATTT
TGTTTAACTTTAAGAAGGAGATATACATATGAGCGCGTGGAGCCATCCGCAGTTTGAAAAAGGTGCTGTATCCAAGGGCGAAGAGC
TGTTTACGGGGCGTAGTACCGATTTTGGTGGAGCTGGACGGCGATGTGAACGGCCATAAATTTAGTGTGAGCGGGCGAAGGTGAGGGC
GATGCGACATATGGCAAACTGACCCTGAAAATTTATTAGTACCACCGGTAACCTGCCAGTGCCTTGGCCGACGCTGGTTACCACCCCT
GACCTACGGTGTGCAAAATGTTTCGCTCGCTACCCCGACCATATGAAACAGCATGACTTCTTCAAGAGCGCAATGCCGGAAAGGTACG
TGCAGGAGCGTACGATTTTTTCAARAGATGATGGGAATTAACAAGACAGTGGCGAAGTGAATTCGAGGGGGCATACGCTGGTTAAT
CGCATCGAACTGAAAGGCCATCGACTTCAAAGAAGATGGTACATTTCTGGGTACAAGCTTGAATACAACCTACACTCACATAACGT
ATATATCACAGCAGATAAGCAGAAGAATGGTATTAAGGCGAATTTCAAGATCCGTACAATATTGAGGATGGCGGTGTTCACTTAG
CTGATCATTTATCAACAGAACACCCCTATTGGAGATGGCCAGTGTTCGTCGCCAGATAATCATTACCTGTCTACCCAGAGCAAACTG
AGCAAAAGACCCCTAATGAGAAACGTGATCATATGGTCTTACTGGAGTTCGTTACAGCGCGGGGCATTACGCTGGGTATGGATGAGCT
GTATAAGCTGGTTTCTCGCGGGTCTGATCTCTGTGACGCCACTTGCAGTTCGCCAAAGCTATTGACGATTGCCAGAAACAGGCGC
ACCATAGCAACGTTCTGCAGACCTCTGTTTCAGACCACCGCCACTTTCACCAGCATGGACACGTCCTCCAGCTGCCTGGCAACAGCGTG
TTTAAAGGAATGTATGAAACAGAAAGAAGGAGTTCAAAGCCTAAACAAGCCCCGAAAGGAAGCTGAGTTGGCTGCTGCCACCGCTG
AGCAATAACTAGCATAACCCCTTGGGGCCTCTAAACGGGTCTTGAGGGGTTTTTGTCTGAAAGGAGGAACCTATATCCGGATATCCA
CAGGACGGAGGTAGCTCTGGCCCGTGTCTCAAATCTCTGATGTTACATTCACAAAGATAAAAAATATATCATCATGAACAATAAAA
CTGTCTGCTTACATAAACAGTAATAACAAGGGGTGTTATGAGCCATAATCAACGGGAAAGCTCGAGGCCGGGATTAATTTCCAACT
SGATGCTGATTTATATGGGTATAAAATGGGCTCGCGATAATGTCGGGCAATCAGGTGCGCAATCTATCGGTTGTATGGGAAGCCCG
ATGGGCCAGGTTGTTTCTGAAACAATGGCAAAAGGTAGCGTGGCCAAATGATGTTACAGATGAGATGGTCCAGACTAAACTGGCTGACC
GANTTTATGGCTCTTCCGACCATCAAGCATTTTATCCGTACTTCTGGTATGCATGCTTACTCACCACCTGGCAATCCCGGAAAAA
AGCATTCCAGGTATTAGAAGAATATCTGATTCAGGTGAAAATATTGTGATGGCGTGGCAGTCTTCTGGCCGGTTGCATTGCA
TTCCTGTTTGTAAATGTCTTTTAAACAGCGATCGGATTTTCGCCTCGCTCAGGCGCAATCACGAATGAATAACGGTTTGGTTGAT
TCGAGTGAATTTGATGACGAGCGTAATGGCTGGCTGTTGAACAAGTCTGGAAAGAAATGCATAAACTTTTGGCATTTCTAGGGGA
TTCAGTCCCTCACTCATGCTGATTTCTCACTTGATAACCTTATTTTGGACGAGGGGAAATTAATAGGTTGATTTGATGTTGCAAGG
TCGGAATCGCAGACCGATACCAGGATCTTGGCATCCTATGGAAGTGCCTCGGTTGAGTTTCTCTCTTATTACAGAAAAGGCTTTT
CAAAAATATGGTATTGATAATCTGATATGAATAAATTCAGTTTTCATTTGATGCTCGATGAGTTTCTTATTCAGAAATTGGTTAA
TTGGTTGTACATTATTAGATTGGGCCCGTTCCTACTGAGCGTCAGACCCCGTAGAAAAGATCAAAGGATCTTCTTGAGATCCTT
TTTTTCTGCGGTAATCTGCTGCTTGCAACAAAAAACCACCGCTACCAGCGGTGGTTTGGTTTCCGGATCAAGAGCTACCAACT
CTTTTCCGAAGGTAACCTGGCTTCAGCAGAGCGCAGATACCAAAATCTGTTCTTCTAGTGTAGCCGTAGTTAGGCCACCCTCAA
GAACTCTGTAGCACCGCTACATACTCGCTCTGCTAATCCTGTTACCAGTGGCTGCTGCCAGTGGCGATAAGTCGTGTCTTACCG
GGTTGGACTCAAGACGATAGTTACCGGATAAGGCGCAGCGGTTCGGGCTGAACGGGGGGTTCGTGCACACAGCCAGCTTGGAGCGA
ACGACCTACACCGAACTGAGATACCTACAGCGTGAAGTATGAGAAAGCGCCACGCTTCCCGAAGGAGAAAGCGGACAGGTATCC
GGTAAGCGGCAGGGTCCGAAACAGGAGAGCGCACGAGGGAGCTTCCAGGGGAAACGCTGGTATCTTTATAGTCTGTCCGGTTTC
GCCACCTGACTTGAGCGTCGATTTTGTGATGCTCGTCAGGGGGCGGAGCCTATGGAAAACGCCAGCAACCGCGCCCTTTTAA
CGGTTCCCTGGCTTTTGTGCTGCTTTTGTCTACATGTTCTTTCCTGCGTTATCCCCTGATTCTGTGGATAACCGTATTACCGTAG
CATGGATCTCGGGACGCTAACTACTAAGCGAGAGTAGGAACTGCCAGGCATCAAATAAAACGAAAGGCCAGTCTTCCGACTG
AGCCTTTCTGTTTATCTGTTGTTTTCGGTGAACGCTCTCCTGAGTAGGACAAATCCGCCGGGAGCGGATTTGAACGTTGTGAAGC
AACGGCCCCGAGGGTGGCGGGCAGGACGCCGCCATAAAGTCCAGGCATCAAACCTAAGCAGAAGGCCATCTGACGGATGGCCTT
TTTGGCTTTCTACAACTCTTCTGTTAGTTAGTTACTTAA
```

Supplementary Table 4-S3. Full sequence of lentiviral plasmid C525 (pLV-hEF1a-PACAP-R-IRES-mKate2-2A-bla)

color coding key:

- hEF1a: Human elongation factor 1 alpha promoter
- Transgene cassette:
 - PAC1: Rat PACAP receptor
 - IRES: Internal ribosome entry site
 - mKate2: Red fluorescent protein
 - 2A: Autoproteolytic viral amino acid sequence
 - Bla: Blasticidin resistance gene
- delta_U3 / 3'LTR: HIV 3'LTR with deletion in the U3 region
- AmpR: Ampicillin resistance gene
- pUC origin of replication
- RSV / 5'LTR: Rous Sarcoma Virus / HIV 5'LTR hybrid promoter
- Psi: Lentiviral Psi packaging sequence
- RRE: Rev response element
- CPPT: Central polypurine tract

sequence:

```

CTTTGCAGCTAATGGACCTTCTAGGTCTTGAAGGAGTGGGAATTEGGTCCGGTGCCCGTCAGTGGGCAGAGCGCACATCGCCAC
AGTCCCCGACAAGTTGGGGGGAGGGGTGGCAATTGAACCGGTGCCTAGAGAAGGTGGCGGGGTAAACTGGGAAAGTGAITGTC
TGTAAGTGGCTCCGCCTTTTCCCGAGGGTGGGGGAGAACCCTATATAAGTGCAGTAGTCGCCCGTGAACCTTCTTTTCGCAACGGG
TTTGCCCGCCAGAACACAGGTAAGTGGCGTGTGTGGTTCGCCCGGGCCCTGGCCCTCTTACGGGTATGGCCCTTCGGTGCCTTGAAT
TACTTCCACCTGGCTGCAGTACGTGATTCCTGATCCCGAGCTTCGGSTTGGAAAGTGGTGGGAGAGTTCGAGGCCCTTCGGCTTAAG
GAGCCCCCTTCGCCTCGTCTTGAAGTTGAGCCTGGCCCTGGGGCGTGGGGCCGCCCGTGGGAATCTGGTGGCACCTTCGCCCTGT
CTCGCTGCTTTTGATAAGTCTCTAGCCATTTAAAATTTTGGATGACCTGCTGGGACGCTTTTTTTCTGGCAAGATAGTCTTGTAAA
TGCGGGCCAAGATCTGCACACTGGTATTTCCGGTTTTTGGGGCCCGGGCCGGCAGCGGGGCCCGTGCCTCCCAGCCACATGTTCCGG
CGAGGCGGGGCTGCGAGCCGGCCACCCGAGAATCGGACGGGGTAGTCTCAAGCTGGCCGGCTGCTCTGGTGCCTGGCTTCGGC
CCGGCGTGTATCGCCCCCGCTGGGGGCAAGGCTGGCCGGTCCGACACAGTTGCGTGGAGCGGAAAGATGGCCCGCTTCGCCGGCC
TGCTGCAGGGAGCTCAAAATGGAGGACCGGGCCCTCGGGAGAGCGGGCCGGTGAATCAOCCACACAAAGGAAAAGGGCCTTCCGT
CCTCAGCCGTCGCTTCATGTGACTCCACGGAGTACCGGGCCCGTCCAGGCACCTCGATTAGTTCGAGCTTTGGAGTACGTCG
TCTTTAGGTTGGGGGGAGGGTTTTATGCGATGGAGTTTCCCCACACTGAGTGGGTGGAGACTGAAGTAGGCCAGCTTGGCCTT
GATGTAATCTCCTTGGAAATTTGCCCTTTTGGATTTGGATCTTGGTTCATTTCAAGCCTCAGACAGTGGTCAAAGTTTTTTTC
TTCCATTTCCAGTGTGCTGAGGAATTAGCTTGGTACTAATACGACTCACTATAGCCTGGCCACCATTGGCTCCGTTCTCCAGTGA
GCTTGCAGAGCTCTCCTCCTCCGTGTGCAATCGCTATGCACCTGACTGTATATTCAAAAAGGAAACAGGCTATGTGTTGGAACGC
ATTGAGAGAGCAAAATGACCTCATGGGATGAATGAGTCTCTCCTGGTTGCCAGGTATGTTGGGATAATATAACATGTTGGAAACC
AGCTCAGGTCGGTGAGATGGTTCCTCGTGGTGGCCAGAGGTTTTCCGAATTTTCAACCAGACCAAGTATGGATGACAGAGACTA
TAGGGGATTCGGGGTTCGCAGATCTAATTCTTTGAAAATAACAGATATGGGAGTTGTAGGGAGAAATGTACAGAGGACGGATGG
TCCGAGCCTTTTCCCAATATTTGATGCTTGTGGATTCGACGATATGAGCCAGAGAGCGGAGATCAAGATTACTATTACCTCAG
CGTTAAGGCACTGTATACTGTCGGTTATTCACTTCTCTTGCACACTTACGACTGCCATGTTGATCCTGTGCCGCTTTAGGAAGC
TGCATGTACCCGAAATTTACACACATGAACCTTTTTGTTTCTTTCATGTTGAGAGCCATTTCTGTTTTCAAAAAGATTGGATA
CTCTACGCCGAACAGGACTCTAGCCATTGCTTCGTGAGTACCGTTGAGTGCAGGCTGTTATGGTCTTCTTTCACTATTGGTGGT
TTCAAATATTTCTGGCTTTTATCGAGGGTCTGACTTGTACTCTTCTGGTTGAAACTTTCTTCCAGAAAAGAGATATTCT
ATTGGTATACTATCATTGGATGGGAACTCCGACGGTATGTGTCAGTGTATGGCAGTCTCAGACTCTATTTTCGATGACCGGGC
TGCTGGGACATGAACGATTCACCCGCGCTGTGGTGGTTATCAAGGGACCGGTAGTGGGAGCATTATGGTCAACTTTGTCTTGT
TATCGGTATCATCATCCTCGTTTCAGAACTGCAGTCCCTGATATGGGAGCAACGAATCATCTATTTATCTTACACTTGTCTA
GATCTACATTTGTTGCTCATACTCTCTTTGGCATCCATTATACAGTCTTTGCTTTCAGCCCTGAAAATGTGTCTAAACCGGAGAGA
CTGGTCTTTGAACTCGGCCCTGGATCTTTTCAGGGATTCGTAGTCCGCTGTGCTCTATTGCTTCTTGAATGGAGAAGTGCAGGCTGA
GATAAAGCGCAAAATGGCGATCCTGGAAGGTCAACCGCTATTTACTATGGACTCAAGCACCGCCATCCATCCTTGGCTTCTAGCG
CGTAAACGGAGGTACAAATTTGCTATCCTTTCTAAATCTAGCTCACAACCTTCGCATGTCTAGCCTCCAGCCGATAACCTTGCT
ACTTAGGACTGGGATCCGCCCTCTCCTCCCGCCCTAACCTTACTGCGCAAGCCGCTTGGATAAGGGCCGTGTGCGTTTTG
TCTATATGTTATTTTCCACCATATTGCCGTCTTTTGGCAATGTGAGGGCCCGGAAACCTGGCCCTGCTTCTTACGAGCATTCCT
AGGGGTCTTTCCCTCTCGCCAAAGGAATGCAAGTCTGTTGAATGTGCTGAAGGAAGCAGTTCCCTCGGAAGCTTCTTGAAGACA
AACACGCTCTGTAGCGACCTTTGCAGGCAGCGGAACCCCCACCTGGCGCAGGTCCTCTGCGGCCAAAAGCCAGCTGTATAAG
ATACACCTGCAAAAGGCGGCACAACCCAGTGCACGTTGTGAGTGGATAGTGTGGAAAGAGTCAAATGGCTCTCTCAAGCGTA
TTCAACAAGGGGCTGAAGGATGCCAGAAAGTACCCCATGATGGGACTGATCTGGGGCCTCGGTACACATGCTTTACATGTGT
TTAGTCCGAGGTTAAAAAAGCTTAGGGCCCCCGAACCCAGCGGACGTTGGTTTTCTTTGAAAAACACGATGATAATATGGCCACA
    
```

GCCACCATGGTGAGCGAGCTGATTAAGGAGAACATGCACATGAAGCTGTACATGGAGGGCACCCTGAACAACCACCCTTCAAGTG
CACATCCGAGGGGGAAGGCAAGCCCTACGAGGGCACCCAGACCATGAGAATCAAGGCGGTGAGGGCGGCCCTCTCCCTTCGCCT
TCGACATCCTGGCTACCAGCTTCATGTACGGCAGCAAAACCTTCATCAACCACACCAGGGCATCCCGACTTCTTAAAGCAGTCC
TTCCCCGAGGGCTTCACATGGGAGAGCTCACCACATACGAAGATGGGGCGGTGCTGACCGCTACCCAGGACACCAGCCTCCAGGA
CGGCTGCCTCATCTACAACGTCAAGATCAGAGGGGTGAACCTCCCATCCAACGGGCCCTGTGATGCAGAAAGAAACACTCGGCTGGG
AGGCTCCACCGAGACACTGTACCCCGCTGACGGCGGCCCTGGAAGGCAGAGCCGACATGGCCCTGAAGCTCGTGGGCGGGGCGAC
CTGATCTGCAACCTTAAGACCACATACAGATCCAAGAAACCCGCTAAGAACCTCAAGATGCCCGGCTCTACTATGTGGACAGGAG
ACTGGAAGAATCAAGGAGGCCGACAAAGAGACATACGTGAGCAGCAGAGGTGGCTGTGGCCAGATACTGCGACCTCCCTAGCA
AACTGGGGCACAACCTTAATTCCGCTCAGGGGCGGGCAGCCTGCTGACCTGGGGCCAGTGGAGGAAACCAGGCCCTATGGCT
AAGCCTTTGTCTCAAGAAGAAATCCACCCTCATTTGAAAGAGCAACGGCTACAATCAACAGCATCCCCATCTCTGAAGACTACAGCCT
CGCCAGCCGAGCTCTCTTAGCCGACGGCGCATCTTCACTGGTGTCAATGTATATCATTTTACTGGGGACCTTGTGCAGAACTCG
TGGTCTGGGCACTGCTGCTGCTGCCGAGCTGGCAACCTGACTTGTATCGTCCGATCGGAAATGAGAACAGGGGCATCTTGAGC
CCTGCGGACGGTGCCGACAGGTGCTTCTCGATCTGCATCCTGGGATCAAAGCCATAGTGAAGGACAGTGATGGACAGCCGACGGC
AGTTGGGATTTGGTGAATTTGGTGCCTCTGGTTATGTGTGGGAGGGATAAGGACAGGTGATATCCAGCACAGTGGCGGCCCTCGA
CAATCAACCTCTGGATTACAAAATTTGTGAAAGATTGACTGGTATTCTTAACTATGTTGCTCCTTTTACGCTATGTGGATACGCTG
CTTAAATGCCTTTGTATCATGCTATTGCTTCCCGTATGGCTTTCATTTTCTCCTCTGTATAAATCCTGGTTGCTGTCTTTTAT
GAGGAGTTGTGGCCGTTTGCAGGCAACGTGGCTGGTGTGCACCTGTGTTGCTGACGAACCCCACTGGTTGGGCATTGCCAC
CACCTGTAGCTCCTTCCGGGACTTTCGCTTCCCCCTCCTTATTGCCACGGCGAAGCTCATCGCCGCTGCCTTGCCTGCTGCT
GGACAGGGGCTCGGCTGTTGGGCACTGACAATCCGTGGTGTGTCGGGGAAGCTGACGTCTTCCATGGCTGCTCGCTGTGTT
GCCACCTGGATCTGCGCGGACGTCTTCTGCTACGTCCCTTCGGCCCTCAATCCAGCGGACCTTCTTCCCGCGCCTGCTGCC
GGCTCTGCGGCTCTCCGCGTCTTCGCTTCCGCTCAGACGAGTCCGATCTCCCTTTGGGCGCCCTCCCGCCTGGAATTTGCA
AGATATCCGGTTAGTAAATGAGTTTGAATTAATTTCTGTGAAATGTGTGCTAGTGTGAAAGTCCCAAGCTCCCAAGCTCCCA
GCAGAAAGTATGCAAAAGCATGCATCTCAATTAGTCAGCAACCAGGTGTGAAAGTCCCAAGCTCCCAAGCTCCCAAGCTCCCA
AAGCATGCATCTCAATTAGTCAGCAACCATAGTCCCGCCCTAACTCCGCCATCCCGCCCTAACTCCGCCAGTTCCGCCATT
CTCCGCCCATGGCTGACTAATTTTTTTATTTATGCAAGGCGGAGGCCGCTCTGCTCTGAGCTATTCCAGAAGTAGTGAGGA
GGCTTTTTTGGAGGCTTAGGCTTTTGAAGAAAGCTCCCCCTGTTGACAATTAATCATCGGCATAGTATATCGGCATAGTATAATAC
GACAAGGTGAGAACTAACCATGGCCAAAGTTGACCACTGCGGTTCGGTGTGCTCACCAGCGGACGCTCGCCGAGCTGCGGAT
CTGGACCGACCGCTCGGTTCTCCCGGACTTCCGTGGAGGACACTTCCCGGTGTGGTCCGGGACGACGTGACCCTGTTTATCA
GCGCGGTCCAGGACCAGGTGGTCCGGACAACACCCTGGCTGGGTGTGGGTGCGCGGCTGGACGAGCTGTACCCGAGTGGTCCG
GAGTCTGTCCACGAACCTCCGGGACGCTCCGGGCGGCCATGACCGAGATCGGCAGCAGCCGTGGGGGCGGGAGTTCGCCCT
GCGGACCCGGCCGCAACTGCGTGCCTTCCGTGGCCGAGGAGCAGGACTGACACGTGCTACGAGATTTAAATGGTACTCTTAAAGA
CCAATGACTTACAAGCAGCTGTAGATCTTAGCCACTTTTTAAAAGAAAAGGGGGACCTGGAAGGGCTAGCTCACTCCCAACGAAG
ACAAGATCTGCTTTTTGCTTGTACTGGTCTCTCTGTTAGACCAGATCTGAGCCTGGGAGCTCTGCTGGCTAGGGAACCCAC
TGCTTAAAGCCTCAATAAAGCTTGCCTTGAAGTCTTCAAGTAGTGTGTGCCCGTCTGTTGTGTGACTCTGGTAACTAGAGATCCCTC
AGACCCTTTTAGTCAGTGTGAAATCTTAGCACTAGTAGTTCATGTCACTTATTATTAGTATTATAACTTGCAAGAAATG
AATATCAGAGAGTGAGAGGAACTTGTATTATGCACTTATAATGTTTACAAATAAAGCAATAGCATCACAAATTTACAAATAAAG
CATTTTTTCACTGCATCTAGTTGGTGTGTTGTTCCAACTCATCAATGTATCTTATCATGTCTGGCTTAGCTATCCCGCCCTAA
CTCCGCCAGTTCCGCCCATTCTCCGCCCATGGCTACTAATTTTTTTTATTTATGCAAGGCGGAGGCCAGCTGTGTTTCTTA
GACGTGAGGTGGCACTTTTCCGGGAAATGTGCGCGGAACCCCTATTTGTTTATTTTTCTAAATACATTCAAATATGTATCCGCTCA
TGAGACAATAACCTGATAAATGCTTCAATAATATGAAAAAGGAAGAGTATGAGTATCAACATTTCCGCTGTCGCCCTTATTTCC
TTTTTTGCGGCATTTTGCCTTCTGTTTTGCTCACCAGAAACGCTGGTGAAGTAAAGATGCTGAAGATCAGTTGGGTGCACG
AGTGGGTTACATCGAAGCTGGATCTCAACAGCGGTAAGATCTTGAGGTTTTCGCCCGAAGAAGCTTTTCCAATGATGAGCACTT
TTAAAGTTCTGTATAGTGGCGGTTATTCGGTATGACCGCGGCAAGAGCAACTCGGTCGCCGATCACTATTTCTAGAAT
GACTTGGTTGACTACTCACCAGTACAGAAAAGCATCTTACGGATGGCATGACAGTAAGAGAATTTAGCAGTGTGCCATAACCAT
GAGTGATAACACTGCGGCCAACTTACTTCTGACAACGATCGGAGGACCGAAGGAGCTAACCCTTTTTTGCACAACATGGGGGATC
ATGTAACCTCGCTTGTATGCTTGGGAACCGGAGCTGAATGAAGCCATACCAACGACGAGCGTACACCACGATGCTGTAGCAATG
GCAACAACGTTCCGCAACTATTAACGGCGAACTACTTACTCTAGCTTCCCGGCAACAATTAATAGACTGGATGGAGGCGGATAA
AGTTGCAGGACCACTTCTCGCTCGGCCCTCCGGCTGGCTGGTTATTGCTGATAAATCTGGAGCGGCTGAGCGTGGGCTCGCC
GTATCATTTGCAGCACTGGGGCCAGATGGTAAGCCCTCCGATCTGATGTTATCTACACGACGGGGAGTCAGGCAACTATGGATGAA
CGAAATAGACAGATCGCTGAGATAGGTGCCCTCACTGATTAAGCATTTGGTAACTGTGACACCAAGTTTACTCATATATACTTTAGAT
TGATTTAAACTTCATTTTTAATTTAAAGGATCTAGGTGAAGATCCTTTTTGATAATCTCATGACCAAAATCCCTAACGTGAGT
TTTCGTTCCACTGAGCGTACAGCCCCGTAGAAAAGATCAAAGGATCTTCTTGAGATCCTTTTTTTCTGCGCGTAACTGTGCTGCTT
CAAAACAAAACACCAGCTACCAGCGGTGGTTGTTTGGCCGATCAAGAGCTACCACTCTTTTTCCGAAGGTAACCTGGCTCAG
CAGAGCCAGATAACCAATCTAGTGTAGCCGTAGTGGCCAGTACCAAGACTCTGAGCACCACCTCAAGAATCTGTAGCACCCTCATACC
TCGCTCTGCTAATCCTGTTACCAGTGGCTGCTGCCAGTGGCGATAAGTCTGTCTTACCAGGTTGGACTCAAGACGATAGTTACCG
GATAAGGCGCAGCGGTCCGGCTGACGGGGGTTCTGTGCACACAGCCAGCTTGGAGCGAACGACCTACACCGAAGTACGATACCT
ACAGCGTGTGATGAGAAAGCGCCAGCTTCCGGAAGGGAGAAAGGGCGACAGGTATCCGGTAAGCGGCAGGTCGGAACAGGAG
AGCGCACGAGGGAGCTCCAGGGGAAACGCTGGTATCTTTATAGCTCTGTGGGTTTCCGCACCTCTGACTTGTGAGCGTGTGATTT
TTGTGATGCTCGTCAAGGGGGGAGCCATGGAAGAAACGCGCAGCAACGCGCCCTTTTACGGTCTGGCCTTTTGTGCTGCTTT
TGCTACATGTTCTTTCCCTGCTTATCCCTGATTTCTGTGGATAACCGTATACCCTTTTGTGAGTACTGATACCCTGCTGCGCA
GCCGAACGACCGAGCGCAGCGAGTCACTGAGCGAGGAAGCGGAAGAGCGCCCAATACGCAACCCCTCTCCCGCGGCTTGGCCG
ATTCATTAATGACGCTGGCAGCAGGTTTCCCGACTGGAAGCGGGCAGTGTGAGCGCAACGCAATTAATGTGAGTTAGCTCACTCA
TTAGGACCCCAAGCTTTTACACTTTATGCTTCCGGCTCGTATGTTGTGTGGAATTTGTGAGCGGATAACAATTTACACAGGAAACA

GCTATGACCATGATTACGCCAAGCGCGCAATTAACCCCTCACTAAAGGGAACAAAAGCTGGAGCTGCAGCTTAATGTAGTCTTATG
CAATACCTTGTAGTCTTGCAACATGGTAACGATGAGTTAGCAACATGCCTTACAAGGAGAGAAAAGCACCCTGCATGCCGATTG
GTGGAAGTAAGGTGGTACGATCGTGCCTTATTAGGAAGGCAACAGACGGGTCTGACATGGATTGGACGAACCACTGAATTGCCCGCA
TTGCAGAGATATTGTATTTAAGTGCCCTAGCTCCATAACAATAAACGGGTCTCTCTGGTTAGACCAGATCTGAGCCTGGGAGCTCTCT
GGCTAAC TAGGGAACCACTGCTTAAGCCTCAATAAAGCTTGCCTTGAGTGCTTCAGTAGTGTGTGCCCGTCTGTTGTGTGACTC
TGGTAAC TAGAGATCCCTCAGACCCTTTTAGTCAGTGTGGAAAATCTCTAGCAGTGGCGCCGAACAGGGACCTGAAAGCGAAAGG
GAAACCAGAGCTCTCTCGACGCAGGACTCGGCTTGCTGAAGCGCGCACGGCAAGAGGCGAGGGGCGGCGACTGGTGAGTACGCCAA
AAATTTTGACTAGCGGAGGCTAGAAGGAGAGAGATGGGTGCGAGAGCGTCAGTATTAAGCGGGGAGAATTAGATCGCGATGGGAA
AAAATTCGGTTAAGGCCAGGGGAAAGAAAAATATAAATTA AACATATAGTATGGGCAAGCAGGGAGCTAGAACGATTTCGCAGT
TAATCCTGGCCTGTTAGAAACATCAGAAGGCTGTAGACAAATACTGGGACAGCTACAACCATCCCTTCAGACAGGATCAGAAGAAC
TTAGATCATTATATAATACAGTAGCAACCCCTCTATTGTGTGCATCAAAGGATAGAGATAAAAGACACCAAGGAAGCTTTAGACAAG
ATAGAGGAAGAGCAAAACAAAAGTAAGACCACCGCACAGCAAGCGGCCGCTGATCTTCAGACCTGGAGGAGGAGATATGAGGGACA
ATTGGAGAAGTGAATTATATAAATATAAAGTAGTAAAAATTGAACCATTAGGAGTAGCACCCACCAAGGCAAAGAGAAGAGTGGTG
CAGAGAGAAAAAGAGCAGTGGGAATAGGAGCTTTGTTCCCTGGGTTCTTGGGAGCAGCAGGAAGCACTATGGGCGCAGCCTCAAT
GACGCTGACGGTACAGGCCAGACAATTATTGTCTGGTATAGTGCAGCAGCAGAACAATTTGCTGAGGGCTATTGAGGGCGAACAGC
ATCTGTTGCAACTCACAGTCTGGGGCATCAAGCAGCTCCAGGCAAGAATCCTGGCTGTGGAAAGATACCTAAAGGATCAACAGCTC
CTGGGGATTGGGGTTGCTCTGGAAAACCTATTTGCACCACTGCTGTGCCTTGGAAATGCTAGTTGGAGTAATAAATCTCTGGAACA
GATTGGAATCACACGACCTGGATGGAGTGGGACAGAGAAATTAACAATTACACAAGCTTAATACACTCCTTAATTGAAGAATCGCA
AAACCAGCAAGAAAAGAATGAACAAGAATTATTGGAATTAGATAAATGGGCAAGTTTGTGGAATTGGTTTTAACATAACAAATTGGC
TGTGGTATATAAAATTTATTCATAATGATAGTAGGAGGCTTGGTAGGTTAAGAATAGTTTTTGCTGTACTTTCTATAGTGAATAGA
GTTAGGCAGGGATATTCACCATTCGTTTCAGACCCACCTCCCAACCCGAGGGGACCCGACAGGCCCGAAGGAATAGAAGAAGA
AGGTGGAGAGAGACAGAGACAGATCCATTTCGATTAGTGAACGGATCTCGACGGTTAACTTTTAAAAGAAAAGGGGGGATTGGGG
GGTACAGTGCAGGGGAAAGAATAGTAGACATAATAGCAACAGACATACAACTAAAGAATTACAAAAACAAATTACAAAAATTCAA
AATTTTATTCCAGTGTGGTGAATTCAGTCTGC

Supplementary Table 4-S4. Full sequence of expression plasmid C705 (gWiz-OX26-LC)

color coding key:

CMV: CMV promoter and intron

Expression cassette:

IL-2 leader sequence

OX26 VL light chain variable domain

Murine IgG2a Ckappa domain

PolyA

KanR: Kanamycin resistance gene

pUC origin of replication

sequence:

TCGCGCGTTTCGGTGATGACGGTGAAAACCTCTGACACATGCAGCTCCCGGAGACGGTACAGCTTGTCTGTAAGCGGATGCCGGG
 AGCAGACAAGCCCGTCAGGGCGCGTCAGCGGGTGTGGCGGGTGTGGGGCTGGCTTAACTATGCGGCATCAGAGCAGATTGTA
 GAGAGTGCACCATATGCGGTGTGAAATACCGCACAGATGCGTAAGGAGAAAATACCGCATCAGATTGGCTATGGCCATTGCATAC
 GTTGATCCATATCATAATATGTACATTTATATGGCTCATGTCCAACATTACCGCCATGTTGACATTGATTATTGACTAGTTATT
 AATAGTAATCAATTACGGGGTCATTAGTTTCATAGCCCATATATGGAGTCCCGCGTTACATAAATTACGGTAAATGGCCCGCTGGC
 TGACCGCCCAACGACCCCGCCCATTTGACGTCAATAATGACGTATGTCCCATAGTAAACGCCAATAGGGACTTTCCATTGACGTCA
 ATGGGTGGAGTATTTACGGTAAACTGCCCACTTGGCAGTACATCAAGTGTATCATATGCCAAGTACGCCCCCTATTGACGTCAATG
 ACGGTAATGGCCCGCTGGCATTATGCCAGTACATGACCTPATGGGACTTTCCCTACTTGGCAGTACATCTACGTATFAGTCATC
 GCTATTACCATPGETGATGCGGTTTTGGCAGTACATCAATGGCGTGGATAGCGGTTTGGACTCACGGGGATTTCACAGTCTCCACCC
 CATTGACGTCAATGGGAGTTTGTGGTGGCACCAAAATCAACGGGACTTTCCAAAATGTCTGTAACAACTCCGCCCCATTGACGCAAA
 TGGGCGGTAGGGCGTGTACGGTGGGAGGTCTATAAAGCAGAGCTCGTTTAGTGAACCGTACAGATCGCCTGGAGACGCCATCCACGC
 TGTTTTGACCTCCATAGAACACACCGGACCGGATCCAGCCCTCCCGGGCCGGGAACGGTGCATTGGAACCGGGATTCCCGGTGCCAA
 GAGTGACGTAAGTACCGCTATAGACTCTATAGGCACACCCCTTTGGCTCTTATGCATGCTATACTGTTTTTGGCTTGGGGCTAT
 ACACCCCGCTTCCCTTATGCTATAGGTGATGGTATAGCTTAGCCTATAGGTGTGGTTATTGACCATTATTGACCCTCCCTATT
 GGTGACCACTTTCCATTAATAACATAACATGGCTCTTGGCACAACTATCTCTATTGGCTATATGCCAATACTCTGTCTCTC
 AGAGACTGACACGGACTCTGTATTTTACAGGATGGGGTCCCATTTATTTACAAATTCACATATACAACAACGCCCTCCCGG
 TGCCCGCAGTTTTTATTAACATAGGGTGGGATCTCCACGGGAATCTCGGGTACGTGTTCCGGACATGGGCTCTTCTCCGGTAGCG
 GCGGAGCTTCCACATCCGAGCCCTGGTCCCATGCTCCAGCGGCTCATGGTCCCTCGGCAGCTCCTTGCTCTAACAGTGGAGGCC
 AGACTTAGGCACAGCACAATGCCACCACCACAGTGTGCCGCACAAGGCCGTGGCGGTAGGGTATGTGTCTGAAAATGAGCGTGG
 AGATTGGGCTCGCACGGCTGACGCAGATGGAAGACTTAAGGCAGCGGCAGAAAGCATGACAGGCAGCTGAGTTGTTGATTTCTGAT
 AAGAGTCAGAGGTAACCTCCGTTGCGGTTGCTGTAAACGGTGGAGGGCAGTGTAGTCTGAGCAGTACTCGTTGGTGGCCGCGCGCC
 ACCAGACATAAATAGCTGACAGACTAACAGACTTCTCTTCCATGGTCTTTTCTGCAATCACCGTCTGTCGACAGCCGCCACCATTG
 TACAGGATGCAACTCCTGTCTTGCATTGCACTAAGTCTTGCACCTTGTCAAAAACAGTATATCGTGATCACCCAATCTCCATCCAG
 TCTGTCTGCATCCCTTGGCGACACAATTTCTCATCACTTGGCATGCCAGTCAGAACATTAATGTTGGTAAAGTGGTCCAGCAGA
 AACCAGGAAATGCTCCTAAACTGTTGATCTATAAGGCTTCCAACCTGACACAGGGCTCCCATCAGATTTAGTGGCAGTGGATCT
 GGAACAGGTTTCCATTAACCATCAGCAGCCTCCAGCCTGAAGACATTTGCCACTTACTACTGTCAACAGGGTCAAAGTTATCCGGT
 GACCTTCGGTGGAGGCCAAGCTGGAAATCAAAGGGCAGATGCTGCACCAACTGTATCCATCTTCCACCAATCCAGTGGAGAGT
 TACGATCTGGAGGTGCTCAGTCTGTCTTCTTGAACAACCTTCTACCCCAAAAGACATCAATGTCAAGTGGAAAGATTGATGGCAGT
 GAHCGACAAAATGGCGTCTTGAACAGTTGGACTGATCAGGACAGCAAAAGACAGCACTTACAGCATGAGCAGCACCTCAGCTTGAC
 CAAGGAGGATGATGAACGACATAACAGCTATACCTGTGAGGCCACTCACAAGACATCAACTTCAAGCATTGTCAAGAGSTTCAACA
 GGAATGAGTGTATCCGGATCCAGATCACTTCTGGCTAATAAAAGATCAGAGCTCTAGAGATCTGTGTGTTGGTTTTTTGTGGATCT
 GCTGTGCCCTTCTAGTTGCCAGCCATCTGTGTTTGGCCCTCCCGGTCCTTCCCTTGACCCTGGAAGGTGCCACTCCCCTGTCTCT
 TTCCATAAAAATGAGCAAAATGCAATCGCATGTCTGATAGTTGCTTCTATTTCTATTCTGGGGGTGGGCTGGGGCAGCAGCAAGG
 CGGAGGATTGGGAAGACAATAGCAGGCATGCTGGGGATGCGGTGGGCTCTATGGGTACCTCTCTCTCTCTCTCTCTCTCTCTCT
 CTCTCTCTCTCTCGGTACCT
 GTTCCCTCCTGGGCCAGAAAAGCAGGCACATCCCCTTCTCTGTGACACACCCTGTCCACGCCCTGGTTCTTAGTCCAGCCCCA
 CTCATAGGACACTATAGCTCAGGAGGGCTCCGCCCTCAATTTCCACCCCGCTAAAGTACTTGGAGCGGACTCTCCCTCCCTCATCAG
 CCCACAAACCAACCTAGCTCCAAGAGTGGGAAGAAATTAAGCAAGATAGGCTATTAAGTGCAGAGGGAGAGAAAATGCCCTCC
 AACATGTGAGGAAGTAAATGAGAGAAATCATAGAATTTCTCCGCTTCCCTCGTCACTGACTCGTCCGCTCGCTCGCTCGCTCGC
 GCGAGCGGTATCAGCTCAAAAGCGGTAATACGGTTATCCACAGAATCAGGGGATAACGCAGGAAAGAATGTGAGCAAAAAG
 GCCAGCAAAAAGCCAGGAACCGTAAAAGGCCGCGTGTGGCGTTTTTCCATAGGCTCCGCCCCCTGACGAGCATCACAAAAT
 CGACGCTCAAGTCAAGGTTGGCGAAACCCGACAGGACTATAAAGATACCAGGCGTTTCCCGCTGGAAGCTCCCTCGTGGCTCTCC
 ATGTTCCGACCCTGCCGTTACCGGATACCTGTCCGCTTCTCCCTTCCGGGAAGCGTGGCGCTTCTCAATGCTCAGCTGTAGGT
 TCTCAGTTCCGGTGTAGTCCAAACCGGTAAGACACGACTTATCGCCACTGCGAGCAGCCACTGGTAACAGGATTAGCAGAGGGTA
 AACTATCGTCTTGAAGTCCAAACCGGTAAGACACGACTTATCGCCACTGCGAGCAGCCACTGGTAACAGGATTAGCAGAGGGTA
 TGTAGGCGGTGCTACAGAGTTCTTGAAGTGGTGGCCTACTACGGCTACACTAGAAGGACAGTATTTGGTATCTGCGCTCTGCTGA
 AGCCAGTTACCTTCGAAAAAGAGTTGGTAGCTTTGATCCGGCAAAACAAACCACCGCTGGTAGCGGTGGTTTTTTTGTGTTGCAAG
 CAGCAGATTACGCGCAGAAAAAAGGATCTCAAGAAATCCTTTGATCTTTTCTACGGGGTCTGACGCTCAGTGGAAACGAAAACCTC

ACGTTAAGGGATTTTGGTCATGAGATTATCAAAAAGGATCTTCACCTAGATCCTTTTAAATTA AAAATGAAGTTTTAAATCAATCT
AAAGTATATATGAGTAAACTTGGTCTGACAGTTACCAATGCTTAATCAGTGAGGCACCTATCTCAGCGATCTGTCTATTTTCGTTCA
TCCATAGTTGCCTGACTCCGGGGGGGGGGGGCCTGAGGTCTGCCTCGTGAAGAAGGTGTTGCTGACTCATACCAGGCCTGAATCG
CCCCATCATCCAGCCAGAAAGTGAGGGAGCCACGGTTGATGAGAGCTTGTGTAGGTGGACCAGTTGGTGATTTTGAACTTTTGC
TTTGCCACGGAACGGTCTGCGTTGTCGGGAAGATGCGTGATCTGATCCTTCAACTCAGCAAAAAGTTTCGATTTATTCAACAAAGCCG
CCGTCCCCTCAAGTCAGCGTAATGCTCTGCCAGTGTACAAACCAATTAACCAATTCTGATTAGAAAACTCATCGAGCATCAAATG
AAACTGCAATTTATTTCATATCAGGATTATCAATACCATATTTTGGAAAAAGCCGTTTCTGTAATGAAGGAGAAAACTCACCGAGGC
AGTTCCATAGGATGGCAAGATCCTGGTATCGGTCTGCGATTCCGACTCGTCCAACATCAATACAACCTATTAATTTCCCTTCGTCA
AAAATAAGGTATCAAGTGAGAAATCACCATGAGTGACGACTGAATCCGGTGAGAATGGCAAAAAGCTTATGCATTTCTTTCCAGAC
TTGTTCAACAGGCCAGCCATTACGCTCGTCATCAAAATCACTCGCATCAACCAAACCGTTATTCAATTCGTGATTGCGCCTCAGCGA
GACGAAATACGCGATCGCTGTTAAAAGGACAATTACAACAGGAATCGAATGCAACCCGGCGCAGGAACACTGCCAGCGCATCAACA
ATATTTTCACCTGAATCAGGATATTCTTCTAATACCTGGAATGCTGTTTCCCGGGGATCGCAGTGGTGAGTAACCATGCATCATC
AGGAGTACGGATAAAAATGCTTGATGGTCCGAAGAGGCATAAATTCGGTCAGCCAGTTAGTCTGACCATCTCATCTGTAACATCAT
TGGCAACGCTACCTTTGCCATGTTT CAGAAACA ACTCTGGCGCATCGGGCTTCCCATACAATCGATAGATTGTGCGACCTGATTGC
CCGACATTTATCGCGAGCCCATTTATACCCATATAAATCAGCATCCATGTTGGAATTTAATCGCGGCCTCGAGCAAGACGTTTCCCG
TTGAATATGGCTCAT AACACCCCTTGATTACTGTTTATGTAAGCAGACAGTTTTATTGTTTCATGATGATATATTTTTATCTTGTG
CAATGTAACATCAGAGATTTTGAGACACAACGTGGCTTTCCCCCCCCCATTATTGAAGCATTATCAGGGTTATTGTCTCATG
AGCGGATACATATTTGAATGATTTAGAAAAATAAACAATAGGGGTTCCGCGCACATTTCCCGGAAAAGTGCCACCTGACGTCTA
AGAAACCATTATTATCATGACATTAACCTATAAAAATAGGCGTATCACGAGGCCCTTTCGTC

Supplementary Table 4-S5. Sequence of expression cassette for C707 (gWiz-OX26-LC-Th-Max-sII)

color coding key:

IL-2 leader sequence

OX26 VL light chain variable domain

Murine IgG2a Ckappa domain

Linker: (G₄S)₂-LVPR

Max: GSIL-maxadilan-StreptII

sequence:

```
ATGTACAGGATGCAACTCCTGTCTTGCATTGCACTAAGTCTTGCACCTTGTACAAACAGT GATATCGTGATCACCCAATCTCCATC
CAGTCTGTCTGCATCCCTTGGCGACACAATTCTCATCACTTGCCATGCCAGTCAGAACATTAATGTTTGGTTAAGTTGGTTCCAGC
AGAAACCAGGAAATGCTCCTAAACTGTTGATCTATAAGGCTTCCAACTTGCACACAGGCGTCCCATCAAGATTTAGTGGCAGTGGG
TCTGGAACAGGTTTCACATTAACCATCAGCAGCCTCCAGCCTGAAGACATTGCCACTTACTACTGTCAACAGGGTCAAAGTTATCC
GTGGACGTTCCGGTGGAGGCACCAAGCTGGAAATCAAA CGGGCAGATGCTGCACCAACTGTATCCATCTTCCACCATCCACTGACC
AGTTAAACATCTGGAGGTGCCTCAGTGGTGTGCTTCTTGAACAACCTCTACCCCAAAGACATCAATGTCAAGTGAAGATTGATGGC
AGTGAACGACAAAAATGGCGTCTTGAACAGTTGGACTGATCAGGACAGCAAAGACAGCACCTACAGCATGAGCAGCACCCCTCAAGTT
GACCAAGGACAGATATGAACGACATAACAGGTATACCTGTGAGGGCCACTCACAAAGACATCAACTTCACCCATTTGTCAAGAGGTTCA
ACAGGAATCAGTCTGGTGGCGGTGGCTCCGGTGGTGGAGGTTCCCTGGTGCCGCGTGGTTCGATTCTGTGCGACGCGACTTGTCAG
TTTCGTAAAGCGATTGACGATTGCCAGAAGCAGGCTCACCCTCCAACGTTCTGCAGACCTCTGTTCAAACGACTGCAACGTTTAC
TTCCATGGACACGTCGCAGTTACCGGGTAATAGCGTGTTTAAAGAGTGCATGAAACAGAAGAAAAAGAATTCAAGGCGAGCGCTT
GGAGTCATCCGCAATTCGAAAAGGGCGCATAA
```


Supplementary Table 4-S6. Sequence of expression cassette for C708 (gWiz-OX26-LC-Max-sII)

color coding key:

IL-2 leader sequence

OX26 VL light chain variable domain

Murine IgG2a Ckappa domain

Linker: (G₄S)₂

Max: GSIL-maxadilan-StreplI

sequence:

ATGTACAGGATGCAACTCCTGTCTTGCATTGCACTAAGTCTTGCCTTGTGCACAAACAGT GATATCGTGATCACCAATCTCCATC
CAGTCTGTCTGCATCCCTTGGCGACACAATTCTCATCACTTGCCATGCCAGTCAGAACATTAATGTTGGTTAAGTTGGTTCCAGC
AGAAACCAGGAAATGCTCCTAAACTGTTGATCTATAAGGCTTCCAACCTGCACACAGGCGTCCCATCAAGATTTAGTGGCAGTGG
TCTGGAACAGGTTTCACATTAACCATCAGCAGCCTCCAGCCTGAAGACATTGCCACTTACTACTGTCAACAGGGTCAAAGTTATCC
GTGGACGTTCCGGTGGAGGCACCAAGCTGGAATCAAA CGGGCAGATGCTGCACCAACTGTATCCATCTTCCACCATCCAGTGAG
AGTTAAACATCTGGAGGTCCCTCAGTCTGTGCTTCTTGAACAACCTTACCCCAAGACATCAATGTCAAGTGGAGATTTGATGGC
AGTGAACGACAAAATGGCGTCCCTGAACAGTTGCACTGATCAGGACAGCAGAGACAGCACCTACAGCTGAGCAGCACCCCTCAGGTT
GACCAAGGACGAGTATGAACCACATAACAGCTATACCTGTGAGGCCACTCAACAAGACATCAACTTCCACCCATTTGTCAAGAGCTTCA
ACAGGAATCAGTGGTGGCGGTGGCTCCGGTGGTGGAGGTTCCGGTTCGATTCTGTGCGACGCGACTTGTGAGTTTCGTAAAGCG
ATTGACGATTGCCAGAAGCAGGCTCACCACTCCAACGTTCTGCAGACCTCTGTTCAACGACTGCAACGTTTACTTCCATGGACAC
GTCGCAGTTACCGGGTAATAGCGTGTTTAAAGAGTGCATGAAACAGAAGAAAAAGAATTCAGGGCGAGCGCTTGGAGTCATCCGC
AATTCGAAAAGGGCGCATAA

Supplementary Table 4-S7. Sequence of expression cassette for C709 (gWiz-OX26-LC-His6)

color coding key:

IL-2 leader sequence

OX26 VL light chain variable domain

Murine IgG2a Ckappa domain

Linker and tag: (G₄S)₂-LPETGGG-H₆

sequence:

```
ATGTACAGGATGCAACTCCTGTCTTGCATTGCACTAAGTCTTGCACAAACAGT GATATCGTGATCACCCAATCTCCATC
CAGTCTGTCTGCATCCCTTGGCGACACAATTCTCATCACTTGCCATGCCAGTCAGAACATTAATGTTGGTTAAGTTGGTTCCAGC
AGAAACCAGGAAATGCTCCTAAACTGTTGATCTATAAGGCTTCCAACCTGCACACAGGCGTCCCATCAAGATTTAGTGGCAGTGGG
TCTGGAACAGGTTTCACATTAACCATCAGCAGCCTCCAGCCTGAAGACATTGCCACTTACTACTGTCAACAGGGTCAAAGTTATCC
GTGGACGTTCCGGTGGAGGCACCAAGCTGGAAATCAAA CCGGCAGATGCTGCACCAACTGTATCCATCTTCCACCATCCAGTGAGC
AGTTAACAATCTGGAGGTGCTCAGTGGTGTGCTTCTTGAACAACCTTCTACCCCAAGACATCAATGTCAAGTGGAGATTTGATGGG
AGTGAACGACAAAATGGCGTCTTGAACAGTTGGACTGATCAGGACAGCAAGACAGCAACCTACAGCATGAGCAGCACCCCTCAGGTT
GACCAAGCAGGAGTATGAACGACATAACAGCTATACCTGTGAGGBCACTCACAAAGACATCAACTTCACCCATTTGCAAGAGCTTCA
ACAGGAAATGAGTGGGAGGAGGTGGCTCGGGTGGAGGCGGTTGCTGCCGGAACGGGTGGTGGCCACCATCATCATCATCATTAA
```

Supplementary Table 4-S8. Sequence of expression cassette for C710 (gWiz-OX26-HC)

color coding key:

IL-2 leader sequence

OX26 VH heavy chain variable domain

Murine IgG2a heavy chain constant domains

sequence:

```
ATGTACAGGATGCAACTCCTGTCTTGCATTGCACTAAGTCTTGCACCTGTCACAAACAGT CAGGTGCAGCTCCAGCAGCCTGGGGC
TGCGCTGGTGAGGCCTGGAGCTTCAATGAGGCTGTCTTGCAGGCTTCTGGCTACTCCTTCACCACCTACTGGATGAACTGGGTGA
AGCAGAGGCCTGGACAAGGCCTTGAGTTGATTGGCATGATTCATCCTTCCGATAGTGAAGTTAGGTAAATCAGAAATTCAAGGAC
AAGGCCACATTTGACTGTTGACACATCCTCCAGCACAGCCTACATGCAACTCAACAGCCCGACATCTGAGGACTCTGCGGTCTATTA
CTGTGCAAGATTGCGCCTTGACTACTGGGGCCAAGGCACCACTCTCACAGTCTCCTCC GCTAAAACAACAGCCCCATCGGTCTATC
CACTGGCCCTGTGTGTGGAGATACAACCTGGCTCCTCGGTGACTCTAGGATGCCTGGTCAAGGGTTATTTCCCTGAGCCAGTGACC
TTGACCTGGAACCTCTGGATCCCTGTCCAGTGGTGTGCACACCTTCCCAGCTGTCTCCAGTCTGACCTCTACACCTCAGCAGCTC
AGTGACTGTAACCTCGAGCACCTGGCCAGCCAGTCCATCACCTGCAATGTGGCCACCCGGCAAGCAGCACCAAGGTGGACAAGA
AAATTGAGCCAGAGGGCCACAATCAAGCCCTGTCTCCATGCAAAATGCCAGCACCTAACCTCTTGGGTGGACCATCCGCTTC
ATCTTCCCTCCAAAGATCAAGGATGTACTCATGATCTCCTGAGCCCATAGTCACATGTGTGGTGGTGGATGTGAGCGAGGATGA
CCCAGATGTCCAGATCAGCTGGTTTGTGAACAACGTGGAAGTACACACAGCTCAGACACAACCATAGAGAGGATTACGGCAGTA
CTCTCCGGGTGGTCAAGTGCCTCCCATCCAGCACAGGACTGGATGAGTGGCAAGGAGTTCAAATGCAAGTCAACAACAAGAC
CTCCAGCGCCCATCGAGAGAACCATCTCAAAACCCAAAGGGTCAAGTAAAGAGCTCCACAGGTATATGTCTTGCCTCCACCAGAAGA
AGAGATGACTAAGAAACAGGTCACTCTGACCTGCATGGTCAAGACTTCATGCCTGAAGACATTTACGTGGAGTGGACCAACAACG
GGAAAACAGAGCTAAACTACAAGAACACTGAACCAGTCTGGACTCTGATGGTTCTTACTTCATGTACAGCAAGCTGAGAGTGGAA
AAGAAGAACTGGGTGGAAGAAATAGCTACTCTGTTCAGTGGTCCACGAGGGTCTGCACAATCACCACAGGACTAAGAGCTTCTC
CCGGACTCCGGGTAATGA
```

Supplementary Table 4-S9. Sequence of expression cassette for C711 (gWix-OX26-Fab-HC-His)

color coding key:

IL-2 leader sequence

OX26 VH heavy chain variable domain

Murine IgG2a heavy chain constant domains (Fab only)

Linker and tag: G₄S-H₆

sequence:

ATGTACAGGATGCAACTCCTGTCTTGCATTGCACTAAGTCTTGCACCTTGTACAAACAGT CAGGTGCAGCTCCAGCAGCCTGGGGC
TGCGCTGGTGAGGCCTGGAGCTTCAATGAGGCTGTCTGCAAGGCTTCTGGCTACTCCTTCACCACCTACTGGATGAACTGGGTGA
AGCAGAGGCCTGGACAAGGCCTTGAGTTGATTGGCATGATTCATCCTCCGATAGTGAAGTTAGGTTAAATCAGAAATCAAGGAC
AAGGCCACATTGACTGTTGACACATCCTCCAGCACAGCCTACATGCAACTCAACAGCCCGACATCTGAGGACTCTGCGGTCTATTA
CTGTGCAAGATTTCGGCCTTGACTACTGGGGCCAAGGCACCACTCTCACAGTCTCCTCC GCTAAAACAACAGCCCCATCGGTCTATC
CACTGGCCCTGTGTGGAGATACTGGCTCCTCGGTGACTCTAGGATGCCTGGTCAAGGGTTATTTCCCTGAGCCAGTGACC
TTGACCTGGAACCTGGATCCCTGTCCAGTGGTGTGCACACCTTCCCAGCTGTCTCCAGTCTGACCTCTACACCCTCAGCAGCTC
AGTGACTGTAACCTCGAGCACCTGGCCAGCCAGTCCATCACCTGCAATGTGGCCACCCGGCAAGCAGCACCAAGGTGGACAAGA
AAATTGAGCCAGAGGGCCACAATCAAGGGAGAGGTGGCTCGCACCATCATCATCATCATTAA

Supplementary Table 4-S10. Sequence of expression cassette for C712 (gWix-OX26-Fab-HC-sII)

color coding key:

IL-2 leader sequence

OX26 VH heavy chain variable domain

Murine IgG2a heavy chain constant domains (Fab only)

Linker and tag: G₄S-StreptII

sequence:

```
ATGTACAGGATGCAACTCCTGTCTTGCATTGCACTAAGTCTTGCACAAACAGT CAGGTGCAGCTCCAGCAGCCTGGGGC
TGCGCTGGTGAGGCCTGGAGCTTCAATGAGGCTGTCTGCAAGGCTTCTGGCTACTCCTTCACCACCTACTGGATGAACTGGGTGA
AGCAGAGGCCTGGACAAGGCCTTGAGTTGATTGGCATGATTCATCCTTCCGATAGTGAAGTTAGGTAAATCAGAAATTCAGGAC
AAGGCCACATTGACTGTTGACACATCCTCCAGCACAGCCTACATGCAACTCAACAGCCCGACATCTGAGGACTCTGCGGTCTATTA
CTGTGCAAGATTCGGCCTTGACTACTGGGGCCAAGGCACCACTCTCACAGTCTCCTCCGCTAAAACAACAGCCCCATCGGTCTATC
CACTGGCCCTGTGTGTGGAGATACAACCTGGCTCCTCGGTGACTCTAGGATGCCTGGTCAAGGTTATTTCCCTGAGCCAGTGACC
TTGACCTGGAACTCTGGATCCCTGTCCAGTGGTGTGCACACCTTCCCAGCTGTCTCCAGTCTGACCTCTACACCCTCAGCAGCTC
AGTGACTGTAACCTCGAGCACCTGGCCAGCCAGTCCATCACCTGCAATGTGGCCACCCGGCAAGCAGCACCAAGGTGGACAAGA
AAATTGAGCCAGAGGGCCACAATCAAGGGAGGAGGTGGCTCGGCTTGAGTTCATCCGCAATTCGAAAAGGGCGCATAA
```

Supplementary Table 4-S11. Sequence of expression cassette for C714 (gWiz-OX26-LC-long-Th-Max-sII)

color coding key:

IL-2 leader sequence

OX26 VL light chain variable domain

Murine IgG2a Ckappa domain

Linker: (G₄S)₄-LVPR

Max: GSIL-maxadilan-StrepII

sequence:

```
ATGTACAGGATGCAACTCCTGTCTTGCATTGCACTAAGTCTTGCACCTTGTACAAACAGT GATATCGTGATCACCAATCTCCATG
CAGTCTGTCTGCATCCCTTGGCGACACAATTCTCATCACTTGCCATGCCAGTCAGAACATTAATGTTGGTTAAGTTGGTTCCAGC
AGAAAACCAGGAAATGCTCCTAAACTGTTGATCTATAAGGCTTCCAAGTTCACACACAGGCGTCCCATCAAGATTAGTGGCAGTGGG
TCTGGAACAGGTTTCACATTAACCATCAGCAGCCTCCAGCCTGAAGACATGCCCACTTACTACTGTCAACAGGGTCAAAGTTATCC
GTGGACGTTTCGGTGGAGGCACCAAGCTGGAAATCAAA CCGGCAGATGCTGCACCAACTGTATCCATCTTCCCACCATCCACTGAGC
AGTTACATCTGGAGGTGCCTCAGTGGTGTGCTTCTTGAACAACCTCTACCCCAAAGACATCAATGTCAAGTGGAAAGATTGATGGG
AGTGAACGACAAAATGGCGTCTTGAACAGTTGGACTGATCAGGACAGCAAAGACAGCACCTACAGCATGAGCAGCACCCCTCACGTT
GACDAAGGACGAGTATGAACGACATAACAGCTATACTGTGAGGCCACTCACAAAGACATCAAACTTCAACCCATTGTCAAGAGCTTCA
ACAGCAATGAGTGGAGGCGGTGGCTCAGGTGGCGGAGGTTCCGGTGGCGGTGGCTCCGGTGGTGGAGGTTCCCTGGTGCCGCGT
GGTTCCGATTCGTGCGACGCGACTTGTCAAGTTTCGTAAAGCGATTGACGATTGCCAGAAGCAGGCTCACCACTCCAACGTTCTGCA
GACCTCTGTTCAAACGACTGCAACGTTTACTTCCATGGACACGTCGCAGTTACCGGTAATAGCGTGTTTAAAGAGTGCATGAAAC
AGAAGAAAAAGAATTCAAGGCGAGCGCTTGGAGTCATCCGCAATTCGAAAAGGGCGCATAA
```

Supplementary Table 4-S12. Sequence of expression cassette for C715 (gWiz-OX26-HC-long-Th-Max-sII)

color coding key:

IL-2 leader sequence

OX26 VH heavy chain variable domain

Murine IgG2a heavy chain constant domains

Linker: (G₄S)₄-LVPR

Max: GSIL-maxadilan-StrepII

sequence:

```
ATGTACAGGATGCAACTCCTGTCTTGCATTGCACTAAGTCTTGCACCTTGTGCAAAACAGT CAGGTGCAGCTCCAGCAGCCTGGGGC
TGCGCTGGTGAGGCCTGGAGCTTCAATGAGGCTGTCTGCAAGGCTTCTGGCTACTCCTTCACCACCTACTGGATGAACCTGGGTGA
AGCAGAGGGCTGGACAAGGCCTTGAGTTGATTGGCATGATTCATCCTCCGATAGTGAAGTTAGGTAAATCAGAAATTCAGGAC
AAGGCCACATTGACTGTTGACACATCCTCCAGCACAGCCTACATGCAACTCAACAGCCCGACATCTGAGGACTCTGCGGTCTATTA
CTGTGCAAGATTTCGGCCTTGACTACTGGGGCCAAGGCACCACTCTCACAGTCTCCTCCGCTAAAACAACAGCCCCATCGGTCTATC
CACTGGCCCCCTGTGTGGAGATACTGGCTCCTCGGTGACTCTAGGATGCCTGGTCAAGGGTTATTTCCCTGAGCCAGTGACC
TTGACCTGGAACCTGGATCCCTGTCCAGTGGTGTGCACACCTTCCCAGCTGTCTCCAGTCTGACCTCTACACCCTCAGCAGCTC
AGTGACTGTAACTCGAGCACCTGGCCAGCCAGTCCATCACCTGCAATGTGGCCACCCGGCAAGCAGCACCAAGGTGGACAAGA
AAATTGAGCCAGAGGGGCCACAATCAAGCCCTGTCTCCATGCAAATGCCAGCACCTAACCTCTTGGGTGGACCATCCGTCTTC
ATCTTCCCTCCAAAGATCAAGGATGTACTCATGATCTCCCTGAGCCCCATAGTCACATGTGTGGTGGTGGATGTGAGCGAGGATGA
CCAGATGTCCAGATCAGCTGGTTTGTGAACAACGTGGAAGTACACACAGCTCAGACACAAACCCATAGAGAGGATTACGGCAGTA
CTCTCCGGGTGGTCAAGTGCCTCCCATCCAGCACCAAGGACTGGATGAGTGGCAAGGAGTTCAAATGCAAGGTCAACAACAAGAC
CTCCAGCGCCCATCGAGAGAACCATCTCAAAACCCAAAGGGTCAAGTAAGAGCTCCACAGGTATATGTCTTGCCTCCACCAGAAGA
AGAGATGACTAAGAAACAGGTCACTTGACCTGCATGGTACAGACTTCATGCCTGAAGACATTTACGTGGAGTGGACCAACAACG
GGAAAACAGAGCTAAACTACAAGAACACTGAACCAGTCTGGACTCTGATGGTTCTTACTTCATGTACAGCAAGCTGAGAGTGGAA
AAGAAGAAC TGGGTGAAAGAATAAGCTACTCCTGTTCCAGTGGTCCACGAGGGTCTGCACAATCACCACACGACTAAGAGCTTCTC
CCGCACTCCGGGTAAA GGAGGCGGTGGCTCAGGTGGCGGAGGTTCCGGTGGCGGTGGCTCCGGTGGTGGAGGTTCCCTGGTGCCGC
GTGGTTCGATTCTGTGCGACGCGACTTGTCAAGTTTCGTAAGCGATTGACGATTGCCAGAAGCAGGCTCACCCTCCAACGTTCTG
CAGACCTCTGTTCAAACGACTGCAACGTTTACTTCCATGGACACGTCGCAGTTACCGGTAATAGCGTGTTTAAAGAGTGCATGAA
ACAGAAGAAAAAGAATTCAAGGCGAGCGCTTGGAGTCATCCGCAATTCGAAAAGGGCGCATAA
```

Supplementary Table 4-S13. Sequence of expression cassette for C722 (gWiz-FC5-Fc)

color coding key:

IL-2 leader sequence

FC5

Human Fc region (with T299A mutation)

sequence:

```
ATGGACTGGACATGGCGAGTGTCTGTCTGCTGGCTGTGGCACCAGGGGCCATTCTGACGTTCAACTGCAGGCTAGTGGTGGTGG
GCTCGTGCAGGCTGGCGGCTCCTTGAGACTCTCCTGCGCCGCCAGTGGTTTCAAAATCACTCACTACACAATGGGTGGTTTCGGC
AAGCACCCGGAAAAGAACGGGAATTTGTGTCCAGGATTACCTGGGGGGGAGACAACACGTTCTATAGCAATAGTGTCAAAGGTAGA
TTCACCATTTCCCGCGACAACGCACAAAAACACGGTGTATCTGCAGATGAACTCACTGAAACCCGAGGATACAGCCGACTATTATTG
TGCAGCCGGCTCCACTTCTACCGCCACCCCCCTGAGGGTGGATTATTGGGTAAGGGCACACAGGTGACAGTTTCAAGCCGAGAAC
CTAAAAGCTGTGACAAAACACACCTGTCTCCTGCCCTGCACCCGAACTGCTCGGTGGCCCTTCCGTGTTCTTTTCCCACCC
AAACCCAAGGACACCCTCATGATTAGCCGGACCCCTGAGGTCACATGCGTTGTGGTGGACGTGTCACATGAAGACCCTGAGGTCAA
ATTCAACTGGTACGTGGACGGAGTGAAGTGCATAATGCCAAGACAAAACCTCGGGAAGAGCAATACAACAGCGCGTACAGGGTGG
TGTCTGTACTACCGTCTCCACCAGGACTGGTTGAACGGTAAAGAGTACAAATGTAAAGTCAGTAACAAGGCACTGCCAGCCCT
ATTGAAAAGACCATCTCAAAGCCAAGGGTCAGCCCCGCGAGCCTCAGGTGTACACACTGCCCCCGTCCCGCGACGAGCTCACGAA
GAATCAGGTGAGCCTTACCTGCCTGGTCAAAGGATTCTATCCATCAGACATTGCGGTGGAATGGGAATCAAACGGTCAACCCGAAA
ACAATTATAAAACACACCCGCGGTCTCGATAGTGACGGAAGCTTCTTTCTGTATTCTAAGCTCACCGTGGATAAGTCTCGGTGG
CAGCAGGGCAATGTCTTTTCTGCAGCGTGATGCACGAGGCTCTGCACAACCACTACACACAGAAAAGCCTCAGCCTCTCACCTGG
TAAATGA
```


Supplementary Table 4-S14. Sequence of expression cassette for C723 (gWiz-FC5-Fc-long-Max)

color coding key:

IL-2 leader sequence

FC5

Human Fc region (with T299A mutation)

Linker: (G₄S)₄

Max: GSIL-maxadilan

sequence:

```
ATGGACTGGACATGGCGAGTGTCTGTCTGCTGGCTGTGGCACCAGGGGCCATTCTGACGTTCAACTGCAGGCTAGTGGTGGTGG
GCTCGTGCAGGCTGGCGGCTCCTTGAGACTCTCCTGCGCCGCCAGTGGTTTCAAATCACTCACTACACAATGGGTGGTTTCGGC
AAGCACCCGGAAAAGAACGGGAATTTGTGTCCAGGATTACCTGGGGGGGAGACAACACGTTCTATAGCAATAGTGTCAAAGGTAGA
TTCACCATTTCCCGCGACAACGCCAAAAACACGGTGTATCTGCAGATGAACTCACTGAAACCCGAGGATACAGCCGACTATTATTG
TGCAGCCGGCTCCACTTCTACCGCCACCCCCCTGAGGGTGGATATTGGGGTAAGGGCACACAGGTGACAGTTTCAAGCGCAGAAC
CTAAAAGCTGTGACAAAACACACCTGTCCCTCCCTGCCCTGCACCGGAACCTGCTCGGTGGCCCTTCCGTGTTTCTTTCCACCC
AAACCCAAGGACACCCTCATGATTAGCCGGACCCCTGAGGTCACATGCCGTTGTGGTGGACGTGTCACATGAAGACCCTGAGGTCAA
ATTCAACTGGTACGTGGACGGAGTGAAGTGCATAATGCCAAGACAAAACCTCGGGAAGAGCAATACAACAGCGCGTACAGGGTGG
TGTCTGTACTCACCGTCTCCACCAGGACTGGTTGAACGGTAAAGAGTACAAATGTAAAGTCAGTACAAGGCACTGCCAGCCCT
ATTGAAAAGACCATCTCAAAGGCCAAGGGTCAGCCCCGCGAGCCTCAGGTGTACACACTGCCCCCGTCCCGCGACGAGCTCACGAA
GAATCAGGTGAGCCTTACCTGCCTGGTCAAAGGATCTATCCATCAGACATGCGGTGGAATGGGAATCAAACGGTCAACCCGAAA
ACAATTATAAAACACACCCCGGTCTCGATAGTACGGAAGCTTCTTTCTGTATTCTAAGCTCACCGTGGATAAGTCTCGGTGG
CAGCAGGGCAATGTCTTTTCTGCGAGCGTGATGCACGAGGCTCTGCACAACCCTACACACAGAAAAGCCTCAGCCTCTCACCTGG
TAAAGGAGGCGGTGGCTCAGGTGGCGGAGGTTCCGGTGGCGGTGGCTCCGGTGGTGGAGGTTCCGGTTCGATTCTGTGCGACGCGA
CTTGTCAAGTTTCGTAAAGCGATTGACGATTGCCAGAAGCAGGCTCACCACTCCAACGTTCTGCAGACCTCTGTTCAACGACTGCA
ACGTTTACTTCCATGGACACGTGCGAGTACCGGGTAATAGCGTGTTTAAAGAGTGCATGAAACAGAAAGAAAAAGAGTTCAAGGC
GTGA
```

Supplementary Table 4-S15. Sequence of expression cassette for C724 (gWiz-FC5-Fc-long-Th-Max)

color coding key:

IL-2 leader sequence

FC5

Human Fc region (with T299A mutation)

Linker: (G₄S)₄-LVPR

Max: GSIL-maxadilan

sequence:

```
ATGGACTGGACATGGCGAGTGTCTGTCTGCTGGCTGTGGCACCAGGGGCCATTCTGACGTTCAACTGCAGGCTAGTGGTGGTGG
GCTCGTGCAGGCTGGCGGCTCCTTGAGACTCTCCTGCGCCGCCAGTGGTTTCAAAATCACTCACTACACAATGGGTGGTTTCGGC
AAGCACCCGAAAAGAACGGGAATTTGTGTCCAGGATTACCTGGGGGGGAGACAACACGTTCTATAGCAATAGTGTCAAAGGTAGA
TTCACCATTTCCCGCGACAACGCAAAAAACACGGTGTATCTGCAGATGAACTCACTGAAACCCGAGGATACAGCCGACTATTATTG
TGCAGCCGGCTCCACTTCTACCGCCACCCCTGAGGGTGGATTATTGGGGTAAGGGCACACAGGTGACAGTTTCAAGCGCAGAAC
CTAAAAGCTGTGACAAAACACACCTGTCTCCCTGCCCTGCACCGGAACTGCTCGGTGGCCCTTCCGTGTTCTTTTCCCACCC
AAACCCAAGGACACCCCTCATGATTAGCCGGACCCCTGAGGTACATGCGTTGTGGTGGACGTGTCACATGAAGACCCCTGAGGTCAA
ATTCAACTGGTACGTGGACGGAGTCGAAGTGCATAATGCCAAGACAAAACCTCGGGAAGAGCAATACAACAGCGCGTACAGGGTGG
TGTCTGTACTCACCGTCTCCACCAGGACTGGTTGAACGGTAAAGAGTACAAATGTAAAGTCAGTAACAAGGCACTGCCAGCCCT
ATTGAAAAGACCATCTCAAAGGCCAAGGGTCAGCCCCGCGAGCCTCAGGTGTACACACTGCCCCCGTCCCGCGAGGAGCTCAGGAA
GAATCAGGTGAGCCTTACCTGCCTGGTCAAAGGATTCTATCCATCAGACATGCGGTGGAATGGGAATCAAACGGTCAACCCGAAA
ACAATTATAAAACCACACCCGGTCTCGATAGTGACGGAAGCTTCTTCTGTATTCTAAGCTCACCGTGGATAAGTCTCGGTGG
CAGCAGGGCAATGTCTTTTCTGACGGTGATGCACGAGGCTCTGCACAACCCTACACACAGAAAAGCCTCAGCCTCTCACCTGG
TAAAGGAGGCGGTGGCTCAGGTGGCGGAGGTTCCGGTGGCGGTGGCTCCGGTGGTGGAGGTTCCCTGGTGCCCGCTGGTTCGATTC
TGTGCGACCGCACTTGTGAGTTTCGTAAAGCGATTGACGATTGCCAGAAGCAGGCTCACCCTCCAACGTTCTGCAGACCTCTGTT
CAAACGACTGCAACGTTTACTTCCATGGACACGTCGCAGTTACCGGGTAATAGCGTGTTTAAAGAGTGCATGAAACAGAAGAAAAA
AGAGTTCAAGGCGTGA
```

Supplementary Table 4-S16: Plasmid combinations used for antibody expressions

Construct	Name	Plasmids
(1)	OX26 IgG	C709, C710
(2)	OX26 IgG-Max	C708, C710
(3)	OX26 IgG-Th-Max	C707, C710
(4)	OX26 Fab	C709, C712
(5)	OX26 Fab-Th-Max	C707, C711
(6)	OX26 Fab-long-Th-Max	C711, C714
(7)	OX26 IgG-long-Th-Max	C710, C714
(8)	OX26 IgG-HC-Th-Max	C705, C715
(9)	FC5-Fc	C722
(10)	FC5-Fc-long-Max	C723
(11)	FC5-Fc-long-Th-Max	C724

Supplementary Table 4-S17: Predicted molecular masses and extinction coefficients

Construct	Mass (Da)	ϵ_{280} ($\text{cm}^{-1} \text{M}^{-1}$)
GFP-LVPR-GSIL-Max	35,921	25,940
(1) OX26 IgG	148,826	224,840
(2) OX26 IgG-Max	163,056	237,180
(3) OX26 IgG-Th-Max	163,986	237,180
(4) OX26 Fab	50,024	85,550
(5) OX26 Fab-Th-Max	57,689	86,030
(6) OX26 Fab-long-Th-Max	58,320	86,030
(7) OX26 IgG-long-Th-Max	165,248	237,180
(8) OX26 IgG-HC-Th-Max	165,220	237,180
(9) FC5-Fc	78,724	120,220
(10) FC5-Fc-long-Max	95,694	121,180
(11) FC5-Fc-long-Th-Max	96,926	121,180

Note: For antibody constructs (1) to (11), values are given for the secreted species (multimer, without leader peptide).

Supplementary Table 4-S18: Fitted potencies and 95% confidence intervals for PAC1 activation in cell culture

Construct	Uncleaved		Cleaved	
	Log(EC ₅₀)	95% CI	Log(EC ₅₀)	95% CI
PACAP-38 (Sigma)	-10.9	(*)		
GFP-LVPR-GSIL-Max	-9.5	[-9.7, -9.3]		
(2) OX26 IgG-Max	-8.5	[-8.6, -8.3]		
(3) OX26 IgG-Th-Max	-8.7	[-8.9, -8.5]	-11.0	(*)
(5) OX26 Fab-Th-Max	-9.5	[-9.9, -9.1]	-10.4	[-11.5, -9.4]
(6) OX26 Fab-long-Th-Max	-9.5	[-9.7, -9.3]	-10.3	[-10.5, -10.2]
(7) OX26 IgG-long-Th-Max	-9.1	[-9.2, -9.0]	-11.0	(*)
(8) OX26 IgG-HC-Th-Max	-9.7	[-10.0, -9.4]	-11.0	(*)
(10) FC5-Fc-long-Max	-9.8	[-9.9, -9.8]		
(11) FC5-Fc-long-Th-Max	-9.9	[-10.0, -9.9]	-11.1	[-11.1, -11.0]

(*) denotes samples with high potency for which strong receptor activation occurred at concentrations $\leq 10^{-10}$ M and for which no 95% confidence interval could be computed for the best-fit Log(EC₅₀).

Conclusions and future directions

Synopsis, significance, and impact

We have established a novel principle for high-sensitivity molecular imaging *in vivo* which successfully circumvents many of the limitations traditionally associated with molecular MRI probes for brain imaging in particular. By using blood hemoglobin as an abundant endogenous contrast agent, our approach of artificially perturbing bloodflow renders the concentration requirement for the molecular imaging sensor entirely independent of the concentration requirement for the contrast agent. Since imaging of changes in cerebral bloodflow is a long-established technique using common and well-optimized equipment and routines, we thus reduce the problem of molecular imaging to a problem of molecular sensing and of perturbing vascular tone effectively.

We demonstrate the feasibility of imaging the action of CGRP as a highly potent vasoactive peptide at nanomolar concentrations in a manner that can be validated by other modalities and that can be pharmacologically isolated by inhibiting other molecular pathways for vasodilation. We further show that caged forms of CGRP can serve as protease sensors, with differences in potency before and after uncaging of up to several orders of magnitude. Beyond serving as a proof-of-concept of analyte-activatable imaging probes based on CGRP, such protease-responsive agents could potentially be used to report on disease-relevant biomarkers in animal models in basic research or drug development, or even clinically once minimally invasive delivery has been established. For example, noninvasive evaluation of the activity of FAP could be used to guide therapeutic decisions in cancer treatment⁵¹, and in Alzheimer's disease, beta-secretase as a cell membrane-associated protease is both a drug target and could serve as a diagnostic biomarker for patient selection and treatment monitoring^{99,100}.

By successfully using a cassette encoding prepro-CGRP as a genetic reporter, we illustrate not only the versatility of imaging with vasoactive probes but also a qualitative practical benefit of the nanomolar potency of such probes: namely, that they can be produced and secreted *in situ* at effective concentrations, obviating the need for delivery by invasive injection or by delivery across the BBB in settings where genetic targeting prior to the imaging experiment is feasible. Cell tracking, as we demonstrate, is one application where constitutively secreted and constitutively active vasoprobe can be useful and could serve to track tumor xenografts or cell populations descended from stem cells, for example. One interesting potential application is their use as reporters for viral gene delivery and expression, especially in conjunction with viral vectors that efficiently transduce the central nervous system¹⁰¹. Finally, combining genetic expression with molecularly responsive probes, for example (but not limited to) protease sensors as discussed above, suggests the intriguing possibility of minimally invasive imaging of such analytes in transgenic or virally transduced animals.

Fusing maxadilan to known BBB-penetrating antibodies represents an important step toward minimally invasive vasoprobe delivery to the brain. While local expression of genetically encoded probes can potentially obviate the need for brain delivery via the periphery, the kinds of vasoactive probes that can be used with it are limited (e.g. probes with synthetic chemical entities attached cannot be used), experimental protocols are constrained, and for the time being is not suitable for clinical translation into human patients. Delivery across the BBB would address these problems. With our results so far, we have shown that maxadilan can be recombinantly expressed in both bacterial and mammalian systems and that it retains low nanomolar potency when fused to different BBB-penetrating antibodies. If in future work *in vivo* we can successfully establish imaging of brain entry by vasoprobe-antibody fusions, this will not only lay the foundation for delivery of analyte-responsive probes but could also be of more immediately utility for evaluating BBB-crossing antibodies in order to optimize them or to translate them across species.

In sum, we have succeeded in establishing a novel molecular imaging paradigm which combines the widely-appreciated advantages of MRI with greatly improved sensitivity. We have moreover illustrated some of the broad versatility of vasoactive imaging and hope to inspire its further exploitation in the future.

Limitations

Technical limitations of the method

Despite the advantages and potential utility of molecular imaging with vasoactive probes, several limitations of this approach need to be kept in mind. The characteristics of the vasculature and of bloodflow mean that the specificity of imaging with vasoactive agents is inherently constrained. In contrast to radionuclide-based probes, vasoactive agents will always yield images with substantial background signal and changes in background signal. While we have shown that inhibitors of the NO pathway do not interfere with CGRP-based probes and are known to attenuate the hemodynamic signal changes underlying BOLD fMRI, there is no way to entirely isolate the action of vasoactive imaging probes from all other physiological effects on bloodflow.

Furthermore, dependence on the vasculature imposes a floor for spatial and temporal resolution. We have not attempted to probe the limits of this resolution, but a few useful mechanistic and comparative comments can be made. As we noted, any point in the brain has a mean distance from the nearest capillary on the order of $10\ \mu\text{m}$ ³⁶, while BOLD fMRI can achieve a spatial resolution on the order of $1\ \text{mm}$ ¹⁰². Since the neuronal activity and metabolic demand underlying the BOLD fMRI signal are usually dispersed (i.e. don't originate from a single cell), the spatial resolution limit for vasoactive imaging likely lies between the length scale of microvascularization and common BOLD fMRI measurements. This compares favorably with the resolution of radionuclide-based methods, but it is important to note that the superior potential resolution of invasive optical or photoacoustic imaging could be better suited for

investigating single-cell or subcellular phenomena. The temporal resolution of imaging with vasoactive probes depends on the specific pathway used for evoking vascular responses. We chose to use vasoactive peptides which act through GPCRs to cause vasodilation within seconds and a return to baseline within tens of minutes. On the other hand, BOLD fMRI has a resolution of seconds. If a faster temporal resolution is needed than our existing implementation affords, it could in principle be achieved; alternative implementations (e.g. using the NO pathway or engineering direct analyte sensing by smooth muscle cells) are discussed below under “future work”. It must be acknowledged, however, that some important phenomena such as millisecond-scale electrical firing of neurons or subsecond-scale neurotransmitter release cannot be fully resolved with vasoactive probes, although “bulk” measurements of increased average activity during a window of time may be feasible.

Moreover, quantitative interpretation of the imaging signal may be challenging due to the nonlinear nature of vasodilatory responses and due to heterogeneity of receptor expression and probe distribution. In cases where one is only interested in localizing a signal (such as cell tracking) or in a qualitative assessment (such as determining whether an analyte is expressed or secreted), this may not be prohibitive. Semi-quantitative measurements (i.e. is a signal stronger or weaker) should also generally be possible. However, the near-linear and fully quantifiable signal strength characteristic of many radioactive probes and some optical sensors over a wide range of analyte concentrations might be difficult to achieve with hemodynamic probes.

Toxicity and perturbations of endogenous physiology

We have observed no acute toxicity of intracranially injected CGRP or of CGRP secreted from implanted cells over several days. It is also worth highlighting that changes in vascular tone and in bloodflow occur continuously during the healthy physiological operation of the brain, suggesting that a technique based on triggering similar effects in response to analytes could in principle operate with minimal invasiveness.

However, a much more thorough investigation of the effects of vasoactive probes on the organism is warranted. Some applications will require consideration of only the most severe kinds of toxicity. Examples might include the use of vasoactive probes to assess brain entry by a biologic or tumor engraftment in an animal model. In order to use vasoactive probes for molecular imaging of cognitive or behavioral phenomena in animals, or for translation into humans, it would be essential to ensure they don't interfere unduly with neurological or vascular function, don't increase the risk of bleeding or hemorrhage, and are not immunogenic for repeat administration. Maxadilan in particular, due to its origin in flies, might be recognized by the human or other mammalian immune systems.

The role of CGRP in migraine was discussed in Chapter 1 and is thought to involve action on the trigeminal nerve outside the brain¹⁰³. This role did not impede or experiments using intracranial injection and may also not interfere with the use of CGRP-based probes expressed in animal brains *in situ*, but could pose a problem for the delivery of CGRP after peripheral injection. Peripheral action of maxadilan would also require further assessment.

It should be noted that if a particular toxic effect were found, it would still be possible to attempt to engineer the vasoactive molecular imaging probe to fulfill its intended purpose while minimizing the undesirable side effect.

Specific applications

This final, important limitation to be acknowledged concerns the scope of the work presented in this dissertation. We demonstrate a proof of concept for a novel imaging strategy. However, as with any imaging technique, it will ultimately depend on the specific question under investigation whether the capabilities and constraints of our method render it suitable for the task at hand.

Future work

We envision several future experimental directions based on the work presented in this dissertation. Firstly, the possibility of delivering vasoactive probes across the BBB after peripheral injection and imaging the brain entry of such antibody fusions by MRI should be investigated *in vivo*. This may require re-optimization of the protocols for image acquisition, normalization, and data analysis because the kinetics of brain entry and especially accumulation in the brain are likely to be substantially slower than those of receptor activation by the probe (on the order of hours rather than seconds). If successful, such a technique could then be used to assess the effect of point mutations in the RMT antibody on the efficacy of brain delivery.

Secondly, molecular imaging probes based on vasoactive peptides for the detection of ligand binding events should be created. Conceptually, the mechanism of action of vasoactive peptides - i.e. receptor binding and activation - immediately suggests the feasibility of this by implementing protein architecture where its ligand binding domain is fused to vasoactive moiety in such a way that access of the vasoactive agent to its receptor is modulated by ligand binding. This could be accomplished via a conformational change (allosteric regulation) or it could be accomplished by sterically masking access to the vasoactive moiety. Switching by ligand binding has been implemented in the variety of protein architectures, including optical imaging probes, suggesting that the powerful techniques of protein engineering could be used to accomplish the same to create ligand-responsive vasoactive probes. Attractive ligands for which to design sensors may include neurotransmitters, neuropeptides such as oxytocin, or small molecule drugs whose delivery to the brain could be monitored.

Thirdly, alternative pathways for implementing molecular imaging with artificial hemodynamic changes should be explored. The nitric oxide pathway is one example of this. Another example of great conceptual appeal would be the heterologous expression of GPCRs already specific for the desired ligand directly in vascular smooth muscle cells. This would turn smooth muscle into a cell-based molecular imaging sensor, analogous to existing cell-based optical imaging sensors¹⁵. By using

alternative pathways for vasodilation, it will be possible to implement a variety of molecular imaging strategies with different advantages and trade-offs so as to enable different applications.

Finally, the ultimate validation of the utility of molecular imaging with engineered hemodynamic responses will lie in successful specific applications. This entails not only the development and characterization of probes or protocols, but successfully using such an imaging strategy to answer significant open questions in fundamental neuroscience or to usefully apply it to a real problem in drug development or in clinical radiology.

References

1. Bhatia, S.N. & Ingber, D.E. Microfluidic organs-on-chips. *Nat. Biotechnol.* **32**, 760-772 (2014).
2. Lancaster, M.A. & Knoblich, J.A. Organogenesis in a dish: modeling development and disease using organoid technologies. *Science* **345**, 1247125 (2014).
3. Esch, E.W., Bahinski, A. & Huh, D. Organs-on-chips at the frontiers of drug discovery. *Nat. Rev. Drug Discov.* **14**, 248-260 (2015).
4. Yin, X., *et al.* Engineering Stem Cell Organoids. *Cell Stem Cell* **18**, 25-38 (2016).
5. James, M.L. & Gambhir, S.S. A molecular imaging primer: modalities, imaging agents, and applications. *Physiol. Rev.* **92**, 897-965 (2012).
6. Willmann, J.K., van Bruggen, N., Dinkelborg, L.M. & Gambhir, S.S. Molecular imaging in drug development. *Nat. Rev. Drug Discov.* **7**, 591-607 (2008).
7. Price, J.C. Molecular brain imaging in the multimodality era. *J. Cereb. Blood Flow Metab.* **32**, 1377-1392 (2012).
8. Keyes, J.W., Jr., Orlandea, N., Heetderks, W.J., Leonard, P.F. & Rogers, W.L. The Humongotron--a scintillation-camera transaxial tomograph. *J. Nucl. Med.* **18**, 381-387 (1977).
9. Vandenberghe, R., Adamczuk, K., Dupont, P., Laere, K.V. & Chetelat, G. Amyloid PET in clinical practice: Its place in the multidimensional space of Alzheimer's disease. *Neuroimage Clin* **2**, 497-511 (2013).
10. Zimmer, L. & Luxen, A. PET radiotracers for molecular imaging in the brain: past, present and future. *NeuroImage* **61**, 363-370 (2012).
11. Hillman, E.M. Optical brain imaging in vivo: techniques and applications from animal to man. *J Biomed Opt* **12**, 051402 (2007).
12. Wang, L.V. & Hu, S. Photoacoustic tomography: in vivo imaging from organelles to organs. *Science* **335**, 1458-1462 (2012).

13. Taruttis, A. & Ntziachristos, V. Advances in real-time multispectral optoacoustic imaging and its applications. *Nature Photonics* **9**, 219-227 (2015).
14. Grienberger, C. & Konnerth, A. Imaging calcium in neurons. *Neuron* **73**, 862-885 (2012).
15. Nguyen, Q.T., *et al.* An in vivo biosensor for neurotransmitter release and in situ receptor activity. *Nat. Neurosci.* **13**, 127-132 (2010).
16. Wang, X., *et al.* Noninvasive laser-induced photoacoustic tomography for structural and functional in vivo imaging of the brain. *Nat. Biotechnol.* **21**, 803-806 (2003).
17. Lelyveld, V.S., Atanasijevic, T. & Jasanoff, A. Challenges for molecular neuroimaging with MRI. *Int. J. Imag. Syst. Tech.* **20**, 71-79 (2010).
18. Sherry, A.D. & Woods, M. Chemical exchange saturation transfer contrast agents for magnetic resonance imaging. *Annu. Rev. Biomed. Eng.* **10**, 391-411 (2008).
19. Ogawa, S., Lee, T.M., Kay, A.R. & Tank, D.W. Brain magnetic resonance imaging with contrast dependent on blood oxygenation. *Proc. Natl. Acad. Sci. U. S. A.* **87**, 9868-9872 (1990).
20. Lin, Y.J. & Koretsky, A.P. Manganese ion enhances T1-weighted MRI during brain activation: an approach to direct imaging of brain function. *Magn. Reson. Med.* **38**, 378-388 (1997).
21. Lee, T., Cai, L.X., Lelyveld, V.S., Hai, A. & Jasanoff, A. Molecular-level functional magnetic resonance imaging of dopaminergic signaling. *Science* **344**, 533-535 (2014).
22. Sosnovik, D.E. & Weissleder, R. Emerging concepts in molecular MRI. *Curr. Opin. Biotechnol.* **18**, 4-10 (2007).
23. Hsieh, V. & Jasanoff, A. Bioengineered probes for molecular magnetic resonance imaging in the nervous system. *ACS Chem. Neurosci.* **3**, 593-602 (2012).
24. Major, J.L. & Meade, T.J. Bioresponsive, cell-penetrating, and multimeric MR contrast agents. *Acc. Chem. Res.* **42**, 893-903 (2009).
25. Li, W.H., Fraser, S.E. & Meade, T.J. A calcium-sensitive magnetic resonance imaging contrast agent. *J. Am. Chem. Soc.* **121**, 1413-1414 (1999).

26. Kanal, E. & Tweedle, M.F. Residual or retained gadolinium: practical implications for radiologists and our patients. *Radiology* **275**, 630-634 (2015).
27. Thorek, D.L., Chen, A.K., Czupryna, J. & Tsourkas, A. Superparamagnetic iron oxide nanoparticle probes for molecular imaging. *Ann. Biomed. Eng.* **34**, 23-38 (2006).
28. Bulte, J.W. In vivo MRI cell tracking: clinical studies. *AJR Am. J. Roentgenol.* **193**, 314-325 (2009).
29. Atanasijevic, T., Shusteff, M., Fam, P. & Jasanoff, A. Calcium-sensitive MRI contrast agents based on superparamagnetic iron oxide nanoparticles and calmodulin. *Proc. Natl. Acad. Sci. U. S. A.* **103**, 14707-14712 (2006).
30. Matsumoto, Y., Chen, R., Anikeeva, P. & Jasanoff, A. Engineering intracellular biomineralization and biosensing by a magnetic protein. *Nat Commun* **6**, 8721 (2015).
31. Gilad, A.A., *et al.* Artificial reporter gene providing MRI contrast based on proton exchange. *Nat. Biotechnol.* **25**, 217-219 (2007).
32. Viale, A. & Aime, S. Current concepts on hyperpolarized molecules in MRI. *Curr. Opin. Chem. Biol.* **14**, 90-96 (2010).
33. Logothetis, N.K. What we can do and what we cannot do with fMRI. *Nature* **453**, 869-878 (2008).
34. Logothetis, N.K. The underpinnings of the BOLD functional magnetic resonance imaging signal. *J. Neurosci.* **23**, 3963-3971 (2003).
35. Sourbron, S., Ingrisch, M., Siefert, A., Reiser, M. & Herrmann, K. Quantification of cerebral blood flow, cerebral blood volume, and blood-brain-barrier leakage with DCE-MRI. *Magn. Reson. Med.* **62**, 205-217 (2009).
36. Tsai, P.S., *et al.* Correlations of neuronal and microvascular densities in murine cortex revealed by direct counting and colocalization of nuclei and vessels. *J. Neurosci.* **29**, 14553-14570 (2009).
37. van den Pol, A.N. Neuropeptide transmission in brain circuits. *Neuron* **76**, 98-115 (2012).

38. Brain, S.D. & Grant, A.D. Vascular actions of calcitonin gene-related peptide and adrenomedullin. *Physiol. Rev.* **84**, 903-934 (2004).
39. Russell, F.A., King, R., Smillie, S.-J., Kodji, X. & Brain, S.D. Calcitonin gene-related peptide: physiology and pathophysiology. *Physiol. Rev.* **94**, 1099-1142 (2014).
40. Chin, S.Y., Hall, J.M., Brain, S.D. & Morton, I.K. Vasodilator responses to calcitonin gene-related peptide (CGRP) and amylin in the rat isolated perfused kidney are mediated via CGRP1 receptors. *J. Pharmacol. Exp. Ther.* **269**, 989-992 (1994).
41. Logothetis, N.K. & Wandell, B.A. Interpreting the BOLD signal. *Annu. Rev. Physiol.* **66**, 735-769 (2004).
42. Logothetis, N.K., Pauls, J., Augath, M., Trinath, T. & Oeltermann, A. Neurophysiological investigation of the basis of the fMRI signal. *Nature* **412**, 150-157 (2001).
43. Yao, J. & Wang, L.V. Breakthroughs in Photonics 2013: Photoacoustic Tomography in Biomedicine. *IEEE Photon. J.* **6**, 0701006 (2014).
44. Patterson, A.P., Booth, S.A. & Saba, R. The Emerging Use of In Vivo Optical Imaging in the Study of Neurodegenerative Diseases. *BioMed Res. Int.* **2014**, 401306 (2014).
45. Stefanovic, B., Schwandt, W., Hoehn, M. & Silva, A.C. Functional uncoupling of hemodynamic from neuronal response by inhibition of neuronal nitric oxide synthase. *J. Cereb. Blood Flow Metab.* **27**, 741-754 (2007).
46. Hortobágyi, L., *et al.* Adaptation of the hypothalamic blood flow to chronic nitric oxide deficiency is independent of vasodilator prostanoids. *Brain Res.* **1131**, 129-137 (2007).
47. Choi, K.Y., Swierczewska, M., Lee, S. & Chen, X. Protease-activated drug development. *Theranostics* **2**, 156-178 (2012).
48. Turk, B. Targeting proteases: successes, failures and future prospects. *Nat. Rev. Drug Discov.* **5**, 785-799 (2006).
49. Sanman, L.E. & Bogoy, M. Activity-based profiling of proteases. *Annu. Rev. Biochem.* **83**, 249-273 (2014).

50. Watkins, H., Rathbone, D.L., Barwell, J., Hay, D.L. & Poyner, D.R. Structure-activity relationships for alpha-calcitonin gene-related peptide. *Br. J. Pharmacol.* **170**, 1308-1322 (2013).
51. Brennen, W.N., Isaacs, J.T. & Denmeade, S.R. Rationale behind targeting fibroblast activation protein-expressing carcinoma-associated fibroblasts as a novel chemotherapeutic strategy. *Mol. Cancer Ther.* **11**, 257-266 (2012).
52. Ahrens, E.T. & Bulte, J.W.M. Tracking immune cells in vivo using magnetic resonance imaging. *Nat. Rev. Immunol.* **13**, 755-763 (2013).
53. Naumova, A.V., Modo, M., Moore, A., Murry, C.E. & Frank, J. Clinical imaging in regenerative medicine. *Nat. Biotechnol.* **32**, 804-818 (2014).
54. Silva, M.T. Secondary necrosis: The natural outcome of the complete apoptotic program. *FEBS Lett.* **584**, 4491-4499 (2010).
55. Maueröder, C., *et al.* Tumor Immunotherapy: Lessons from Autoimmunity. *Front. Immunol.* **5**, 212 (2014).
56. Melis, M.H.M., *et al.* Sustained tumour eradication after induced caspase-3 activation and synchronous tumour apoptosis requires an intact host immune response. *Cell Death Differ.* **20**, 765-773 (2013).
57. Laxman, B., *et al.* Noninvasive real-time imaging of apoptosis. *Proc. Natl. Acad. Sci. U. S. A.* **99**, 16551-16555 (2002).
58. Edgington, L.E., *et al.* Noninvasive optical imaging of apoptosis by caspase-targeted activity-based probes. *Nat. Med.* **15**, 967-973 (2009).
59. Li, J., *et al.* Activatable near-infrared fluorescent probe for in vivo imaging of fibroblast activation protein-alpha. *Bioconj. Chem.* **23**, 1704-1711 (2012).
60. Mizukami, S., *et al.* Paramagnetic relaxation-based ¹⁹F MRI probe to detect protease activity. *J. Am. Chem. Soc.* **130**, 794-795 (2008).
61. Ye, D., *et al.* Caspase-responsive smart gadolinium-based contrast agent for magnetic resonance imaging of drug-induced apoptosis. *Chem. Sci.* **5**, 3845-3852 (2014).

62. Research, T.F.I.f.M. Fluorodeoxyglucose F18 Injection: Highlights of prescribing information. (Manhasset, New York, 11030, 2012).
63. Pardridge, W.M. & Boado, R.J. Reengineering biopharmaceuticals for targeted delivery across the blood-brain barrier. *Methods Enzymol.* **503**, 269-292 (2012).
64. Durham, P.L. Calcitonin gene-related peptide (CGRP) and migraine. *Headache* **46**, S3-8 (2006).
65. Fischer, M.J.M., Uchida, S. & Messlinger, K. Measurement of meningeal blood vessel diameter in vivo with a plug-in for ImageJ. *Microvasc. Res.* **80**, 258-266 (2010).
66. Cox, R.W. AFNI: software for analysis and visualization of functional magnetic resonance neuroimages. *Comput. Biomed. Res.* **29**, 162-173 (1996).
67. Swanson, L.W. *Brain Maps: Structure of the Rat Brain*, (Elsevier Science, 1992).
68. Forman, S.D., *et al.* Improved assessment of significant activation in functional magnetic resonance imaging (fMRI): use of a cluster-size threshold. *Magn. Reson. Med.* **33**, 636-647 (1995).
69. Xiong, J., Gao, J.-H., Lancaster, J.L. & Fox, P.T. Clustered pixels analysis for functional MRI activation studies of the human brain. *Hum. Brain Mapp.* **3**, 287-301 (1995).
70. Campeau, E., *et al.* A versatile viral system for expression and depletion of proteins in mammalian cells. *PLoS One* **4**, e6529 (2009).
71. Engler, C., Kandzia, R. & Marillonnet, S. A one pot, one step, precision cloning method with high throughput capability. *PLoS One* **3**, e3647 (2008).
72. Suzuki, T., *et al.* Development of cysteine-free fluorescent proteins for the oxidative environment. *PLoS One* **7**, e37551 (2012).
73. Szymczak, A.L., *et al.* Correction of multi-gene deficiency in vivo using a single 'self-cleaving' 2A peptide-based retroviral vector. *Nat. Biotechnol.* **22**, 589-594 (2004).
74. Fitzsimmons, T.J., Zhao, X. & Wank, S. The extracellular domain of receptor activity-modifying protein 1 is sufficient for calcitonin receptor-like receptor function. *J. Biol. Chem.* **278**, 14313-14320 (2003).

75. Fan, F., *et al.* Novel genetically encoded biosensors using firefly luciferase. *ACS Chem. Biol.* **3**, 346-351 (2008).
76. Taylor, A., Wilson, K.M., Murray, P., Fernig, D.G. & Levy, R. Long-term tracking of cells using inorganic nanoparticles as contrast agents: are we there yet? *Chem. Soc. Rev.* **41**, 2707-2717 (2012).
77. Pereira, S.M., Moss, D., Williams, S.R., Murray, P. & Taylor, A. Overexpression of the MRI Reporter Genes Ferritin and Transferrin Receptor Affect Iron Homeostasis and Produce Limited Contrast in Mesenchymal Stem Cells. *Int. J. Mol. Sci.* **16**, 15481-15496 (2015).
78. Srivastava, A.K., *et al.* Advances in using MRI probes and sensors for in vivo cell tracking as applied to regenerative medicine. *Dis. Model. Mech.* **8**, 323-336 (2015).
79. Pardridge, W.M. Blood-brain barrier delivery. *Drug Discov. Today* **12**, 54-61 (2007).
80. Banks, W.A. From blood-brain barrier to blood-brain interface: new opportunities for CNS drug delivery. *Nat. Rev. Drug Discov.* (2016).
81. Lajoie, J.M. & Shusta, E.V. Targeting receptor-mediated transport for delivery of biologics across the blood-brain barrier. *Annu. Rev. Pharmacol. Toxicol.* **55**, 613-631 (2015).
82. Triguero, D., Buciak, J. & Pardridge, W.M. Capillary depletion method for quantification of blood-brain barrier transport of circulating peptides and plasma proteins. *J. Neurochem.* **54**, 1882-1888 (1990).
83. Gosk, S., Vermehren, C., Storm, G. & Moos, T. Targeting anti-transferrin receptor antibody (OX26) and OX26-conjugated liposomes to brain capillary endothelial cells using in situ perfusion. *J. Cereb. Blood Flow Metab.* **24**, 1193-1204 (2004).
84. Niewoehner, J., *et al.* Increased brain penetration and potency of a therapeutic antibody using a monovalent molecular shuttle. *Neuron* **81**, 49-60 (2014).
85. Yu, Y.J., *et al.* Therapeutic bispecific antibodies cross the blood-brain barrier in nonhuman primates. *Sci. Transl. Med.* **6**, 261ra154 (2014).

86. Yu, Y.J., *et al.* Boosting brain uptake of a therapeutic antibody by reducing its affinity for a transcytosis target. *Sci. Transl. Med.* **3**, 84ra44 (2011).
87. Farrington, G.K., *et al.* A novel platform for engineering blood-brain barrier-crossing bispecific biologics. *FASEB J.* **28**, 4764-4778 (2014).
88. Jolivel, V., *et al.* Distribution and functional characterization of pituitary adenylate cyclase-activating polypeptide receptors in the brain of non-human primates. *Neuroscience* **160**, 434-451 (2009).
89. Vaudry, D., *et al.* Pituitary adenylate cyclase-activating polypeptide and its receptors: 20 years after the discovery. *Pharmacol. Rev.* **61**, 283-357 (2009).
90. Lerner, E.A. & Shoemaker, C.B. Maxadilan. Cloning and functional expression of the gene encoding this potent vasodilator peptide. *J. Biol. Chem.* **267**, 1062-1066 (1992).
91. Lanzaro, G.C., *et al.* Variation in the salivary peptide, maxadilan, from species in the *Lutzomyia longipalpis* complex. *Insect Mol. Biol.* **8**, 267-275 (1999).
92. Reddy, V.B., Iuga, A.O., Kounga, K. & Lerner, E.A. Functional analysis of recombinant mutants of maxadilan with a PAC1 receptor-expressing melanophore cell line. *J. Biol. Chem.* **281**, 16197-16201 (2006).
93. Nokihara, K., Yasuhara, T., Nakata, Y., Lerner, E.A. & Wray, V. Chemical Synthesis of Maxadilan, a Non-mammalian Potent Vasodilatory Peptide Consisting of 61 Amino Acids with Two Disulfide Bridges, and Its Related Peptides. *Int. J. Pept. Res. Ther.* **13**, 377-386 (2007).
94. Moro, O., *et al.* Functional characterization of structural alterations in the sequence of the vasodilatory peptide maxadilan yields a pituitary adenylate cyclase-activating peptide type 1 receptor-specific antagonist. *J. Biol. Chem.* **274**, 23103-23110 (1999).
95. Bickel, U., Yoshikawa, T., Landaw, E.M., Faull, K.F. & Pardridge, W.M. Pharmacologic effects in vivo in brain by vector-mediated peptide drug delivery. *Proc. Natl. Acad. Sci. U. S. A.* **90**, 2618-2622 (1993).

96. Li, J.Y., *et al.* Genetically engineered brain drug delivery vectors: cloning, expression and in vivo application of an anti-transferrin receptor single chain antibody-streptavidin fusion gene and protein. *Protein Eng.* **12**, 787-796 (1999).
97. Muruganandam, A., Tanha, J., Narang, S. & Stanimirovic, D. Selection of phage-displayed llama single-domain antibodies that transmigrate across human blood-brain barrier endothelium. *FASEB J.* **16**, 240-242 (2002).
98. Farrington, G.K. & Sisk, W. Enhancement of transport of therapeutic molecules across the blood brain barrier. (2013).
99. Decourt, B. & Sabbagh, M.N. BACE1 as a potential biomarker for Alzheimer's disease. *J. Alzheimers Dis.* **24 Suppl 2**, 53-59 (2011).
100. Perneczky, R., Alexopoulos, P. & Kurz, A. Soluble amyloid precursor proteins and secretases as Alzheimer's disease biomarkers. *Trends Mol. Med.* **20**, 8-15 (2014).
101. Deverman, B.E., *et al.* Cre-dependent selection yields AAV variants for widespread gene transfer to the adult brain. *Nat. Biotechnol.* **34**, 204-209 (2016).
102. Zarahn, E. Spatial localization and resolution of BOLD fMRI. *Curr. Opin. Neurobiol.* **11**, 209-212 (2001).
103. Russell, F.A., King, R., Smillie, S.J., Kodji, X. & Brain, S.D. Calcitonin gene-related peptide: physiology and pathophysiology. *Physiol. Rev.* **94**, 1099-1142 (2014).